



**HAL**  
open science

# Contribution to Face Analysis from RGB Images and Depth Maps

Elhocine Boutellaa

► **To cite this version:**

Elhocine Boutellaa. Contribution to Face Analysis from RGB Images and Depth Maps. Computer Vision and Pattern Recognition [cs.CV]. Ecole nationale Supérieure en Informatique Alger, 2017. English. NNT: . tel-01452378v1

**HAL Id: tel-01452378**

**<https://theses.hal.science/tel-01452378v1>**

Submitted on 1 Feb 2017 (v1), last revised 13 Feb 2017 (v2)

**HAL** is a multi-disciplinary open access archive for the deposit and dissemination of scientific research documents, whether they are published or not. The documents may come from teaching and research institutions in France or abroad, or from public or private research centers.

L'archive ouverte pluridisciplinaire **HAL**, est destinée au dépôt et à la diffusion de documents scientifiques de niveau recherche, publiés ou non, émanant des établissements d'enseignement et de recherche français ou étrangers, des laboratoires publics ou privés.

Ecole Nationale Supérieure d'Informatique



## Contribution to Face Analysis from RGB Images and Depth Maps

Elhocine Boutellaa

A dissertation submitted for the degree of Doctor of Philosophy

Supervisors:

Mr.	Samy Ait-Aoudia	Prof	ESI
Mr.	Abdenour Hadid	Prof	University of Oulu

Publicly defended on 31/01/2017 before the jury composed of:

Mr.	Walid Khaled HIDOUCI	Prof	ESI	President
Mr.	Amar BALLA	Prof	ESI	Examiner
Mr.	Hamid HADDADOU	MCA	ESI	Examiner
Mr.	Youcef ZAFFOUNE	MCA	USTHB	Examiner
Mr.	Samy AIT AOUDIA	Prof	ESI	Thesis Director

## Abstract

Automatic human face analysis refers to the processing of facial images by machines in order to infer useful information, such as identity, gender, ethnicity, mood, etc. Face analysis has many interesting applications in security, human computer interaction, social media analysis, etc. Therefore, though face analysis is an well-established computer vision problem, it is still an active research topic attracting considerable attention from researchers. The research community mainly aims to develop more robust systems with the ability to fulfill the requirements of current applications.

This thesis contributes to a number of face analysis tasks: face verification and identification, gender recognition, ethnicity recognition and kinship verification. Faces from three different imaging supports i.e. RGB images, depth maps and videos are used throughout the thesis. We present novel approaches and in-depth studies for solving and improving the face analysis problem.

First, we tackle face verification problem from RGB images. The local binary patterns based face verification scheme has been revised through proposing novel efficient representations, which cope with the original approach drawbacks while improving the verification performance.

Next, the problems of identity, gender and ethnicity recognition are investigated from both RGB and depth images. The aim is to assess the usefulness low-quality depth images, acquired with Microsoft Kinect low-cost sensor, in coping with facial analysis tasks. The performance of RGB images and depth maps are compared to show the ability of the latter ones to deal with sever environment illumination circumstances.

Furthermore, the thesis contributes to the problem of kinship verification from videos, where the family relationship between two persons is checked by comparing their facial attributes. The dynamics of faces are efficiently coded by the means of spatio-temporal descriptors and deep features. The value of using videos in kinship problem is shown by comparing their performance against that of still images.

Throughout the thesis, various benchmark databases are used and extensive experiments are carried out to validate our proposed approaches and developed methods. Besides, the results of the proposed approaches are compared against the state of the art, highlighting our contributions and showing improvements. Future directions for the presented contributions are outlined at end of the thesis.



## Acknowledgments

This thesis has been carried out within the biometric team, Telecom Laboratory of Centre de développement des Technologies Avancées (CDTA), Algiers, Algeria. I have been working as a research associate within CDTA during the thesis work.

First of all, I express my profound gratitude to my supervisors, Professor Samy Ait-Aoudia and Professor Abdenour Hadid, for their guidance, support and encouragements. I am thankful for their precious advices and fruitful discussions for improving each paper and the thesis. I also acknowledge their patience and help during the whole thesis work period.

I am grateful to all Biometric team members in CDTA as well as other co-authors for the fruitful collaboration we established. I acknowledge the help I received and the exchange I had, which made the work of the thesis easier.

I am thankful for Professor Mohamed Cheriet for hosting me in his research laboratory Synchormedia at Ecole de Technologie Supérieure in Montreal Canada for one month. I am also thankful for Professor Matti Pietikäinen for hosting me in Center for Machine Vision of University of Oulu in Finland for a period of eighteen months. Both visits had a significant impact on my research. These two research visits have been funded by CDTA and the Algerian ministry of higher education and scientific research.

Finally, my deep gratitude is addressed to my parents, family members and friends for their endless support and encouragement.



# Abbreviations

AAM active appearance models

ANN artificial neural networks

ASM active shape model

BSIF binarized statistical image features

CNN convolutional neural networks

DET detection error trade-off

DLQP depth local quantized pattern

DPM deformable parts-based model

EER equal error rate

FAR false acceptance rate

FRR false rejection rate

GMM Gaussian mixture model

GPU graphics processing unit

HoG histograms of oriented Gradients

HTER half total error rate

ICA independent component analysis

ICP iterative closest point

LBG Linde-Buzo-Gray

LDA linear discriminant analysis

LLR log likelihood ratio

LBP local binary patterns

LPQ local phase quantization

MAP maximum *a posteriori*

MLP multi-layer perception

MSE mean squared error

NIR near infrared

NN nearest neighbor

OCLBP over-complete LBP

PCA principal component analysis  
RBF radial basis function  
ROC receiver operating characteristics  
ROI regions of interest  
SIFT scale invariant feature transform  
STFT short-term Fourier transform  
SRC sparse representation classifier  
SVM support vector machines  
TOP three orthogonal planes  
UBM universal background model  
VQ vector quantization





# Contents

<b>1</b>	<b>Introduction</b>	<b>19</b>
1.1	Thesis contributions . . . . .	20
1.2	Thesis organization . . . . .	22
<b>2</b>	<b>Background</b>	<b>26</b>
2.1	Face analysis tasks . . . . .	26
2.2	Applications and motivation . . . . .	28
2.2.1	Security . . . . .	28
2.2.2	Social media analysis . . . . .	29
2.2.3	Human computer interaction . . . . .	29
2.2.4	Automatic health assessment . . . . .	29
2.3	Generic face analysis framework . . . . .	30
2.3.1	Face detection and tracking . . . . .	31
2.3.2	Face description . . . . .	33
2.3.3	Face modeling and classification . . . . .	34
2.4	Challenges and remedies . . . . .	36
2.4.1	Illumination . . . . .	37
2.4.2	Head pose and viewpoint change . . . . .	38
2.4.3	Occlusion . . . . .	38
2.5	Summary . . . . .	39
<b>3</b>	<b>Face verification</b>	<b>41</b>
3.1	Motivations and approach overview . . . . .	42

3.2	The local binary patterns . . . . .	43
3.3	Face representation using LBP . . . . .	46
3.4	Face verification using LBP and VQMAP . . . . .	48
3.4.1	LBP Quantization . . . . .	48
3.4.2	VQMAP model . . . . .	50
3.4.3	Face verification system . . . . .	51
3.5	Face verification using adapted LBP histograms . . . . .	53
3.6	Experimental analysis . . . . .	55
3.6.1	Databases . . . . .	55
3.6.2	Setup . . . . .	57
3.6.3	Results and discussion . . . . .	58
3.7	Conclusion . . . . .	61
<b>4</b>	<b>Face analysis from Kinect data</b>	<b>64</b>
4.1	Kinect sensors . . . . .	65
4.2	Review of works using Kinect for face analysis . . . . .	67
4.2.1	Face detection and tracking, pose estimation . . . . .	67
4.2.2	Face recognition . . . . .	69
4.2.3	Gender and expression recognition . . . . .	71
4.2.4	Face modeling, reconstruction and animation . . . . .	72
4.2.5	Discussion and contribution motivation . . . . .	72
4.3	A framework for face analysis from Kinect data . . . . .	73
4.3.1	Preprocessing . . . . .	73
4.3.2	Feature extraction . . . . .	74
4.3.3	Classification . . . . .	80
4.4	Experiments and results . . . . .	81
4.4.1	Databases . . . . .	81
4.4.2	Setup . . . . .	83
4.4.3	Experimental results . . . . .	84
4.5	Conclusion . . . . .	87

<b>5</b>	<b>Kinship verification from videos</b>	<b>90</b>
5.1	Background and motivation . . . . .	91
5.2	Video-based kinship verification . . . . .	92
5.2.1	Approach overview . . . . .	93
5.2.2	Face detection and tracking . . . . .	95
5.2.3	Face description . . . . .	96
5.2.4	Classification . . . . .	102
5.3	Experiments . . . . .	102
5.3.1	Database and test protocol . . . . .	102
5.3.2	Results and analysis . . . . .	104
5.4	Conclusion . . . . .	114
<b>6</b>	<b>Summary and future work</b>	<b>116</b>
6.1	Summary . . . . .	116
6.2	Future directions . . . . .	118
<b>A</b>	<b>Vector quantization maximum <i>a posteriori</i></b>	<b>121</b>
A.1	Modeling VQ as a Gaussian mixture . . . . .	122
A.2	Defining the prior density . . . . .	122
A.3	MAP estimates for vector quantization . . . . .	123

# List of Figures

1-1	Main content of the thesis. . . . .	24
2-1	Training phase of face analysis system. . . . .	31
2-2	Operational phase of face analysis system. . . . .	31
2-3	Illustration of face detection. . . . .	32
2-4	Different strategies for extracting local face features from: a) face grid, b) face regions, c) face landmarks [69]. . . . .	35
2-5	Examples of challenging face images. . . . .	37
3-1	The basic LBP operator. . . . .	44
3-2	The uniform patterns in $LBP_{8,R}$ configuration [95]. . . . .	45
3-3	Some texture primitives detected by the LBP operator [95]. . . . .	46
3-4	Face description using LBP. . . . .	47
3-5	Face block description: LBP histogram against VQ-LBP codebook. The histograms are larger and sparse while the codebooks are dense and compact . . . . .	49
3-6	LBP-face quantization. . . . .	50
3-7	LBP-VQMAP face verification system. . . . .	52
3-8	LBP histograms of the same block from three face images of a subject, taken in the same session, and their adapted histogram. . . . .	53
3-9	Example of XM2VTS face images of the same person across different sessions. . . . .	55
3-10	Example of BANCA face images from the three acquisition conditions : controlled (left), degraded (middle) and adverse (right). . . . .	57

3-11	DET curve for baseline LBP, our two approaches (VQMAP and AH) and their fusion (VQMAP-AH) on BANCA database for the pooled protocol P. . . . .	61
4-1	Comparing face images acquired with Minolta VIVID 910 scanner (left) against Kinect (right). . . . .	66
4-2	Examples of 2D cropped image (left) and corresponding 3D face image (right) obtained with the Microsoft Kinect sensor after preprocessing.	74
4-3	Examples of results after applying the four descriptors to face texture and depth images. From left to right: the original face image (top: texture image and bottom: its corresponding depth image) and the resulting images after the application of LBP, LPQ, HoG and BSIF descriptors, respectively. . . . .	80
4-4	Face images samples from a subject of the CurtinFaces database. Top: RGB faces, middle: their corresponding raw depth maps and bottom: depth cropped face. . . . .	83
4-5	Classification accuracy for identity, gender and ethnicity using RGB and depth on FaceWarehouse database. . . . .	86
5-1	Overview of the proposed approach for kinship verification from videos.	94
5-2	Example of face cropping: (left) a frame annotated with the detected landmarks, and (right) the cropped and aligned face region. . . . .	95
5-3	Illustration of three orthogonal planes used to extract dynamic textural face descriptors from a video. . . . .	97
5-4	Division of video into region volumes. . . . .	98
5-5	Three plan feature vector. . . . .	98
5-6	Example of a convolutional neural network. . . . .	100
5-7	Samples of pair images form UvA-NEMO Smile database for different kin relations. Positive pairs are combinations of first row with second row (green rectangles) and negative pairs are combinations of second row with third row (red rectangles). . . . .	103

5-8	Comparing deep vs. shallow features on UvA-NEMO Smile database.	107
5-9	Comparing videos vs. still images for kinship verification on UvA-NEMO Smile database. . . . .	110
5-10	Performance of our approach against the best state-of-the-art one. . .	112
5-11	Examples of correctly classified positive kin pairs by our approach using both spatio-temporal features and deep features. . . . .	113
5-12	Examples of wrongly classified positive kin pairs by our approach using both spatio-temporal features and deep features. . . . .	113

# List of Tables

3.1	Partitioning of the XM2VTS database according to the two configurations. . . . .	56
3.2	Partitioning of Banca database for MC, UA and P configurations. . .	57
3.3	HTER (%) on XM2VTS database using LPI and LPII protocols for different configurations of LBP baseline and our proposed methods. . .	58
3.4	HTER (%) on BANCA database for MC, UA and P protocols using different configurations of LBP baseline and our proposed methods. . .	60
3.5	HTER (%) for state of the art methods on BANCA database. . . . .	60
4.1	Comparing Kinect and Minolta VIVID 910 3D scanning devices. . . . .	67
4.2	Kinect face databases employed in our experiments. . . . .	83
4.3	Mean classification rates (%) and standard deviation using RGB and depth for face identity classification on FaceWarehouse, IIIT-D and CurtinFaces databases. . . . .	84
4.4	Mean classification rates (%) and standard deviation using RGB and depth for face gender classification on FaceWarehouse, IIIT-D and CurtinFaces databases. . . . .	85
4.5	Mean classification rates (%) and standard deviation using RGB and depth for facial ethnicity classification on FaceWarehouse and CurtinFaces database. Results are not provided for IIIT-D database as only one ethnicity is represented in this database. . . . .	85
4.6	Summary of reported performance of literature work on face analysis using Kinect sensor. . . . .	87



5.1	VGG-face CNN architecture. . . . .	101
5.2	Kinship statistics of UvA-NEMO Smile database. . . . .	103
5.3	Accuracy (in %) of kinship verification using spatio-temporal and deep features on UvA-NEMO Smile database. . . . .	105
5.4	Comparison of our approach for kinship verification against state of the art on UvA-NEMO Smile database. . . . .	111



# List of publications

This thesis is based on the following publications:

- I** . E. Boutellaa, F. Harizi, M. Bengherabi, S. Ait-Aoudia, and A. Hadid. Face verification using local binary patterns and maximum a posteriori vector quantization model. In *Advances in Visual Computing*, pages 539-549. Springer, 2013.
- II** . E. Boutellaa, F. Harizi, M. Bengherabi, S. Ait-Aoudia, and A. Hadid. Face verification using local binary patterns and generic model adaptation. *International Journal of Biometrics*, 7(1):31-44, 2015.
- III** . E. Boutellaa, M. Bengherabi, S. Ait-Aoudia, and A. Hadid. How much information Kinect facial depth data can reveal about identity, gender and ethnicity? In L. Agapito, M. M. Bronstein, and C. Rother, editors, *Computer Vision - ECCV 2014 Workshops*, volume 8926 of *Lecture Notes in Computer Science*, pages 725-736. Springer International Publishing, 2015.
- IV** . E. Boutellaa, A. Hadid, M. Bengherabi, and S. Ait-Aoudia. On the use of Kinect depth data for identity, gender and ethnicity classification from facial images. *Pattern Recognition Letters*, 68, Part 2:270-277, 2015.
- V** . E. Boutellaa, M. Bordallo, S. Ait-Aoudia, X. Feng, and A. Hadid. Kinship Verification from Videos using Spatio-Temporal Texture Features and Deep Learning, *International Conference on Biometrics (ICB)*, Accepted, 2016.



# Chapter 1

## Introduction

Human face is involved in an impressive variety of different activities. It houses the majority of our sensory apparatus - eyes, ears, mouth, and nose - allowing the bearer to see, hear, taste, and smell. Apart from these biological functions, it also provides a number of signals about our health, emotional state, identity, age, gender, etc. Humans have an impressive ability to read faces. Indeed, inspecting a person's face, one can easily know whether the person is male or female, Asian or Caucasian, happy or sad, healthy or sick, etc. The aim of automatic face analysis is to make machines able to perform such tasks.

Machine analysis of faces plays a key role in many emerging applications of computer vision, including biometric recognition systems, human-computer interfaces, smart environments, visual surveillance, and content-based retrieval of images from multimedia databases. Due to its many potential applications, automatic face analysis which includes, e.g., face detection, face recognition, gender classification, age estimation and facial expression recognition, has become one of the most active topics in computer vision research [69].

Despite of the considerable research advance achieved in the past years in various face analysis problems, the topic is still very active attracting attention by researchers from computer vision, pattern recognition and machine learning disciplines. This interest is not only motivated by the increasing robustness requirements of current applications but also by encountered challenges that prevent developing robust

systems for real world applications. A widely varied and extremely complicated challenges limit the development of ideal face analysis systems. On one hand, human face is inherently a non rigid 3D object which deforms and moves (due, for example, to expressions and head poses) in complex ways making considerable changes to its ordinary shape. Other face-internal changes may appear because of some face parts like hair, mustache and beard as well as change occurring because of age. On the other hand, various effects external to face, such as garments (e.g., glasses, make up, hat, mask, scarf, etc.) and environment illumination, significantly affect face analysis tasks. Finally, combinations of the previously mentioned constraints make the face analysis task extremely hard to perform.

To overcome the above challenges, face analysis has been studied from different sensing technologies. While mostly RGB images have been employed, other image types have also been studied but with less magnitude. For instance, 3D face scans have been used to overcome the head pose, facial expression and illumination change. Face videos have also been used in order to take face dynamics into account. On the other hand, to address these challenges, various feature extraction methods and classification approaches have been investigated to increase the robustness of face analysis systems.

The present thesis aims to study some still open issues within face analysis research. A particular emphasis is given to feature extraction and modeling stages. The contributions are summarized in the following section.

## 1.1 Thesis contributions

This thesis contributes to different stages of face analysis systems. Various face analysis tasks (i.e., identity, gender, ethnicity and kinship) are investigated by considering several imaging technologies (i.e. RGB images, depth images and videos).

The thesis mainly focuses on developing powerful face descriptors and models which are evaluated on various face analysis tasks. First of all, the successful local binary patterns (LBP) descriptor is revisited addressing some of its inherent short-

comings in face description. Specifically, we propose an efficient and compact LBP-based face representation using vector quantization maximum *a posteriori* adaptation modeling. Additionally, we have proposed an improved version of the original LBP-histogram representation. To enhance the face description, we build a generic face using a pool of face images from a background population and derive a specific user histogram representation by adapting the generic model to each person. The two proposed approaches are evaluated, each one separately as well as their combination, on the problem of face verification from RGB images. The results of these investigations are published in Papers I and II.

Another contribution is concerns the use of novel low-cost depth sensing devices for face analysis tasks. We have investigated face identification, gender classification and ethnicity recognition using depth images acquired with Microsoft Kinect sensors. We aimed to study the feasibility and usefulness of employing low resolution depth images for automatically inferring meaningful face information. For this purpose, we employed four different feature extraction methods (Local Binary Patterns (LBP), Local Phase Quantization (LPQ), Histogram of Oriented Gradients (HOG) and Binarized Statistical Image Features (BSIF)) for representing face depth images. Besides, the performance of depth images has been compared against RGB counterparts to analyze the benefits of each type of images. The contributions of this part of the thesis are published in Papers III and IV.

The thesis contributes also to face analysis from videos where the problem of kinship verification has been investigated. To account for the dynamics of the face, face videos are represented by three spatio-temporal descriptors as well as the powerful deep features. Deep features are extracted by an efficient deep convolutional neural networks architecture. The spatio-temporal features are extensions of LBP, LPQ and BSIF features to enable describing video sequences in three dimensional planes. Furthermore, to highlight the importance of using videos for solving kinship verification problem, we carry out a comparison of videos performance against those of still images. The contributions of this part of the thesis are published in Paper V.

## 1.2 Thesis organization

The thesis is organized as follows:

- In Chapter 2, we introduce some background and preliminaries. First, we introduce the main face analysis tasks mostly studied in the literature. Next, potential applications and motivations for the research on face analysis topics are discussed. Then, we depict the generic scheme for face analysis and explain the details of each component involved in the global system. The chapter presents also the challenges related to face image analysis and summarizes some existing solutions.
- In Chapter 3, we tackle face verification problem using LBP features. Two face verification approaches are proposed. The first one [19] is based on the quantization of LBP codes and modeling the resulting vectors by the maximum a posterior paradigm. The second approach [20] enhances the histogram representation in LBP-baseline of face recognition. The new histogram representation results from weighting a generic face histogram and the targeted person histogram. Both approaches are further fused to improve the verification performance. The evaluation is performed using two publicly available face databases showing significant improvements.
- In Chapter 4, we study three face analysis tasks, namely identity, gender and ethnicity recognition, from both RGB and depth images acquired by Microsoft Kinect sensor. We present the Microsoft Kinect sensor and review its use for different face analysis tasks [16, 18]. The study of this chapter involves four different local descriptors. We extend the LBP used for describing faces from RGB images in Chapter 3, as well as three other descriptors (LPQ, HOG and BSIF) for describing faces from low resolution depth images. Extensive evaluation and analysis of the proposed approach is performed on four different Kinect databases. Furthermore, comparisons between results of different features and image types for the studied problems are discussed.



- In Chapter 5, we address the problem of kinship verification from face videos [17]. We first present some analysis of recent works on Kinship verification problem to identify the important and less investigated issues. Based on this analysis, we propose an efficient approach to cope with kinship verification problem. The proposed approach is based on the combination of spatio-temporal features and the recently widely successful deep features and support vector machines for classification. Spatio-temporal features are extensions of the features used in Chapter 4, for RGB and depth images, to describe faces from videos. We extensively evaluate the proposed approach on a kinship video database and compare our results against state-of-the-art.
- In Chapter 6, we summarize the thesis work, present our conclusions and draw some future directions.

The main content of the thesis is summarized in Fig. 1-1.





# Chapter 2

## Background

In this chapter, we introduce the background information and the notions required for understanding the thesis. After introducing the main face analysis tasks, we enumerate their extensive applications which justify the ongoing research interest in the topic. Next, we present a generic face analysis flow chart and detail its different components. We also overview the challenges related to face analysis and present the main remedies proposed by state-of-the-art works. Throughout the sections of the chapter, a brief survey pointing out the major achievements will be provided.

### 2.1 Face analysis tasks

A wide range of information can be automatically inferred from human faces. This section overviews the main face analysis tasks.

*Face recognition* [69] is the most researched task and it has a big influence on other face analysis tasks. As a biometric, a face has many advantages above the other modalities. Capturing a face image is a non-intrusive process since usually less, or even no, cooperation of the person is required. Another important reason making face among the top biometric modalities is the omnipresence of cameras, which facilitates the face acquisition. Face recognition encompasses two different operational modes: verification and identification. The former, also known as authentication, is the process of checking whether a given face corresponds to a claimed identity. In

this first mode, a unique matching of the test face against the claimed person face is needed. On the other hand, face identification refers to finding out whether a probe face belongs to one person among the population of a face database. In face identification, the matching of the probe face against the whole database is indispensable. Though, the first research on automatic face recognition is originated by Woodrow Bledsoe in 1964 [15], the topic is still today among the most active in computer vision, pattern recognition and machine learning research communities.

*Expression classification* [42] is also an important research topic in automatic face analysis. Facial expressions can reflect different information about the person including emotions, mental activities, social interaction and physiological signals. Psychologists identified six prototypic primary facial expressions called basic emotions: happiness, sadness, fear, disgust, surprise and anger. These expressions are universal across human ethnicities. Automatic facial expression recognition is accomplished by the classification of face motion and face deformation into different classes based on face visual information. The research on facial expression analysis dates back to 1978, by the pioneer work of Suwa et al. [108], then gained much interest since the 1990s.

Human face holds also a variety of *demographic information* [125], such as *age, gender and ethnicity*. These facial information has been extremely useful in many fields such as forensics, customer analysis, surveillance, biometrics and video indexing. For instance, demographic facial information can help boosting face recognition algorithms [57]. While face based gender and ethnicity classification are challenging tasks, age estimation is harder to perform, mainly because age changes with time while gender and ethnicity remain the same for a given person.

*Automatic kinship verification* from faces is an emerging task that aims at determining whether two persons have a biological kin relation or not by comparing their facial attributes. Kinship verification is important for automatically analyzing the huge amount of photos daily shared on social media. It helps understanding the family relationships in these photos. Kinship verification is also useful in case of missing children and elderly people with Alzheimer as well as in kidnapping cases. Kinship verification can also be used for automatically organizing family albums and

generating family trees.

## 2.2 Applications and motivation

A key issue that motivates the ongoing and growing research on face analysis topics is the wide range of their important applications. This section gives an overview of current and potential face analysis applications.

### 2.2.1 Security

Security is a crucial concern of today's world with cross-countries terrorism threat. Face plays an important role in establishing security. One of the most important and worldwide spread applications is biometrics which aims at identifying or authenticating persons based on their physiological or behavioral traits. Along with fingerprint, face is the most widely used biometric modality. Face biometrics are used in identity documents, such as passports, national identity cards, driving licenses, etc. Border control of immigrants is another important issue for many countries where face-based identification is used to prevent illegal immigration. Other applications for face as a biometric include secure access to buildings, electronic devices, e-commerce services, etc.

Surveillance is another important security issue where face analysis and recognition plays an important role. Surveillance cameras are today deployed everywhere and the automatic analysis of the huge data collected by these cameras is crucial. For instance, face recognition has been applied to identify the suspects of Boston Marathon bombings [62] by inspecting the data collected by the surveillance cameras around the place.

Face analysis finds also important applications in forensics [58] by analyzing evidences collected from crime scenes in order to reconstruct and describe events in a legal setting. For example, facial sketches created based on eyewitness description are of great use in law enforcement to help identifying suspects involved in a crime. Automatic matching of the drawn sketch against criminals databases may accelerate

capturing dangerous criminals and hence preventing more crimes.

### **2.2.2 Social media analysis**

Today, social networks are powerful tools that influence many aspects of human life including culture, economy, politics, etc. Automatic analysis of the huge amount of daily shared data on social networks is very important for building strategies and future visions in various fields. Photos and videos of individuals, family, friends, group of people, etc. are among the most shared types of data in social networks. Therefore, developing effective automatic face analysis tools for analyzing, understanding and exploiting these data gained a remarkable attention these last years [115, 27, 44].

### **2.2.3 Human computer interaction**

To make human computer interaction more natural, face [11], gesture and speech analysis have been extensively considered. Robots that read the facial expression of the person, deduce the actual emotion and react accordingly have been recently developed. Moreover, face analysis has been useful for user immersion in virtual reality and game applications. Fatigue detection by analyzing car drivers face has been investigated to prevent car accidents.

### **2.2.4 Automatic health assessment**

As human face holds information about the health status of the person, there were an interest in automatically assessing a person health by analyzing the face. Many works are inspired by traditional Chinese medicine. Automatic pain detection, which is useful for elderly people surveillance, has been the subject of many studies [8]. Researchers have also estimated the heart rate from face videos by inspecting the change in the face color [70].

## 2.3 Generic face analysis framework

We distinguish two different stages in building a face analysis system: the training stage (Fig. 2-1), where the system is built, tested and optimized, and the operational stage (Fig. 2-2), where the system is deployed in a targeted environment to fulfill the desired application.

The process of face analysis starts by capturing the face using a sensor (e.g., camera, depth camera). Then, the face needs to be located within the captured image. This step is called face detection (or localization). In case of video data, the detected face can be tracked along the video sequence. Once detected, the face region is segmented from the image and forwarded to the next component. In the preprocessing step, the face image undergoes a number of treatments in order to enhance it and to mitigate different artifacts. Usually, this step involves photometric and geometric normalizations. Next, a feature extraction method is applied to characterize the face in a distinguishable way. A mathematical model is afterward built for the extracted descriptors, where the aim is to categorize the descriptors in a specific class depending on the face analysis task being performed. In the training step, the specific parameters of each component of the system are optimized on a given database according to certain performance metric. The output of the training stage are the models and the optimal parameters for the whole system components.

In the operational stage (Fig.2-2), the system captures new instances of faces which are submitted to face detection, preprocessing and description components successively. All these three steps are executed with the optimal parameters obtained at the training stage. Once the face features are extracted, they are matched to the trained models and attributed to the most likely class the input face may belong to. According to the performed face analysis task, the output of the system this time is the predicted class.

More technical details on the framework components is provided in the following subsections.



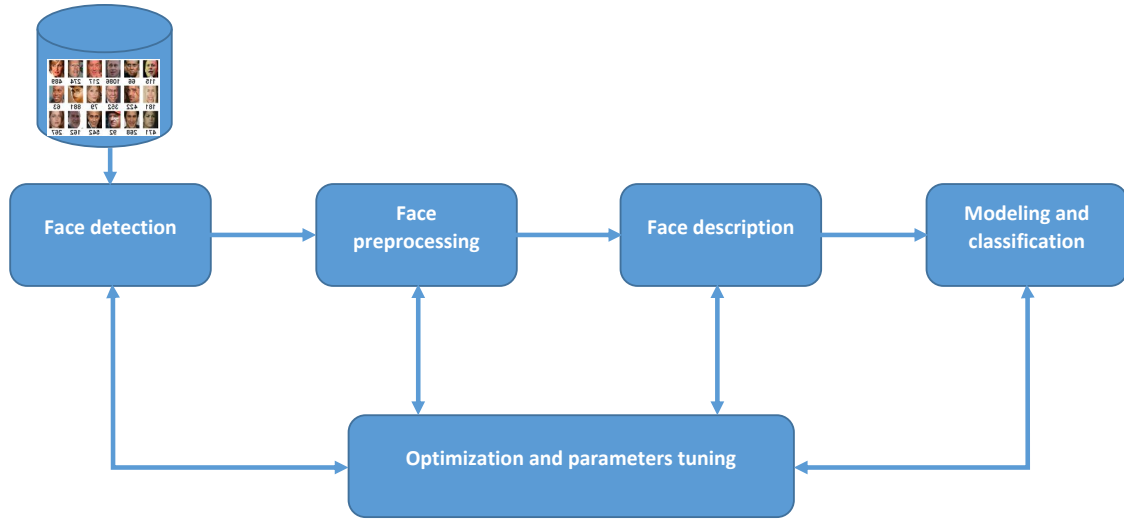


Figure 2-1: Training phase of face analysis system.

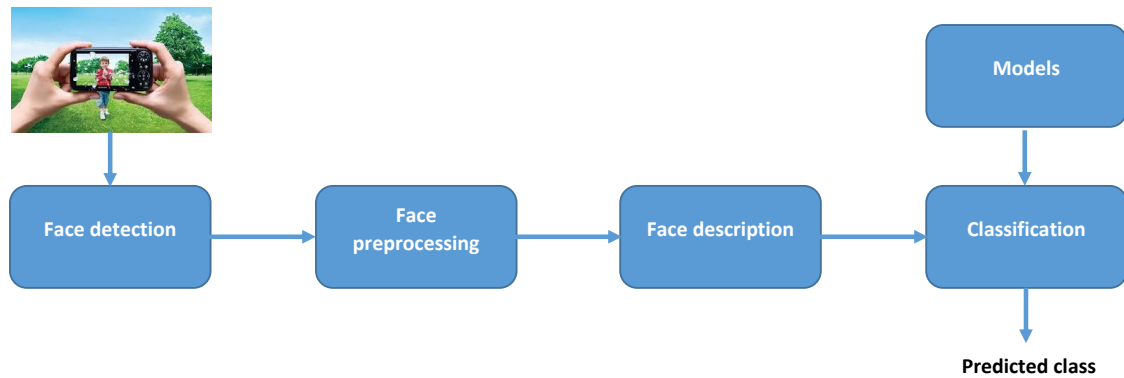


Figure 2-2: Operational phase of face analysis system.

### 2.3.1 Face detection and tracking

Face detection [126, 124] knew a tremendous progress during the past years thanks to the availability of in-the-wild data (i.e. faces captured in unconstrained conditions), collected from the Internet, with its publicly available benchmarking and the development of robust computer vision algorithms. The goal of face detection is to predict whether or not an image contains one or more human faces. The face detection algorithm returns the rectangles indicating the location of each detected face in the image (see Fig. 2-3). Yang et al [124] categorized the various face detection methods

into four groups: i) knowledge-based methods use pre-defined rules based on human knowledge in order to detect a face; ii) feature invariant approaches aim to find face structure features that are robust to pose and lighting variations; iii) template matching methods use pre-stored face templates to locate a human face in an image; and iv) appearance based methods learn face models from a set of representative training face images which are used for face detection.



Figure 2-3: Illustration of face detection.

The Viola-Jones face detector [114] is considered as the most inspiring method for face detection. The detector is based on three main ideas that make it powerful and running in real time. The first concept is the use of integral image or summed area table algorithm, which quickly and efficiently computes the sum of values in a rectangle, for rapid computation of Haar-like features. The second technique is the classifier learning with AdaBoost, which is a method for building highly accurate classifier by combining many weak ones, each with moderate accuracy. Finally, the third idea is the attentional cascade structure, where sub-windows of the image undergo a series of weak classifiers that reject the majority of negative sub-windows making the detection extremely fast. Viola and Jones method made face detection practically feasible in real-world applications and today it is widely implemented in digital cameras and photo software.

Another important face detection algorithm is the so-called deformable parts-based model (DPM) or pictorial structures model [43]. DPM qualitatively describes the visual appearance of an object. Its basic idea is to represent an object by a collection of parts organized in a deformable configuration. The appearance of each part of the object is modeled separately and the deformable configuration is represented by connections between the pairs of parts. One way of implementing DPM is to describe the pictorial structure of objects via an undirected graph. In the case of face, the set of graph vertices correspond to facial parts, and the set of edges indicates the connection between facial parts. The parts may correspond to semantically meaningful facial landmarks (such as mouth, nose, eyes, etc.) or can be automatically learned through training examples. The major drawback of DPM models is their high computational complexity.

In the case of face analysis from video, it is important to keep the trace of a face, previously located with a face detector in a given frame, along the next frames until it disappears from the scene. Face tracking algorithms employ both spatial and motion information in sequences of frames to continuously follow the movements of previously detected faces. Face tracking algorithms are mainly divided into two categories. The first one is feature-based tracking, which matches local interest-points between successive frames and updates the tracking parameters. An example of this first category is the 3D deformable face tracking [129]. The second category is appearance-based approach, which tracks faces by matching a statistical model of face appearance to the image. Examples of this category include 2D Active Appearance Models (AAM) [31].

### **2.3.2 Face description**

The literature overview reveals a plethora of face descriptors that have been investigated for various face analysis tasks. There are several ways to categorize different face description approaches [69]. One of the most widely used divisions is to distinguish whether the method is based on representing the feature statistics of small local face patches (i.e. local) or computing features directly from the entire image or video

(i.e. global or holistic).

Typical holistic features include subspace methods, which project the data into a low dimensional space, such as the Eigenfaces [113] and Fisherfaces [12]. The former approach is based on Principal Component Analysis (PCA), which aims to represent the data by minimizing its reconstruction error. The PCA seeks a data representation in the orthogonal directions corresponding to the highest variances. The principal component axes are defined by the eigenvectors corresponding to the highest eigenvalues of the covariance matrix of the face data. The face data is projected into the subspace spanned by these directions. The latter approach is based on Linear Discriminant Analysis (LDA), which seeks discriminant features subspace by taking into account the data classes. LDA finds a subspace in which the within class variability is minimized and the between class variability is maximized. To handle the nonlinear nature of face data, PCA and LDA have been extended [104, 123] by applying a nonlinear mapping, using some kernel functions, of the input data to a new space.

Among the popular and successful state-of-the-art local face descriptors are Scale Invariant Feature Transform (SIFT) [74], Histograms of oriented Gradients (HoG) [32], Gabor wavelets [73], Local Binary Patterns (LBP) [88], etc. Generally, these features characterize the information around a set of points or from face regions (see Fig. 2-4) then aggregate the features in a vector by the means of some methods such as histograms and bag of features [87]. The local methods have proved to be more effective in real world conditions given their ability to handle small changes in local face areas. However, the global methods have been employed to complement the local descriptors giving a third feature category termed hybrid features.

### **2.3.3 Face modeling and classification**

The classifiers that have been investigated for different face analysis tasks are far beyond the coverage of this part. However, in this section, we mention the most commonly used classifiers and face models, especially those which have made a remarkable advance in face analysis research. Firstly, the nearest neighbor classifier is

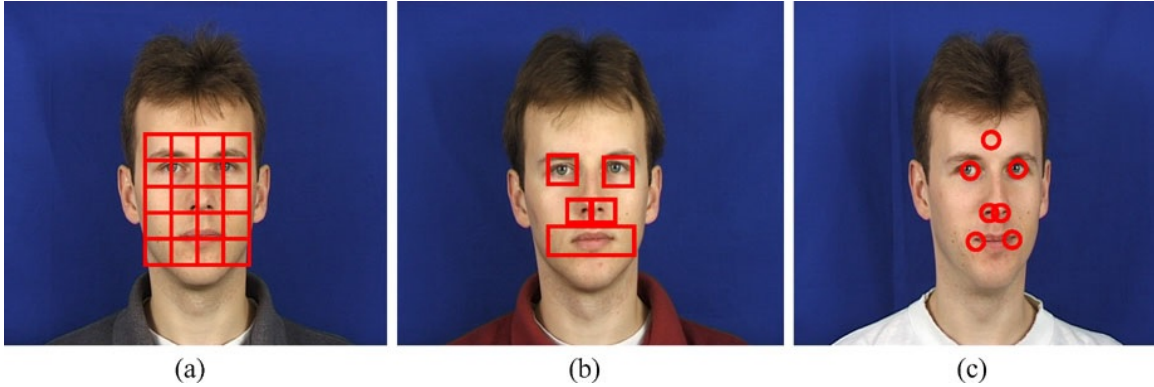


Figure 2-4: Different strategies for extracting local face features from: a) face grid, b) face regions, c) face landmarks [69].

commonly used for classifying similarities, usually computed with a distance function, between face feature vectors. The face sample to classify is attributed to the class with the nearest training samples. Support vector machines (SVM) are also among the most frequently used classifiers for face analysis. SVM builds optimal separating hyperplanes which maximizes the margin between different classes in high dimensional spaces. Other powerful classification tools are artificial neural networks, which automatically learn different classes based on a brain inspired process. The recent findings achieved by employing very deep neural network architectures highly impacted face analysis, thus making impressive advances [110, 107]. Recent face classification trends include the sparse representation classifier (SRC) [120] which represents a facial image as a linear combination of training images from the same class. The class of a given face is recovered by selecting the class corresponding to the smallest reconstruction error (i.e. sparsest representation).

Regarding models, the aim is to build a face model that is able to capture the face variations. A typical example is the elastic bunch graph matching approach [119], where the face is modeled as a graph with nodes are the face landmark points and edges are labeled with distances. The local regions around the landmarks are described with Gabor wavelets. Thus, the face geometry is encoded by the edges while the texture is encoded by the nodes. In order to account for variations, several face graphs are stacked so that all Gabor jets describing the same landmark point are

assembled together in a bunch. Graphs constructed by different combinations of the jets result in variations in different faces. A new face is matched by finding the landmark points that maximize a graph similarity function. Graph similarity is computed as the average of the best possible match between the new face and any face stored within the bunch and normalized with a topographical term which accounts for face distortion. Another successful face model is the 3D morphable model [14]. A 3D model, which encodes both face shape and texture, is first constructed from 3D face scans using computer graphics' techniques. To account for different face variations, the morphable model separates intrinsic parameters of the face from extrinsic imaging parameters. In order to match face images, the images are first parameterized in terms of the morphable model by fitting the model to the face images and similarity between the derived parameters is estimated. Other well established face models include statistical models such as hidden Markov models [102].

## 2.4 Challenges and remedies

Face analysis systems are trained with a limited number of face samples captured under certain conditions while in real life face undergoes huge intrinsic and extrinsic changes. Fig 2-5 illustrates some challenging face images captured in the wild. It is practically impossible to cover all the face variations in the training stage making the face analysis systems fail processing unseen faces with new variations. Furthermore, it has been demonstrated by literature studies [1] that variations (in terms of illumination, head pose, etc.) in different face images of the same person can be larger than variation of faces from different persons. Therefore, face analysis performance degrades remarkably in adverse environments. This section reviews the main challenges that hinder face analysis and refers to the main solutions proposed in the literature.

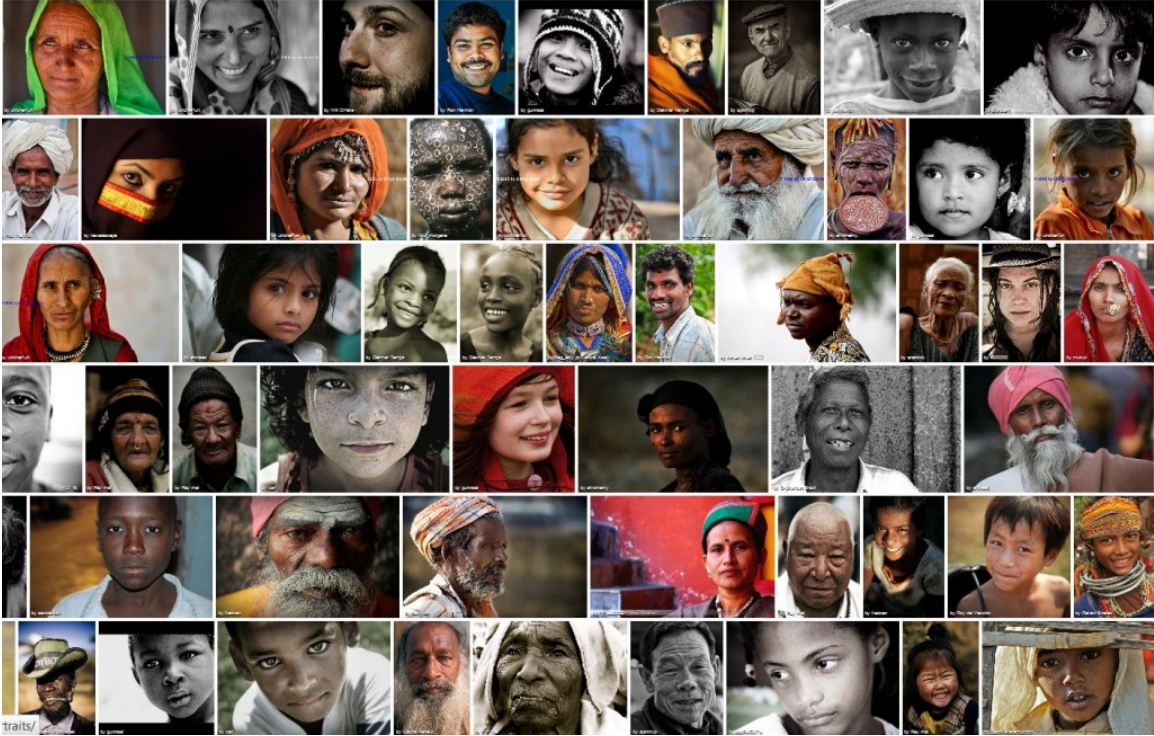


Figure 2-5: Examples of challenging face images.

### 2.4.1 Illumination

Illumination change in uncontrolled environments is one of the biggest challenges to face analysis. Even in controlled environments, illumination is still a big challenge to deal with. Face images are sensitive to the direction of lighting as well as the resultant pattern of shading that alter informative features and lead to fake contours. Specular reflections on eyes, teeth and wet skin are also a type of illumination to count for.

Photometric normalization techniques such as histogram equalization and gamma intensity correction are usually the first preprocessing steps to be applied to face images in order to compensate for face illumination. Among other literature solutions to the problem of illumination is the development of face descriptors robust to illumination change. However, the study by [1], which involved several relatively illumination-insensitive image representations under changes of viewpoint and illumination, demonstrated that no method is completely sufficient to address the problem.

Some researches resort to other sensing technologies which are less prone to illumi-

nation change than intensity images. Therefore, 3D sensors have been used to capture face range images which describe the depth of the scene objects. An alternative to 3D sensors is to reconstruct the face from 2D images by means of computer vision techniques and apply synthetic illumination to the 3D face model. Near infrared (NIR) sensors have also been investigated to overcome the face illumination problem. Thermal imaging is another sensing technology for handling face illumination change. Both NIR and thermal images are inherently less sensitive to illumination change however the former is less efficient in outdoor strong NIR illumination conditions while the latter is affected by the temperature change and opaque to eye glasses.

### **2.4.2 Head pose and viewpoint change**

3D faces, either collected by 3D scanners or reconstructed from 2D images, are useful for dealing with head poses and viewpoint changes. Many approaches for head pose estimation have been proposed in the literature [85]. Once the pose is estimated, the head can be rotated to a normalized position (very often a frontal pose) and the face is further analyzed. One can also deal with head pose by either building a face model from face images of the same individual but with different head orientations [48] or by building separate view-based models for the same face [93]. The pose can also be corrected by fitting a 3D morphable model [14] to the image then generating frontal view of the face. The fitting is achieved based on face landmark correspondence between the 3D model and the face image. This correspondence requires an automatic detection of facial points in the 2D images.

### **2.4.3 Occlusion**

Face analysis in uncontrolled situations is very difficult because of uncooperative users. In face recognition for example, the uncooperative subjects try to fool the system by intentionally disguising. The face or parts of it may be covered using sunglasses, scarf, hat, fake face hair, etc. Many researchers attempted to handle such situations by proposing approaches that are robust to partial face occlusion.



Subspace methods have been used to project the face into a new space and discard the occluded parts. Local face descriptors are shown to be more robust to partial face occlusion than the holistic approaches. Faces are usually partitioned into small blocks and each block is modeled separately. Since, the corresponding blocks are matched, only blocks spanning the occlusion will be affected. The sparse representation [120] has been found to cope well with occlusions. Some other methods [117] attempted to reconstruct the occluded face parts, while others (e.g., [84, 111]) detect the occlusion and use only non-occluded parts for face analysis.

## 2.5 Summary

In this chapter, we presented an overview of automatic face analysis. We discussed some exciting applications and attractive motivations for the continuous research in this topic. The generic face analysis flowchart is depicted and its components are explained. We have also enumerated a number of practical challenges that restrain the face analysis problems. Throughout the chapter, the main milestones that marked the history of face analysis are briefly presented.

The chapter is intended to provide understanding of automatic face analysis concepts pointing out the main state of the art breakthroughs. Literature works, which are close and directly related to our work, will be presented with technical details in the corresponding chapters of the thesis.



# Chapter 3

## Face verification

Biometric systems can run into two fundamentally distinct modes: (i) verification (or authentication) and (ii) recognition (more popularly known as identification). In the former mode, the system aims to confirm or deny the identity claimed by a person (one-to-one matching) while in latter mode the system aims to identify an individual from a database (one-to-many matching). Because of its natural and non-intrusive interaction, identity verification and recognition using facial information is among the most active and challenging areas in computer vision research [69]. However, despite the achieved progress during the recent decades, face biometrics [68] (that is identifying individuals based on their face information) is still a major area of research. Particularly, wide range of viewpoints, aging of subjects and complex outdoor lighting are still challenges in face recognition.

The recent developments in face analysis and recognition have shown that the local binary patterns (LBP) [88] provide excellent results in representing faces [2, 95]. LBP is a gray-scale invariant texture operator which labels the pixels of an image by thresholding the neighborhood of each pixel with the value of the center pixel and considers the result as a binary number. LBP labels can be regarded as local primitives such as curved edges, spots, flat areas etc. The histogram of the labels can be then used as a face descriptor. Due to its discriminative power and computational simplicity, the LBP methodology has attained an established position in face analysis and has inspired plenty of new research on related methods. In the same context,

we present in this chapter a couple of different LBP variants to address the face verification problem.

The rest of the chapter is organized as follows. Section 3.2 describes the original LBP operator and Section 3.3 explains LBP scheme for face recognition. In Section 3.4, our first proposed approach for efficient and compact LBP representation overcoming LBP drawbacks (i.e. sparse and unstable histograms) is introduced. Section 3.5 presents the second proposed approach for robust LBP feature vector estimation. Experimental evaluation is presented in Section 3.6 and conclusions are drawn in Section 3.7.

### 3.1 Motivations and approach overview

The original LBP has some limitations that need to be addressed in order to increase its robustness and discriminative power and to make the operator suitable for the needs of different types of problems. The present thesis proposes new solutions that address inherent problems to the original LBP-based face verification system. One problem with the LBP method, for instance, is the number of entries in the LBP histograms as a too small number of bins would fail to provide enough discriminative information about the face appearance while a too large number of bins may lead to sparse and unstable histograms. To overcome this drawback, we propose an efficient and compact LBP representation for face verification. The face is first divided into several regions from which LBP features are extracted. LBP codes in each region are then quantified into a low-dimensional feature vector. The face is represented by concatenating the vectors from all the regions. We generate reliable face model using vector quantization maximum *a posteriori* adaptation (VQMAP) method [19]. For face verification, we use the mean squared error (MSE) to match a test feature vector to the claimed user model.

Another drawback of the LBP method lays in the feature vector robustness as the histogram estimation is not always reliable. We tackle this problem by first estimating a reliable generic feature vector obtained from a pool of users. Face images are divided

into equal blocks from which LBP features are extracted and LBP histograms over blocks are concatenated to form a feature vector [20]. The adapted histogram of a given block is obtained by weighting its histogram and the generic block one. The Chi-square ( $\chi^2$ ) distance is used to match a probe against the claimed identity model. To compensate the cohort effect introduced by the generic feature vector, we finally normalize the obtained score by subtracting the distance between the probe and the generic feature vectors.

We extensively evaluate our two proposed approaches as well as their fusion on two publicly available benchmark databases, namely XM2VTS and BANCA. We compare our obtained results against not only those of the original LBP approach but also those of other LBP variants, demonstrating very encouraging performance.

## 3.2 The local binary patterns

The LBP operator has been first introduced in [88] as a texture analysis approach. It is defined as a gray-scale invariant texture measure, derived from the image appearance in a local neighborhood of the pixel. It has been shown to be a powerful means of texture description thanks to its properties in real-world applications, such as discriminative power, computational simplicity and tolerance against monotonic gray-scale changes.

The original LBP operator forms labels for the image pixels by thresholding the  $3 \times 3$  neighborhood of each pixel with the center value and considering the result as a binary number. Fig. 3-1 shows an example of an LBP calculation. The histogram of these  $2^8 = 256$  different labels can then be used as the image descriptor.

The operator has been extended to use neighborhoods of different sizes. Using a circular neighborhood and bilinearly interpolating values at non-integer pixel coordinates allow any radius and number of pixels in the neighborhood. The notation  $(P, R)$  is generally used for pixel neighborhoods to refer to  $P$  sampling points on a circle of radius  $R$ . The calculation of the LBP codes can be easily done in a single

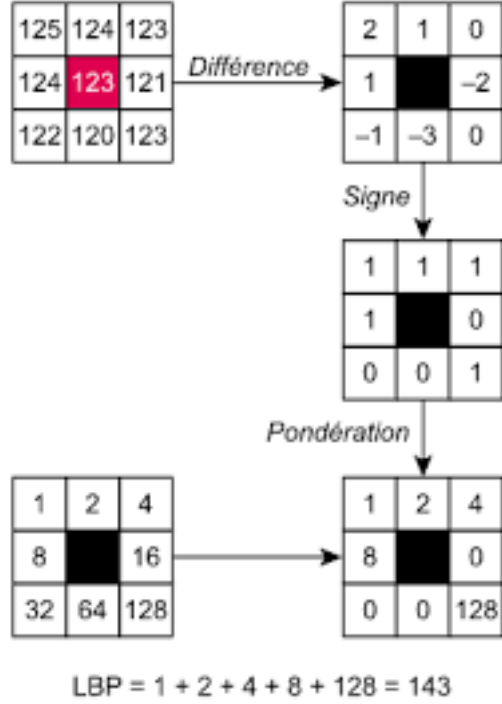


Figure 3-1: The basic LBP operator.

scan through the image. The value of the LBP code of a pixel  $(x_c, y_c)$  is given by:

$$LBP_{P,R} = \sum_{p=0}^{P-1} s(g_p - g_c)2^p, \quad (3.1)$$

where  $g_c$  corresponds to the gray value of the center pixel  $(x_c, y_c)$ ,  $g_p$  refers to gray values of  $P$  equally spaced pixels on a circle of radius  $R$ , and  $s$  defines a thresholding function as follows:

$$s(x) = \begin{cases} 1, & \text{if } x \geq 0; \\ 0, & \text{otherwise.} \end{cases} \quad (3.2)$$

Another important extension to the original operator is the definition of the so called *uniform patterns*. This extension was inspired by the fact that some binary patterns occur more commonly in texture images than others. A local binary pattern is called uniform if the binary pattern contains at most two bitwise transitions from 0 to 1 or vice versa when the bit pattern is traversed circularly. The number of different

labels in uniform patterns configuration is reduced to  $P(P - 1) + 3$ . For instance, the 58 different uniform patterns in  $LBP_{8,R}$  are depicted in Fig. 3-2. In the computation of the LBP labels, uniform patterns are used so that there is a separate label for each uniform pattern while all the non-uniform patterns are labeled with a single label. This yields to the following notation for the LBP operator:  $LBP_{P,R}^{u2}$ . The subscript indicate the use of the operator in a  $(P, R)$  neighborhood. Superscript  $u2$  stands for using only uniform patterns and labeling all remaining patterns with a single label.

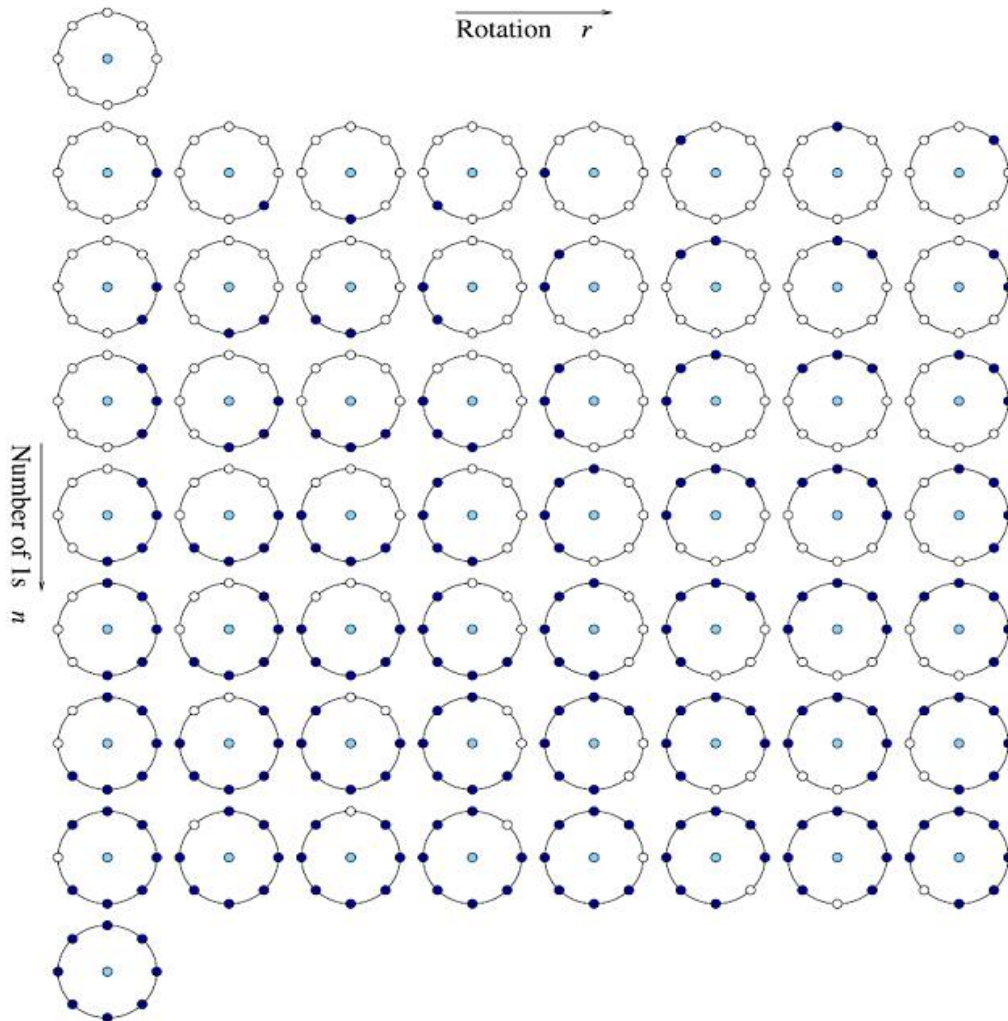


Figure 3-2: The uniform patterns in  $LBP_{8,R}$  configuration [95].

Each LBP label (or code) can be regarded as a micro-texton. Local primitives which are codified by these labels include different types of curved edges, spots, flat

areas, etc. Fig.3-3 illustrates some of the texture primitives detected by the LBP operator.

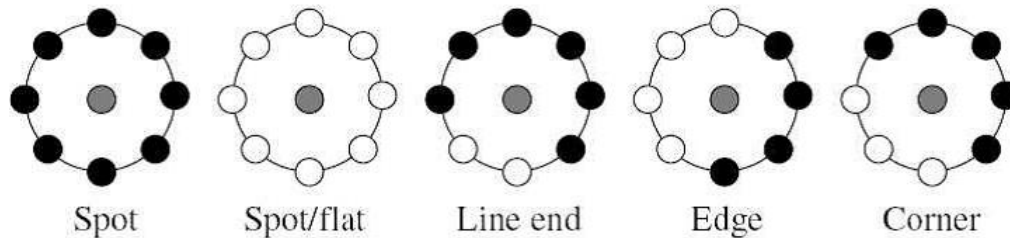


Figure 3-3: Some texture primitives detected by the LBP operator [95].

Since its introduction, LBP gave inspirations to wide range of variants as well as many new descriptors [55]. Furthermore, LBP has been successful in many computer vision problems [95, 21]. For instance, face analysis is one of the application where LBP had a considerable contribution in pushing the state of the art forward. The following section introduces the LBP-based face representation.

### 3.3 Face representation using LBP

In LBP-based approaches, an image is generally described using the histogram of the LBP codes composing the image. This histogram representation does not encompass the location information. Therefore, this representation is not suitable for face images as the face is a structured object, where the position of its parts (i.e., eyes, nose, mouth, etc.) is very important for matching between two facial images. In order to avoid facial spatial information loss, Ahonen et al.[2] subdivided the face images into several small blocks. Then, LBP feature is extracted from each block separately, building a per block local descriptor. The final face descriptor is obtained by combining all the local descriptors from the different blocks. This scheme is illustrated in Fig. 3-4.

The above face description overcome the limitations of the holistic representations. Indeed, it has been shown to be more robust to variations in pose and illumination



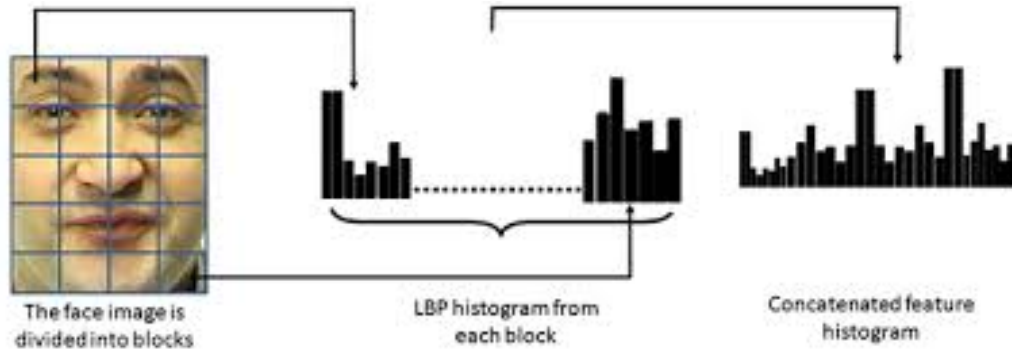


Figure 3-4: Face description using LBP.

than the holistic methods. Moreover, the histogram based face description effectively represents the face on three different locality levels: i) at pixel-level represented by the LBP labels forming the histogram bins, ii) regional level represented by the local histogram, and iii) a global level represented by the concatenation of the regional histograms.

In this original LBP based face representation and most of its variants, extracted histograms over different blocks are generally sparse. In other words, most of bins in the histogram are zero or near to zero, particularly in the case of small face blocks. Indeed, the number of LBP labels in a block depends on its size. On one hand, large blocks produce dense histograms that badly represent local face changes. On the other hand, small blocks are robust to local changes but create unreliable sparse histograms, as the number of histogram bins exceeds by far the number of LBP patterns in the block.

Another problem with LBP representation is that the number of bins in the histogram is function of the number of neighborhood sampling points  $P$ . Therefore, the number of histogram bins grows considerably when  $P$  increases (there are  $2^P$  bins in original LBP and  $P * (P - 1) + 3$  bins in uniform LBP). Hence, small neighborhood yields in compact but poor representation whereas large neighborhood produces huge and unreliable feature vectors. This problem is more serious in many LBP variants, for instance if the face blocks are overlapped, resulting in larger number of local histograms. Another example where the feature size counts is the multi-scale repre-

sentation is adopted [71, 98], in which  $P$  and  $R$  parameters are varied to generate diverse representations of the same block, and the resulting histograms are concatenated. This representation, known as over-complete LBP (OVLBP) [10], generates a very high dimensional feature vector.

Besides, inspecting face representation based on LBP reveals the fact that not all labels are always occurring in some face region. Labels with low occurrences can be considered as noise, produced by one bit transition in the LBP code, and thus are useless for characterizing the face region. Therefore, a block can be efficiently characterized by a more accurate low dimensional vector by discarding such patterns.

The aforementioned shortcomings of the LBP-based face representation lead us to ask the two following questions. The first question is: Is there a better representation than the histogram one that better exploits the LBP power? The second question is: How one can improve the histogram representation in order to overcome its weakness. In the following sections, we answer these two questions by proposing two approaches that deal with the raised problems.

## **3.4 Face verification using LBP and VQMAP**

This section introduces our first approach, which answers the first issue in LBP face representation. We propose an alternative representation instead of the histogram. Specifically, we apply vector quantization to LBP codes in order to derive a compact representation. Afterward, we model the resulting face feature vectors by the MAP paradigm.

### **3.4.1 LBP Quantization**

We apply vector quantification to the LBP codes of each block in the face. This allows to dynamically obtain a more accurate per face-block feature vector that represents the face region in a better way, where only significant patterns are taken into account. Patterns of each block in the face are clustered into a fixed number of groups and the face is represented by resulting codebook. Thus, only relevant LBP labels of a given

block will be represented while other labels, representing noise, are ignored. Fig. 3-5 compares the resulting feature vector using the histogram representation against the vector quantization. The histogram representation generates a high dimensional sparse feature whereas the vector quantization generates a low dimensional dense feature. The gain in terms of feature size proportionally increases with the number of the neighborhood pixels  $P$ . In this example, the size of the block feature vector is 59 and 243 for  $P = 8$  and  $P = 16$ , respectively in the histogram representation while only the VQ-LBP generates a vector of size 32 in both cases.

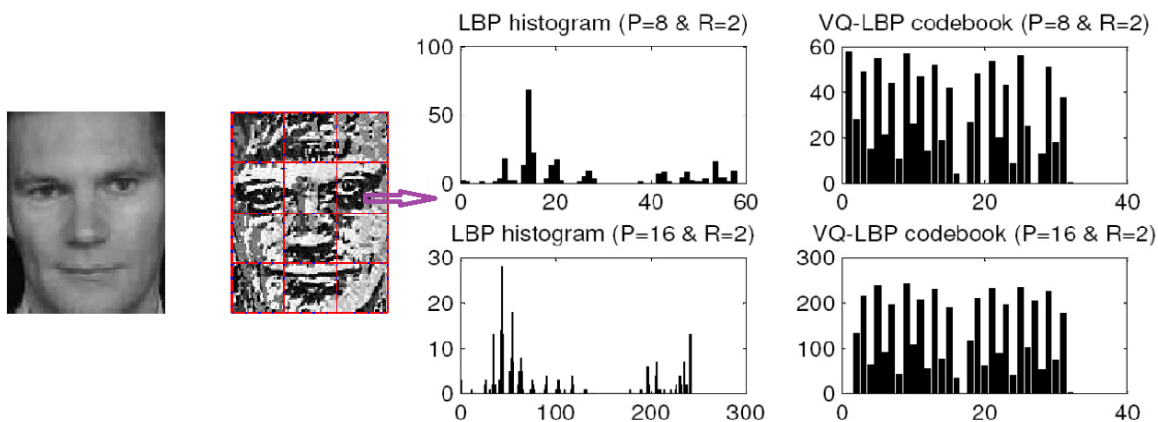


Figure 3-5: Face block description: LBP histogram against VQ-LBP codebook. The histograms are larger and sparse while the codebooks are dense and compact

In this approach, the clustering of LBP labels is achieved by LindeBuzoGray algorithm (LBG) [72]. LBG algorithm is similar to K-means [78] clustering method, which takes a set of vectors  $S = \{x_i \in R^d | i = 1, \dots, n\}$  as input and generates a representative subset of vectors  $C = \{c_j \in R^d | j = 1, \dots, K\}$ , called codebooks, with a specified  $K \ll n$  as output according to the similarity measure. In LBG the number of clusters is a power of two, i.e.  $K = 2^t, t \in N$ . The LBG algorithm is detailed below.

We note that in our case the input vectors are formed by the LBP codes of each face block, as shown in Fig.3-6, of all the training samples. The output of the algorithm is the codebook describing the face. Since LBP labels are discrete values of a defined interval, quantization process is fast, overcoming the main challenge of

---

**Algorithm 1** LBG algorithm

---

- 1: Input training vectors  $S = \{x_i \in R^d | i = 1, \dots, n\}$ .
  - 2: Initiate a codebook  $C = \{c_j \in R^d | j = 1, \dots, K\}$ .
  - 3: Set  $D_0 = 0$  and let  $k = 0$ .
  - 4: Classify the  $n$  training vectors into  $K$  clusters according to  $x_i \in S_q$  if  $\|x_i - c_q\|_p \leq \|x_i - c_j\|_p$  for  $j \neq q$ .
  - 5: Update cluster centers  $c_j, j = 1, \dots, K$  by  $c_j = \frac{1}{|S_j|} \sum_{x_i \in S_j} x_i$ .
  - 6: Set  $k \leftarrow k + 1$  and compute the distortion  $D_k = \sum_{j=1}^K \sum_{x_i \in S_j} \|x_i - c_q\|_p$ .
  - 7: If  $\frac{D_{k-1} - D_k}{D_k} > \epsilon$  (a small number), repeat steps 4 to 6.
  - 8: Output the codebook  $C = \{c_j \in R^d | j = 1, \dots, K\}$ .
- 

Vector Quantization (VQ) on huge continuous data.

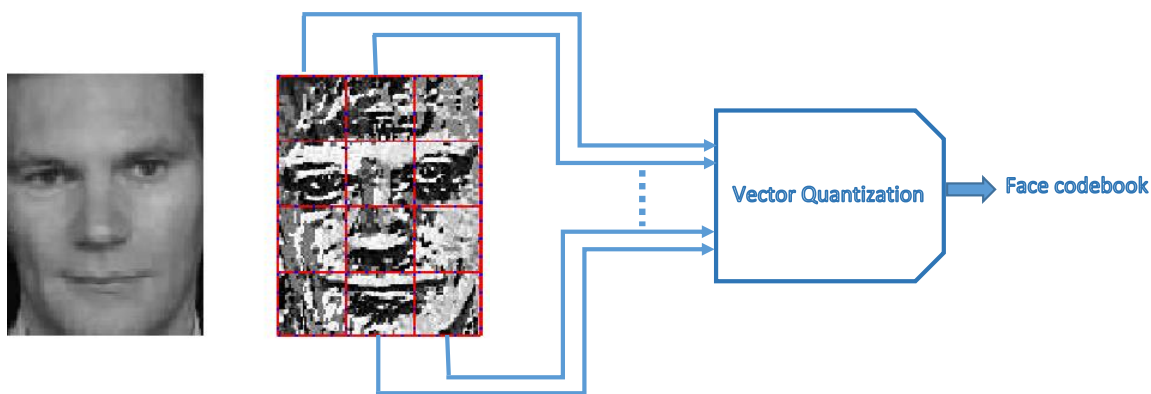


Figure 3-6: LBP-face quantization.

### 3.4.2 VQMAP model

We model faces by maximum *a posteriori* vector quantization (VQMAP) which has the advantage of generating reliable models, especially when only few enrollment faces per user are available.

VQMAP was first formulated by [51] and applied for speaker verification. It is a special case of the Gaussian mixture maximum *a posteriori* method (GMM-MAP) [99]. In this last model, Gaussian mixtures have three sets of parameters to be adapted: mean vectors (centroids), covariance matrices, and weights. VQMAP model is motivated by the fact that accurate models could be obtained by only adapt-

ing the mean vectors in the GMM-MAP approach [99]. By reducing the number of free parameters, the VQMAP model achieves much faster adaptation as well as simpler implementation. Moreover, the similarity computation for a given probe is further simplified by replacing the log likelihood ratio (LLR) computation by the mean squared error (MSE) [51]. Indeed, the speed gain in VQMAP originates mostly from the replacement of the Gaussian density computations with squared distance computations, leaving out the exponentiation and additional multiplications [51].

The main issue in the VQ approach is the estimation of the centroids modeling the face. Let the model parameters noted by  $\theta = (c_1^t, \dots, c_K^t)^t$  where  $c_i$  are the centroids and  $K$  is their number. This estimation has been formulated by MAP. Formally, MAP seeks the parameters  $\Theta$  that maximize the posterior probability density function (pdf):

$$\begin{aligned}\Theta_{MAP} &= \arg \max_{\Theta} P(\Theta/X) \\ &= \arg \max_{\Theta} P(X/\Theta)g(\Theta),\end{aligned}\tag{3.3}$$

where  $P(X/\Theta)$  is the likelihood of the training set  $X = \{x_1, \dots, x_N\}$  given the parameters  $\Theta$  and  $g(\Theta)$  is the prior pdf of the parameters.

The above formulation of VQMAP requires the definition of the likelihood function  $P(X/\Theta)$  as well as the prior distribution  $g(\Theta)$ . The likelihood pdf should take the fact that VQ is non probabilistic model based mean squared error (MSE) into account. Therefore, the likelihood has been modeled as a Gaussian mixture with identity covariances and the prior pdf is modeled by the probability of  $K$  independent Gaussians. The MAP estimates for Vector Quantization is then derived based on k-means algorithm. The detailed formulation and mathematical development of the VQMAP model is provided in Appendix A.

### 3.4.3 Face verification system

The proposed face verification system based on LBP features and VQMAP model is depicted in Fig. 3-7. In the training stage, a model is generated for each autho-

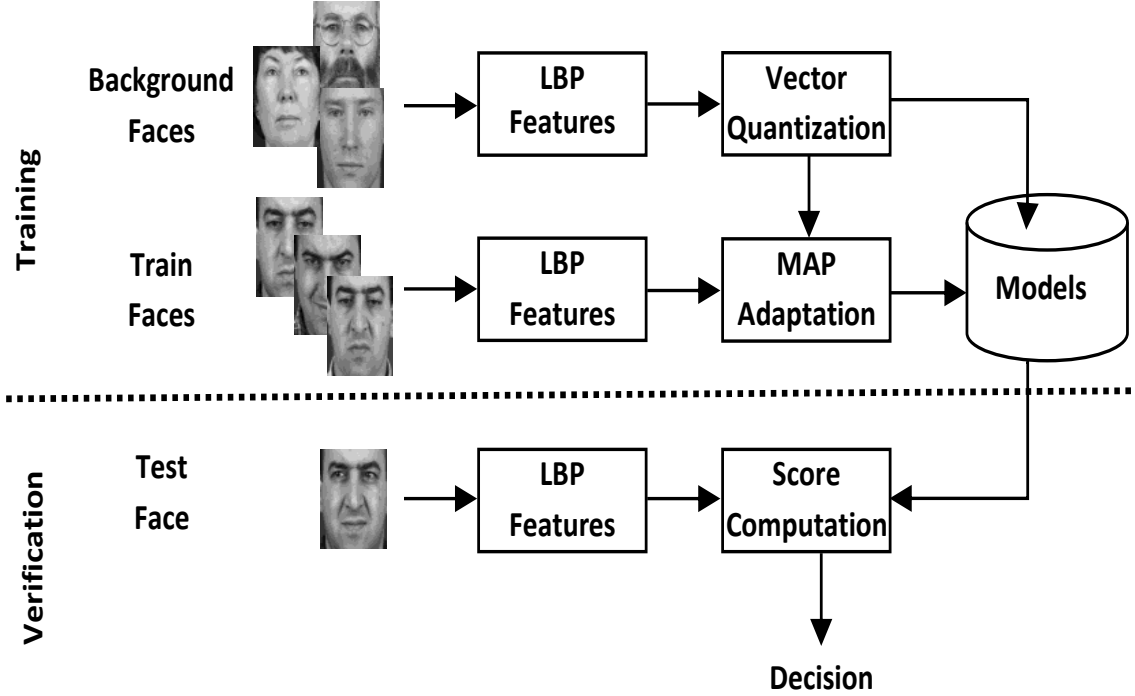


Figure 3-7: LBP-VQMAP face verification system.

alized user of the system. To generate a user model, a generic face model, called universal background model (UBM), is first created using a pool of training faces. After extracting LBP codes from each face, we divide the faces into blocks of equal size. Then, we run LBG algorithm considering together the set of blocks of the same position from all training faces. A codebook representing the background model is obtained. User specific model is then inferred from the global model by applying the MAP adaptation process using the training faces of the user.

In the verification stage, LBP features are extracted from the probe face  $F$  which is divided into blocks with the size set at the training phase. Then, for each block of the probe face, the closest UBM vectors are searched. For the face model, nearest neighbor search is performed on the corresponding adapted vectors only. The match score  $S$  is the difference between the UBM and the target  $C$  quantization errors [61]:

$$S = MSE(F, UBM) - MSE(F, C) \quad (3.4)$$

where:

$$MSE(X, Y) = \frac{1}{|X|} \sum_{x_i \in X} \min_{y_k \in Y} \|x_i - y_k\|^2 \quad (3.5)$$

where  $x_i$  and  $y_k$  are the elements of  $X$  and  $Y$ , respectively.

The resulting score is compared to the decision threshold set at the training phase to decide whether to accept the user as authentic or reject him/her as imposter.

### 3.5 Face verification using adapted LBP histograms

One of the reasons behind the success of LBP methods for face recognition is its simplicity and rapidity. This is mainly due to histogram representation of LBP codes. However, the histogram estimation may not be accurate in some cases, such as small changes in the image, lack of training samples or subdivision of low resolution faces into small boxes. For instance, Fig. 3-8 depicts LBP histogram of the same block (red box) from three images of a person taken in the same session under the same acquisition conditions. Although the three faces are very similar, at the LBP histogram level, noticeable differences could be perceived. In this section, we propose an elegant approach for coping with robust LBP histogram representation.

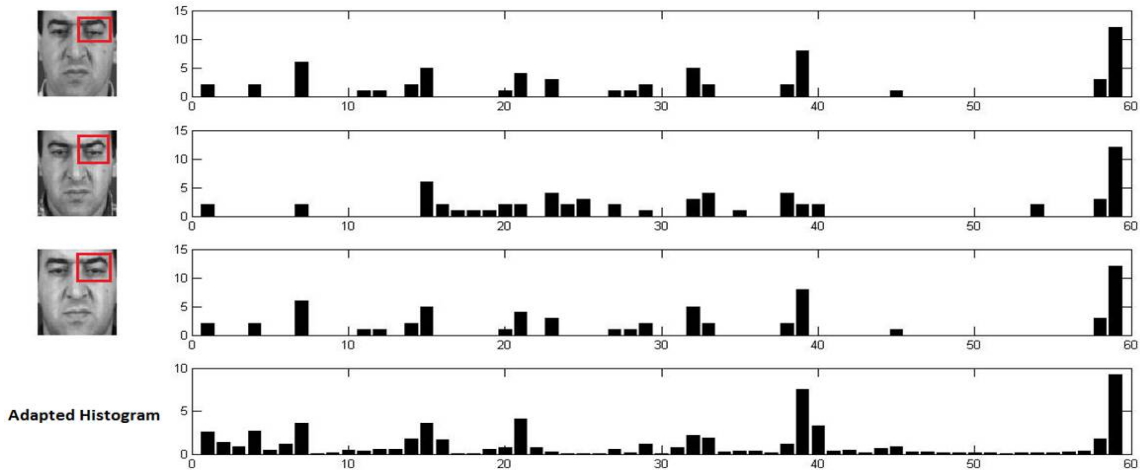


Figure 3-8: LBP histograms of the same block from three face images of a subject, taken in the same session, and their adapted histogram.

Since faces of different persons share some similarities, it is expected that some

LBP codes, which are representative of the face parts (nose, eyes, mouth, etc.), are common between different faces. Here, we make use of this intuition to enhance LBP histogram representation. Our proposed approach consists of creating a generic LBP histogram for each face block computed over the pool of the same region from several users faces. This generic histogram encloses characteristics from all trained users. The generic histogram is then adapted to each user. Hence, a face region is represented by a weighted sum of its LBP histogram and the corresponding generic histogram:

$$\widehat{H}_c^r(l_k) = \alpha H_w^r(l_k) + (1 - \alpha) H_c^r(l_k) \quad (3.6)$$

In Eq. 3.6,  $H_w^r$  denotes the generic histogram of block  $r$ .  $H_w^r$  is estimated using the LBP codes from all the blocks of the same position  $r$  in the world faces.  $H_c^r$  is the histogram of the face block  $r$  for client  $c$  and  $\alpha \in [0, 1]$  is a weighting factor that defines the contribution of each component to the final representation.  $l_k$  is the  $k^{th}$  bin in the histogram.

An example of the adapted histogram is shown in Fig. 3-8. The adapted histogram catches the important information represented by the highest bins in each of the three histograms of individual faces. However some extra bins, known as cohort effect, are introduced by the adaptation. We compensate the cohort effect at the score level.

The feature vector of a given face image is formed by concatenating the different blocks' adapted histograms. For each training face of a given user, we generate a separate feature vector. The score between a training feature vector  $\widehat{H}_c^k$  and a probe one  $H_p^k$  is computed by the  $\chi^2$  histogram similarity measure. In order to eliminate the cohort effect introduced by adapting the global model, we normalize the obtained score by subtracting the similarity between the probe and the generic feature vector (second term in (3.7)). Thus, the normalized score is given by:

$$S = \sum_k (\chi^2(H_p^k, \widehat{H}_c^k) - \chi^2(H_p^k, H_w^k)) \quad (3.7)$$



where

$$\chi^2(X, Y) = \sum_i \frac{(X(i) - Y(i))^2}{X(i) + Y(i)} \quad (3.8)$$

For each probe, the highest score to the claimed user train features is compared to a threshold to decide either to accept or to reject the authentication.

## 3.6 Experimental analysis

In this section, we use two publicly available benchmark databases, namely XM2VTS and BANCA, to evaluate the two proposed approaches, presented in Sections 3.4 and 3.5, and assess their performance. Moreover, we compare the two approaches and their fusion against some recent state-of-the-art methods.

### 3.6.1 Databases

#### XM2VTS

The XM2VTS database [81] contains face videos from 295 subjects. The database was collected in four different sessions separated by one month interval. In each session two videos for each subject of the database were recorded. A set of 200 training clients, 25 evaluation impostors and 70 test impostors contributed in collecting the database. Fig. 3-9 shows an example of one shot from each session for a subject in the XM2VTS database.



Figure 3-9: Example of XM2VTS face images of the same person across different sessions.

Two evaluation configurations, known as *Lausanne protocol configurations* (LPI & LPII), were defined with XM2VTS to assess the biometric systems performance in

verification mode. The two configurations are illustrated in Table 3.1. The database is divided into three subsets: train, evaluation and test. The training data serves for building clients models. Evaluation subset is used to tune system parameters. Finally, system performances are estimated on the test subset, using evaluation parameters. The difference between the two protocols, LPI and LPII, lays in the per-subject number of face samples in each subset and the session these samples are taken from.

Table 3.1: Partitioning of the XM2VTS database according to the two configurations.

Session	Shot	Configuration I			Configuration II		
		Clients	Imposters		Clients	Imposters	
1	1	Training	Evaluation	Test	Training	Evaluation	Test
	2	Evaluation					
2	1	Training					
	2	Evaluation					
3	1	Training					
	2	Evaluation					
4	1	Test					
	2		Test				

## BANCA

The BANCA database [9] contains 52 users (26 male and 26 female). Faces are collected through 12 different sessions with various acquisition devices of different quality and in different environment conditions: controlled (high-quality camera, uniform background, controlled lighting), degraded (web-cam, non-uniform background) and adverse (high-quality camera, arbitrary conditions). Examples of the three conditions are shown in Fig. 3-10. For each session, two videos are recorded: a true client access and an impostor attack.

In the BANCA protocol, seven distinct configurations for the training and testing policy have been defined. In our experiments, we consider the three configurations referred as Matched Controlled (MC), Unmatched Adverse (UA) and Pooled Test (P). As shown in Table 3.2, all of the considered configurations, use the same training conditions: each client is trained using images from the first recording session of the controlled scenario. Testing is then performed on images taken from the controlled



Figure 3-10: Example of BANCA face images from the three acquisition conditions : controlled (left), degraded (middle) and adverse (right).

scenario for MC test and adverse scenario for UA test, while P test is performed by pooling test data from different conditions. The database is divided into two groups, g1 and g2, containing the same number of subjects alternatively used for development and evaluation.

Table 3.2: Partitioning of Banca database for MC, UA and P configurations.

Session	Configuration		
	MC	UA	P
1	Train	Train	Train
2	Test		Test
3	Test		Test
4	Test		Test
5			
6			Test
7			Test
8			Test
9			
10		Test	Test
11		Test	Test
12		Test	Test

### 3.6.2 Setup

In the experiments, we use the same parameters for both databases. We cropped the faces using provided eye positions and resize them to  $80 \times 64$ . Faces are subdivided into equal blocks of  $8 \times 8$  pixels, yielding in 80 blocks per face. We note that no more preprocessing of face images was performed. We consider different LBP parameters

:  $(P, R) \in \{(8, 2), (16, 2), (24, 3)\}$ . Finally, for the sake of comparison, experiments with similar configuration are also carried out for the baseline LBP approach.

We assess the verification performance by the half total error rate (HTER) which is the mean of false acceptance rate (FAR) and false rejection rate (FRR) of the evaluation set :

$$HTER = \frac{FAR(\theta) + FRR(\theta)}{2} \quad (3.9)$$

The threshold  $\theta$  corresponds to the optimal operating point of the development set, defined by the minimal equal error rate (EER).

Finally, to compare different systems, we also draw the detection error trade-off (DET) curve, which plots the FAR vs. FRR and allows comparison at different operating points with an emphasis around the equal error rate (EER) region.

Table 3.3: HTER (%) on XM2VTS database using LPI and LPII protocols for different configurations of LBP baseline and our proposed methods.

Method	Parameters	Protocol	
		LPI	LPII
LBP Baseline	LBP(8,2)	3.0	2.2
Proposed approach 1: VQMAP		3.0	0.8
Proposed approach 2: AH		1.3	0.5
LBP Baseline	LBP(16,2)	2.9	2.0
Proposed approach 1: VQMAP		2.3	1.1
Proposed approach 2: AH		<b>1.2</b>	0.5
LBP Baseline	LBP(24,3)	3.9	2.9
Proposed approach 1: VQMAP		1.9	1.0
Proposed approach 2: AH		1.3	<b>0.3</b>

### 3.6.3 Results and discussion

We report in Tables 3.3 and 3.4 the results of the two proposed approaches as well as those of the baseline LBP system on XM2VTS and BANCA databases. These

results clearly show that the two proposed approaches outperform the original LBP approach in all configurations (i.e. for different parameters and different protocols).

In the VQMAP based approach, the performance gain can be explained by the fact that not all the information present in the baseline LBP representation is discriminative. Indeed, most of the bins in the baseline LBP histograms are close to zero and may represent noise. Hence, vector quantization produces discriminative feature vectors which contain most relevant LBP codes in the face.

In the approach based on the Adapted Histograms (AH), the information from concatenated generic histograms yields more discriminative feature vectors. The proposed normalization plays also an important role in the achieved results. The error rate of the approach based on the Adapted Histograms is nearly one-third of that of the baseline LBP on both databases and for most configurations.

In the experiments on XM2VTS database (Table 3.3), our two proposed approaches outperform the baseline LBP in all the configurations and for both protocols LPI and LPII. Moreover, the two approaches show more robustness to different challenges present in the BANCA database. In fact, they perform better than the baseline LBP in almost all the configurations (Table 3.4). We also note that the best HTERs for the considered protocols are obtained by our approaches.

We also performed a score level fusion of the two proposed approaches by first normalizing the scores using z-norm. Then we used logistic regression to fuse the two systems. The baseline LBP, our two approaches and their fusion systems are compared using the DET curve. Fig. 3-11 show the DET curve for the best configuration on the P protocol of BANCA database including faces from different acquisition conditions (controlled, degraded and adverse). The effectiveness of the proposed approaches over the baseline LBP method for different operating points is clearly shown in Fig. 3-11. Furthermore, the fusion of the two methods enhances the performance, indicating a relative complementary of the two approaches.

Finally, we compare in Table 3.5 our obtained results against those of some state-of-the-art counterpart on the challenging BANCA database. These results indicate that our proposed approaches show competitive results. In the scenario of controlled

Table 3.4: HTER (%) on BANCA database for MC, UA and P protocols using different configurations of LBP baseline and our proposed methods.

Method	Parameters	Protocol		
		MC	UA	P
LBP Baseline	LBP(8,2)	10.5	17.3	25.0
Proposed approach 1: VQMAP		4.0	<b>14.9</b>	16.6
Proposed approach 2: AH		4.2	16.4	<b>12.1</b>
LBP Baseline	LBP(16,2)	10.9	18.5	28.4
Proposed approach 1: VQMAP		3.8	18.8	20.7
Proposed approach 2: AH		<b>3.3</b>	15.8	12.1
LBP Baseline	LBP(24,3)	12.3	25.0	33.3
Proposed approach 1: VQMAP		4.8	18.2	20.4
Proposed approach 2: AH		3.7	17.5	12.6

acquisition conditions (MC) protocols, the best results are given by our adapted LBP histogram method. Furthermore, the fusion of the two proposed approaches yields in the best performance for MC, UA and P protocols. It is also worth noting that, in contrast to the other methods, our proposed approaches also inherit the simplicity and computational efficiency of the original LBP approach.

Table 3.5: HTER (%) for state of the art methods on BANCA database.

Method	Protocol		
	MC	UA	P
LBP Baseline [2]	10.5	17.3	25.0
LBP-MAP [100]	7.3	22.1	19.2
LBP-KDE [3]	4.3	18.1	17.6
Weighted LBP-KDE [3]	3.7	15.1	11.6
Proposed approach 1: VQMAP	3.8	14.9	16.6
Proposed approach 2: AH	3.3	15.8	12.1
Fusion VQMAP-AH	<b>3.3</b>	<b>14.4</b>	<b>11.6</b>

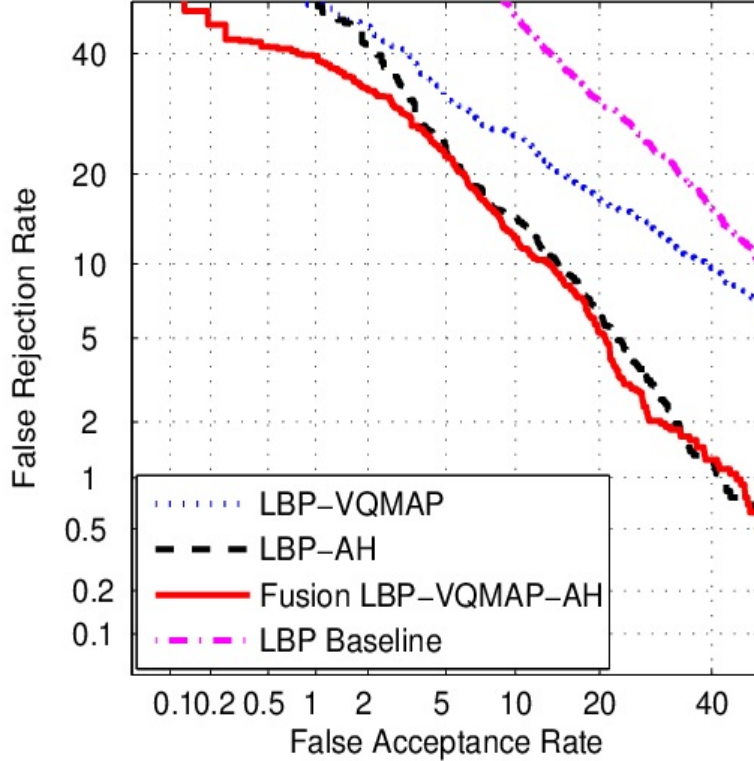


Figure 3-11: DET curve for baseline LBP, our two approaches (VQMAP and AH) and their fusion (VQMAP-AH) on BANCA database for the pooled protocol P.

### 3.7 Conclusion

In this chapter, we revisited the LBP-based face recognition scheme showing its weakness concerning the histogram representation of LBP codes. We presented two novel approaches to deal with the drawbacks of the original LBP-based face representation. The main advantage of the first method is the reduction of the feature vector length using vector quantization. Indeed, competitive results are obtained using very compact feature vectors. Furthermore, the robustness of the system is enhanced by using MAP adaptation to generate the face model.

The second method enhances the robustness of the LBP histograms by adaptation of generic histograms computed over a pool of users' faces. Adapted histograms of face regions are concatenated to form a reliable feature vector. Chi-square distance is used to match a probe face feature vector to the nearest claimed identity feature vector. The obtained similarity is normalized to compensate the cohort effect introduced by

the generic feature vector.

Furthermore, we performed a score level fusion of the two proposed methods using logistic regression after normalizing scores by z-norm. The fusion yields slightly enhanced performance. Compared to state-of-the-art, the error rates on XM2VTS and BANCA databases demonstrated the efficiency of the proposed approaches and their fusion.





# Chapter 4

## Face analysis from Kinect data

Analyzing faces under pose and illumination variations from 2D images is a complex task which can be better handled in 3D [35]. 3D face shapes can be acquired with high resolution 3D scanners. However, conventional 3D scanning devices are usually slow, expensive and large-sized, making them inconvenient for many practical applications. Therefore, assessing new 3D sensing technologies for face analysis applications is an extremely important topic given its direct impact on boosting the system robustness to common challenges.

Fortunately, the recently introduced low-cost depth sensors such as the Microsoft Kinect device allow direct extraction of 3D information, together with RGB color images. This provides new opportunities for computer vision in general and particularly face analysis research. Such sensors are a potential alternative to classical 3D scanners. Hence, low-cost depth sensing has recently attracted a significant attention in the vision research community [50, 6].

This chapter explores the usefulness of the depth images provided by the Microsoft Kinect sensors in different face analysis tasks. We conduct an in-depth study comparing the performance of the depth images provided by Microsoft Kinect sensors against RGB counterpart images in three face analysis tasks, namely identity, gender and ethnicity. Four local feature extraction methods are considered for encoding both face texture and shape: Local Binary Patterns (LBP) [88], Local Phase Quantization (LPQ) [4], Histogram of Oriented Gradients (HoG) [32] and Binarized Statistical

Image Features (BSIF) [60]. Extensive experiments are carried out on three publicly available Kinect face databases, namely FaceWarehouse [23], IIIT-D [47] and CurtinFaces [65].

The chapter is organized as follows. First, the Kinect sensor is briefly introduced in Section 4.1. Section 4.2 overviews the related literature work devoted to the use of Kinect depth images for automatic face analysis. Section 4.3 presents our methodology for studying the usefulness of Kinect depth images in different face analysis tasks. Section 4.4 describes the experiments and discusses the obtained results. Section 4.5 provides the conclusions.

## 4.1 Kinect sensors

The Microsoft Kinect sensor was first introduced in 2009 as a natural user interface of the Microsoft game console Xbox 360. Kinect captures both conventional RGB images and depth maps of the scene. The depth-sensing system is licensed from the PrimeSense Company and the exact technology behind it is still unrevealed. However, the depth computation is, most probably, based on the structured light principle. The depth sensing process is composed of an infrared (IR) projector, which emits an infrared irregular dot distribution, and an IR camera which captures the projected IR pattern to estimate the depth map. In addition to the RGB and depth sensing hardware, Kinect provides also an array of four microphones equipped with enhanced noise suppression capabilities, mainly aimed for voice command in games.

Due to its characteristics, Kinect is a good alternative to expensive high-quality 3D scanners. For instance, a comparison between Kinect and Minolta VIVID 910, used for collecting FRGC face database [94], is provided in Table 4.1 and Fig.4-1. The advantages provided by Kinect in terms of size, weight and price are obvious. However, on the other hand the quality of the 3D scans is very low compared to that provided by existing 3D scanners.

The Kinect sensor provides both color and depth videos as  $640 \times 480$  pixel resolution at 30 fps. However, the Kinect depth data is very noisy and the distance



Figure 4-1: Comparing face images acquired with Minolta VIVID 910 scanner (left) against Kinect (right).

computation of far objects often fails. The maximum distance that can be detected is 4.5 meters. Recently, a more accurate version of the device, namely Kinect 2, has been released. The new Kinect has higher color and depth resolution and can sense far away objects (up to 8 meters) more accurately.

There exist other Kinect-like devices such as Asus Xtion PRO LIVE <sup>1</sup> and Leap Motion <sup>2</sup>. The former is practically similar to Kinect and provides the same functionalities while the latter is a smaller device intended to track the hand gestures. The 3D sensing technology is being embedded in mobile devices, such as Google Tango <sup>3</sup>,

---

<sup>1</sup>[http://www.asus.com/Multimedia/Xtion\\_PRO\\_LIVE/](http://www.asus.com/Multimedia/Xtion_PRO_LIVE/)

<sup>2</sup><https://www.leapmotion.com/>

<sup>3</sup><https://www.google.com/atap/project-tango/>

Table 4.1: Comparing Kinect and Minolta VIVID 910 3D scanning devices.

Device	Kinect	Minolta VIVID 910
Size	$7.3cm \times 28.3cm \times 7.28cm$	$21.3cm \times 41.3cm \times 27.1cm$
Weight	564.5 g	11 Kg
Speed	0.033s	2.5s
Price	< 200 \$	> 50K \$
Color resolution	$640 \times 480$	$640 \times 480$
Depth resolution	$320 \times 240$	$640 \times 480$
Range	0.8 ~ 4 m	0.6 ~ 2.5 m

opening new horizons for wider applications. Similarly to Kinect, these devices are mainly intended for natural user interface applications.

## 4.2 Review of works using Kinect for face analysis

The facial depth images provided by Kinect-like low-cost sensors are unfortunately currently of low-resolution and noisy. This can be due, for instance, to missing data (holes) in some parts of the face, inaccurate depth value computation and limited distance coverage from the sensor (2 to 4 meters). Despite these challenges, many researchers have recently explored Kinect depth images for different facial analysis tasks. The Kinect sensor has been used for face detection and tracking and head pose estimation as well as for inferring and classifying facial information. The face recognition problem is the most studied task while there exist few work dealing with gender and expression recognition. Other use of Kinect includes facial modeling and animation for games and human-computer interaction applications. In the following we review the literature works which utilized Kinect facial images for various applications.

### 4.2.1 Face detection and tracking, pose estimation

As a crucial preprocessing step for various face analysis tasks, Kinect has been used for face detection and segmentation, head pose estimation and normalization and face tracking. Some work make use of depth maps only while others combine both

RGB and depth data. Among the work relying on depth data only, Fanelli et al. [40] presented a system for real time head localization and head pose estimation. The authors extended the random regression forest [38] to classify depth image patches between the head and the rest of the body. Then, a regression is performed in the continuous spaces of head positions and orientations. Experiments on BIWI Kinect head pose database [39] demonstrated good performance as well as robustness to occlusion. In another work, Padeleris et al. [90] rendered auxiliary range images of the reconstructed head from candidate poses and attempted to find the most similar to a reference view obtained at initialization. They formulated the head pose estimation as an optimization problem that quantifies the divergence of the depth measurements between the rendered views and the reference one. Li et al. [67] performed head tracking using iterative closest point (ICP) algorithm by registering a dense face template to depth data captured by Kinect. Niese et al. [86] also fitted a user specific face model with ICP algorithm to determine the head pose. Cao and Lu [24] detected and cropped the head from depth images for fatigue detection application. They split the depth image into different regions, extracted the contour of each region, and then used ellipse fitting algorithm to fit the contour points. The detected head is the region with the lowest fitness cost.

On the other hand, combination of color and depth information for face detection and tracking and head pose estimation has been proven to achieve more robustness than using the two modalities separately. For instance, in order to accelerate face detection, Duc et al. [36] used the depth information from the Microsoft Kinect to estimate the size of the face, thus they limited the range of candidate regions for face detection. They further applied depth-based skin segmentation by imposing geometric constraints, which improved the efficiency of finding human skin as well as reduced the computational cost. Zhang et al. [127] proposed an automatic face segmentation approach employing both color and depth cues. Skin color detection and depth constraint are used together to provide prior information. Given these priors, the segmentation is performed by the local spline regression and active learning framework. Tomari et al. [112] detected and tracked head pose with Kinect for social

robots navigation planning. Initially, possible human regions are segmented out and validated using depth and Hu moment features. Afterward, Haar-like features with the Adaboost classifier are employed to estimate potential head regions within the segmented areas. The obtained head regions are post-validated by examining their dimension and their probability of containing skin. The head pose estimation and tracking is performed by a boosted-based particle filter. Yang et al. [122] combined HoG features extracted from Kinect color and depth images for face detection and head pose estimation. First, they employed nine HoG filters (corresponding to different yaw and pitch angle intervals) trained with support vector machines (SVMs) to achieve a coarse face detection. Then, the detected face location is refined and a feed-forward multi-layer perception (MLP) network is trained to estimate face orientation. Jin et al. [59] used both color and depth acquired with Kinect for face detection, facial region segmentation and head pose estimation. In case of face detection with enough confidence, the head pose is employed to initialize the parameters of the AAM (active appearance model) algorithm [37]. The AAM algorithm, which usually uses the three RGB color channels, is extended to use the face depth information as well. Both face texture and depth are fitted to a model in order to locate the facial features. The authors claimed the ability of their approach to detect faces in presence of complex background and under severe head-pose variations as well as the ability to achieve more accurate facial landmark labeling compared to the traditional AAM algorithm. However, no details about the used experimental data and evaluation protocol were provided.

### **4.2.2 Face recognition**

As stated before, face recognition using Kinect depth images is the most investigated considered among face analysis problems. For instance, Pamplona et al. [91] addressed continuous authentication problem using 3D faces acquired with Kinect. Faces are first detected and normalized using ICP. According to its pose, each face is registered to one of the three positions: frontal, left profile or right profile. HoG features are extracted and matched to corresponding regions of interest (ROI). This

system was evaluated on four 40 minutes long videos with variations in facial expression, occlusion and pose, where an equal error rate of 0.8% was reported. Li et al. [66] tackled face recognition under pose, illumination, expression and disguise using the Kinect sensor. They proposed a preprocessing algorithm that generates a canonical frontal view for both depth map and texture of the face irrespective of its initial position. To this end, after face registration to a reference model, facial symmetry is employed to recover missing face parts, fill holes and smooth the face depth data. Sparse representation classifier (SRC) is used for both depth and texture separately. Evaluation of this system on CurtinFaces dataset [65] yields in 88.7% recognition rate using depth data only and 96.7% when face texture and depth are fused. Min et al. [83] used the PrimeSensor device for real time 3D face identification. To accelerate the processing and meet the real-time constraint, instead of registration to each gallery face, a probe face is registered to a few intermediate references (canonical faces) randomly selected from the gallery. Moreover, ICP algorithm was implemented on a GPU. Good identification results have been reported on a dataset of 20 people with average speed ranging from 0.04s to 0.38s, depending on the number of the canonical faces. However, the experimental analysis does not consider severe challenges like head pose, expression and illumination variations. Goswami et al. [46] proposed a Kinect based face recognition system, where the HoG descriptor is computed on the entropy of RGB-D faces and the saliency of RGB. A random decision forest classifier is used to establish the identity from the concatenation of five HoG descriptors. Ciacio et al. [29] handled the 3D head pose variation problem, by generating different rotated faces either from the probe or the target. The target consists of one frontal face per enrolled subject while the probes can be at any pose angle. For recognition, LBP and covariance matrices are separately used as features and fused after classification at score level. Experiments on faces with variations in six yaw angles demonstrated that using the rendered rotated faces from the target frontal face yields better results than other schemes. Mantecon et al. [80] proposed a face recognition system using the second version of Kinect which provides higher depth resolution. Inspired by LBP, they proposed depth local quantized pattern descriptor (DLQP)



which quantifies the difference between the depth value of a pixel and its neighboring ones. Only depth differences between -35 mm and 35 mm have been quantized as the most relevant depth values of human faces lie in this interval. To keep the DLQP descriptors with a reasonable size, depth differences are coded using 3 bits only. For classification, one-vs-all SVM is adopted. Experiments on HRRFaceD dataset [80] showed some improvements compared to SIFT and LBP features.

### 4.2.3 Gender and expression recognition

Other literature face classification problems studied from Kinect depth data include expression recognition and gender classification. Savran et al. [103] coped with 3D expression recognition using Kinect. Face detection from depth maps is first applied using the approach proposed in [38]. The detected region is transformed to point clouds and cropped to remove the non-facial points. Further, hole filling and noise smoothing is applied on the depth map images. Face is described using surface curvature descriptors computed on point cloud data. Using only Kinect 3D data, the authors obtained 77.4% accuracy in emotion valence detection. Fusing mean curvature features with luminance data boosted the accuracy to 89.4%. Expression recognition using Kinect depth maps has also been studied by Malawski et al. [79]. They used Kinect SDK to locate and track several face landmarks. Histograms of the slopes of line segments connecting the face landmark points are used as features. The best recognition accuracy, on images of 10 individuals with small variations in pose and illumination, was obtained using AdaBoost-based feature selection and SVM classifier.

On the other hand, gender classification using Kinect depth data has been addressed by Huynh et al. [56]. The depth differences are computed at each pixel along different orientations leading to a separate depth difference image corresponding to each orientation. Both depth differences and their signs, at each pixel and through different orientations, are encoded in the range of -8 to 7 in order to form a small sized feature vector, called Gradient-LBP. Evaluation on Eurecom Kinect dataset [56] demonstrated improvements outperforming LBP and 3DLBP features.

#### 4.2.4 Face modeling, reconstruction and animation

In other researches, which are less related to the present thesis, Kinect depth maps are used for modeling faces [106, 116, 26, 53, 82] for computer graphic applications. High resolution 3D faces are reconstructed from Kinect low resolution depth data and used for different applications. Examples of these applications include 3D video conference [5], personalized avatars [135], real-time facial animation [22, 118], etc.

#### 4.2.5 Discussion and contribution motivation

The analysis of the presented review highlights several remarks on the use of the depth maps of faces. Mostly, the depth data has been exploited to preprocess the face and to assist the RGB images based systems. Particularly, depth data has been used in head pose variation to normalize the face into a reference pose. Depth data is also helpful for face detection and segmentation especially in illumination variation situations.

Face description and classification from depth images is less investigated in the literature. While face recognition is the most relatively tackled problem from depth data, only a scarce number of research investigated expression and gender recognition problems. To the best of our knowledge, by the time of the review was being written, no research investigated the other face analysis problems from Kinect depth data including age estimation, ethnicity classification, emotion state, etc.

The review also points out the fact that face depth maps maybe either used solely or combined with RGB channels. However, one notes that there is a lack in comparing the performance of RGB images against depth maps in order to understand the benefits of using depth information.

Another important issue concerns the experimental data and evaluation benchmarks used by the reviewed researches. Most papers make use of private databases which are generally of small size containing a limited number of subjects and/or limited number of samples per subject. Moreover, data is often collected in laboratory environments where real-life challenges are not simulated. Even though few Kinect

face databases are made publically available (See our paper [18] for the detailed description of these databases), the test protocols frequently differ from a paper to another. All the mentioned concerns make the results biased, incomparable and hard to reproduce. These issues hinder the advance in this research topics.

Motivated by the previous limitations, we carry out a study of various face analysis tasks from both RGB images and depth maps. We employ different features to describe faces from both types of images. The best available Kinect face databases are used to evaluate the performances of the studied methods. We also compare depth maps against RGB image in all the study scenarios. The following section provides the details of the proposed framework for our study.

### **4.3 A framework for face analysis from Kinect data**

To gain insights into the usefulness of the depth images in different face analysis tasks, we carried out a comprehensive analysis comparing the performance of the depth images versus RGB counterparts in three face analysis tasks, namely identity, gender and ethnicity recognition, considering four local feature extraction methods. Extensive evaluation is performed on three publicly available benchmark databases. In this Section, we present our experimental framework comprising preprocessing, feature extraction methods and classifier.

#### **4.3.1 Preprocessing**

The depth images acquired by the Kinect sensor usually need to be pre-processed to overcome the noisy and low quality nature of the images. In our framework, the depth images are preprocessed as follows. First, the depth maps provided by Kinect are mapped into real world 3D coordinates. Thus, each pixel is represented by six values:  $x$ ,  $y$  and  $z$  coordinates and the three RGB values. Then, the resulted cloud of points  $C$  is translated so that the nose tip is located at the origin. This is achieved by subtracting the nose coordinates  $(x_{nose}, y_{nose}, z_{nose})$  from the all the points in the

cloud:

$$(x_t, y_t, z_t) = (x, y, z) - (x_{nose}, y_{nose}, z_{nose}), \forall (x, y, z) \in C. \quad (4.1)$$

The face region is extracted using an ellipsoid centered at the nose tip by discarding all the points outside the ellipsoid. Then, the face point cloud is smoothed and re-sampled to a grid of  $96 \times 96$ . Examples of cropped 2D and 3D face images are shown in Fig. 4-2. Finally, for the 3D face part, we drop the  $x$  and  $y$  coordinates and keep only the  $z$  coordinates for describing the face shape.



Figure 4-2: Examples of 2D cropped image (left) and corresponding 3D face image (right) obtained with the Microsoft Kinect sensor after preprocessing.

### 4.3.2 Feature extraction

After preprocessing, four facial local image descriptors are extracted from the depth and RGB images. In contrast to global face descriptors which compute features directly from the entire face image, local face descriptors representing the features in small local image patches have shown to be more effective in real world conditions [52]. The considered local face descriptors in our experiments are LBP, LPQ, HoG and BSIF. LBP and HoG are selected for their popularity in computer vision whereas LPQ and BSIF are recent descriptors which showed very promising results in different problems [7, 97]. To the best of our knowledge, BSIF has never been used to describe Kinect depth face data. While, LBP has been presented in the previous chapter, the description of the three remaining features is given bellow.

## Local Phase Quantization (LPQ)

LPQ was originally proposed for describing and classifying texture blurred images [89] then applied to face recognition from blurred images [4]. The LPQ descriptor bases on the robustness and high insensitivity of the low-frequency phase components to centrally symmetric blur. Therefore, the descriptor uses the phase information of short-term Fourier transform (STFT) locally computed on a window around each pixel of an image. Let  $N_x$  be the  $M^2$  neighborhoods of the pixel  $x$  and let  $f(x)$  be the image function at the bi-dimensional position  $x$ . The output of the STFT at the pixel  $x$  is given by:

$$F(x, u) = \sum_{y \in N_x} f(x - y) e^{-j2\pi u^T y} = W_u^T f_x, \quad (4.2)$$

where  $u$  indicates the bi-dimensional spatial frequency. In the LPQ descriptor, only four complex frequencies are considered:  $u_0 = (\alpha, 0)$ ,  $u_1 = (\alpha, \alpha)$ ,  $u_2 = (0, \alpha)$ ,  $u_3 = (-\alpha, -\alpha)$  where  $\alpha$  is a small scalar frequency ( $\alpha \ll 1$ ) ensuring the blur is centrally symmetric. Hence, each pixel of position  $x$  is characterized by a vector  $F_x$ :

$$\begin{aligned} F_x &= [Re\{F(x, u_0), F(x, u_1), F(x, u_2), F(x, u_3)\}, \\ &Im\{F(x, u_0), F(x, u_1), F(x, u_2), F(x, u_3)\}], \\ &= W f_x, \end{aligned} \quad (4.3)$$

where  $Re\{\cdot\}$  and  $Im\{\cdot\}$  denotes the real part and the imaginary part of a complex number.

In order to derive a binary code for the pixel  $x$ , the vector  $F_x$  needs to be quantized. To maximize the information preservation by the quantization, the coefficients should be statistically independent. Therefore, a de-correlation step, based on a whitening transform, is applied in LPQ before the quantization process. Assuming that the image function  $f(x)$  is a result of a Markov process with the correlation coefficient between two adjacent pixels is  $\rho$  and the variance of each sample is 1, the

covariance between two adjacent pixels  $x_i$  and  $x_j$  is

$$\sigma_{i,j} = \rho^{\|x_i - x_j\|}, \quad (4.4)$$

where  $\|\cdot\|$  denotes the  $L_2$  norm. Using these information, one computes the covariance matrix  $C$  of the  $M^2$  neighborhoods. Hence, the covariance matrix of the transform coefficient vector  $F_x$  can be obtained from:

$$D = WCW^T, \quad (4.5)$$

for  $\rho > 0$ ,  $D$  is not a diagonal matrix, meaning that the coefficients are correlating. Assuming Gaussian distribution, independence can be achieved using the following whitening transform:

$$G_x = V^T F_x, \quad (4.6)$$

where  $V$  is an orthonormal matrix derived from the singular value decomposition (SVD) of the matrix  $D$ , that is:

$$D = U\Sigma V^T. \quad (4.7)$$

$G_x$  is computed for all image positions and subsequently quantized using a simple scalar quantizer:

$$q_i = \begin{cases} 0 & \text{if } g_i < 0 \\ 1 & \text{otherwise} \end{cases}, \quad (4.8)$$

where  $g_i$  is the  $i$ th component of  $G_x$ . Finally, the resulting binary quantized coefficients are represented as integer value in  $[0-255]$  as follows:

$$LPQ(x) = \sum_{i=1}^8 q_i 2^{i-1}. \quad (4.9)$$

## Histogram of Oriented Gradients (HoG)

HoG [32] was initially developed for human detection but later extended and applied to many other computer vision problems. The basic idea behind HoG is that an object appearance and shape can be characterized by the distribution of local intensity gradients or edge directions. To compute the HoG descriptor of a given image  $I$ , the gradients are first obtained at each pixel by computing two 1D derivatives in both horizontal and vertical directions. This is corresponding to filtering the image with the two following filters:

$$D_x = \begin{bmatrix} -1 & 0 & -1 \end{bmatrix}, \quad (4.10)$$

$$D_y = \begin{bmatrix} 1 \\ 0 \\ -1 \end{bmatrix}, \quad (4.11)$$

thus, the  $x$  and  $y$  derivatives are obtained by the convolutions:

$$I_x = I * D_x, \quad (4.12)$$

and

$$I_y = I * D_y. \quad (4.13)$$

The magnitude and orientation of the gradient are then computed as follows:

$$|G| = \sqrt{I_x^2 + I_y^2}, \quad (4.14)$$

$$\theta = \arctan \frac{I_y}{I_x}. \quad (4.15)$$

The image is divided into small spatial regions called cells. The magnitudes of the gradient at each pixel of the cell are accumulated into a histogram according to

the gradient direction. This is equivalent to a weighted vote for an orientation-based histogram, where the weight is the value of the magnitude. In the original work [32], non-signed orientations have been found to perform better. Therefore, a histogram of  $B = 9$  bins (orientations) evenly spaced over 0 to 180 degrees was utilized. To prevent quantization artifacts due to small image changes, each pixel of the cell contributes to two adjacent bins by a fraction of the magnitude.

In order to cope with local changes of illumination and contrast, four adjacent cells ( $2 \times 2$ ) are grouped together forming one block. The blocks in an image are horizontally and vertically overlapped, by two cells in each direction, respectively. The four-cell histograms of each block are concatenated into a vector  $v$ , which is normalized by its Euclidean norm:

$$v_n = \frac{v}{\sqrt{\|v\|^2 + \epsilon}}, \quad (4.16)$$

where the small positive value  $\epsilon$  is added to prevent division by zero.

The final HoG feature vector is formed by concatenating all the normalized block features of the image. Finally, this feature is normalized again to count for the overall image contrast.

### **Binarized Statistical Image Features (BSIF)**

BSIF approach [60] is a relatively recent descriptor inspired by LBP. Instead of using hand-crafted filters, such as in LBP and LPQ, the idea behind BSIF is to automatically learn a fixed set of filters from a small set of natural images. The set of filters are derived based on statistics of training images. Given an image patch  $X$  of size  $l \times l$  pixels and a linear filter  $W_i$  of the same size, the filter response  $s_i$  is obtained by:

$$s_i = \sum_{u,v} W_i(u,v)X(u,v) = w_i^T x, \quad (4.17)$$

where  $w_i$  and  $x$  are vectors containing the pixels of  $W_i$  and  $X$ , respectively. A binary



code chain  $b$  is obtained by binarizing each response  $s_i$  as follows:

$$b_i = \begin{cases} 1, & \text{if } s_i \geq 0 \\ 0, & \text{otherwise} \end{cases}, \quad (4.18)$$

$b_i$  is the  $i$ th element of  $b$ . In the aim to learn a powerful set of filters  $W_i$ , the statistical independence of the responses  $s_i$  should be maximized. Let  $W$  be the matrix of size  $n \times l^2$  formed by stacking the  $n$  filters  $w_i$ . Independent filters estimation is achieved using independent component analysis (ICA). Therefore, one needs to decompose  $W$  into two parts so that the filters responses are rewritten as:

$$S = Wx = UVx = Uz, \quad (4.19)$$

where  $z = Vx$ , and  $U$  is a  $n \times n$  square matrix, and matrix  $V$  simultaneously performs the whitening and dimensionality reduction of training samples  $x$ . The randomly sampled training patches  $x$  are first normalized to zero mean and principal component analysis (PCA) is applied to reduce their dimension to  $n$ . Specifically, let  $C$  denote the covariance matrix of samples  $x$  and its eigen decomposition is  $C = B\Lambda B^T$ , the matrix  $V$  is defined as:

$$V = (\Lambda^{-1/2}B^T)_{1:n}, \quad (4.20)$$

where  $\Lambda$  contains the eigenvalues of  $C$  in descending order, and  $(\cdot)_{1:n}$  denotes the first  $n$  rows of the matrix in parenthesis.

Then, given the zero-mean whitened data samples  $z$ , one may use standard independent component analysis algorithm to estimate an orthoGonal matrix  $U$  which yields the independent components  $S$  of the training data. In other words, since  $z = U^{-1}S$ , the independent components allow to represent the data samples  $z$  as a linear superposition of the basis vectors defined by the columns of  $U^{-1}$ . Finally, the filter matrix  $W = UV$  is computed, which can be directly utilized for calculating BSIF features.

## Face description

Figure 4-3 depicts examples of results when applying the four selected local descriptors on face texture and depth images acquired with Kinect sensor for a subject from the FaceWarehouse database[23]. In our experiments, we extended the BSIF description method to handle depth images by learning the filters using facial depth images from the FRGC database [94] as training data. These filters are then used to compute BSIF features on Kinect depth images. We found this new learning approach yields in better filters, in terms of performances of face classification, than the original ones.

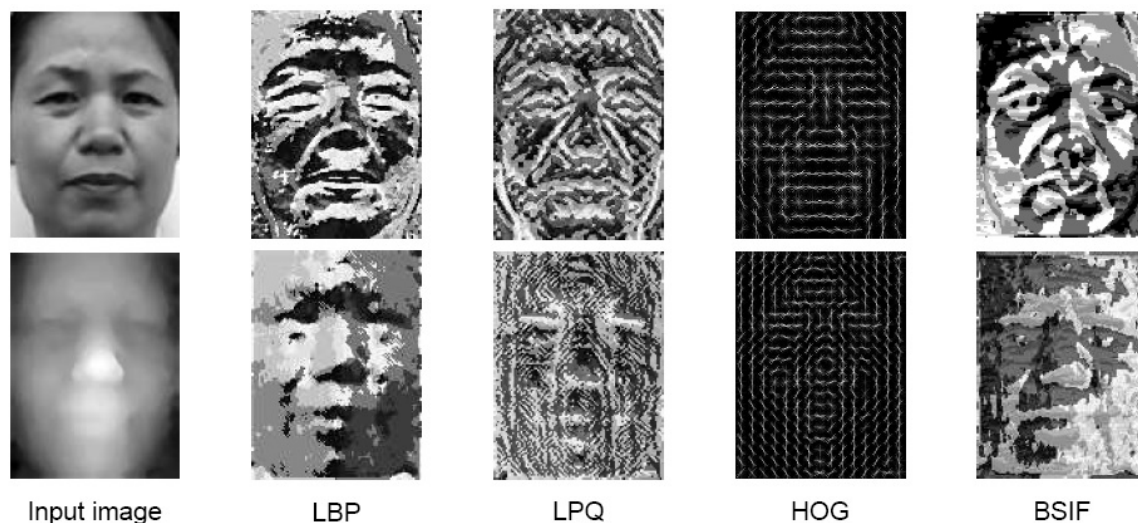


Figure 4-3: Examples of results after applying the four descriptors to face texture and depth images. From left to right: the original face image (top: texture image and bottom: its corresponding depth image) and the resulting images after the application of LBP, LPQ, HoG and BSIF descriptors, respectively.

To form the face feature vector, for each descriptor, the RGB and depth images are first divided into several local regions from which local histograms are extracted and then concatenated into an enhanced feature histogram used for classification.

### 4.3.3 Classification

The classification of both RGB and depth descriptors is performed using a support vector machine classifier (SVM). SVM is a supervised classification algorithm that aims to find the optimal separating hyperplane of the high dimensional training data.

This is achieved via maximization of the margins (distance of closest data, regardless of its class, to the hyperplane). The training feature vectors along with their labels are input to SVM, which outputs a model able to predict the labels of new unseen data. In our case, since we are dealing with nonlinear face feature vectors, we opt for a radial basis function (RBF) kernel. The nonlinear SVM maps the original data into a new space, using the kernel function, in which classes separation is improved.

## 4.4 Experiments and results

We analyzed the performance of the four local descriptors (LBP [88], LPQ [4], BSIF [60] and HoG [32]) presented in Section 4.3.2 on three publicly available Kinect face databases, FaceWarehouse [23], IIIT-D [47] and Curtinfaces [65], containing both RGB and depth facial images acquired with Kinect. We report the results for three different face classification problems: face identification, gender recognition and ethnicity classification. We have used the ground truth data whenever it is available with the database and in case data is not labeled we inferred the needed information from the face images (e.g, gender). We note that we have been limited to the three face analysis tasks mainly because of the available data and meta-data nature. For example, we were unable to perform age estimation because the ages of persons are not provided. The databases, evaluation methodology and results are provided in the following.

### 4.4.1 Databases

FaceWarehouse and IIIT-D databases are selected as these are among the largest available databases (regarding the number of subjects) while CurtinFaces is the most challenging Kinect face database (in terms of head pose, illumination and expression). The three databases are described below.

- **The CurtinFaces Kinect Database**<sup>4</sup> [65] contains over 5000 images of 52

---

<sup>4</sup><https://researchdata.and.s.org.au/curtinfaces-database/3640>

subjects in both RGB and depth maps obtained by Kinect sensor. The participants consist of 10 females and 42 males. The subjects in the database belong to three different ethnic groups (Caucasians, Chinese and Indians). The facial images have various variations in pose, illumination, facial expression as well as sunglasses and hand disguise. The faces of each subject are acquired under many combinations of these challenges. For each subject, there are 49 images under 7 poses and 7 facial expressions, 35 images under 5 illuminations and 7 expressions, and 5 images under disguise (sunglasses and hand). The full set for each person consists of 97 images. CurtinFaces is among the most challenging Kinect face databases.

- **The FaceWarehouse Database**<sup>5</sup> [23] comprises 150 individuals aged from 7 to 80. For each subject, the RGB-D face data is captured for the neutral expression and 19 other expressions. During recording, a guide face mesh for each specific expression is sequentially shown to the person, who is asked to imitate the expression and rotate his/her head within a small angle range, while keeping the expression fixed. For every RGB-D raw data record, a set of facial feature points on the color image are automatically localized, and manually adjusted for better accuracy. A template facial mesh is then deformed to fit the depth data while matching the feature points on the color image to their corresponding points on the mesh. Based on the 20 fitted meshes of each person, 47 individual-specific expression blendshapes per person are constructed.
- **The IIIT-D RGB-D Face Database**<sup>6</sup> [46] comprises 106 male and female subjects. All the subjects are of the same ethnicity (Indian). The number of images per subject varies between 11 and 254 images. The total number of images in the database is 4605. The database is captured in two different sessions. The images are captured under normal illumination with some variations in pose and expression. IIIT-D is the largest Kinect face database in terms of the number of subjects. Since the images are not segmented, the database can

---

<sup>5</sup><http://gaps-zju.org/facewarehouse/>

<sup>6</sup><https://research.iiitd.edu.in/groups/iab/facedatabases.html>

be used for face detection, besides its use for identity and gender recognition.

Table 4.2 outlines the main characteristics of the presented face Kinect databases. For each database, we report the number of subjects, the number of samples per subject and the main challenges presented in the database.

Table 4.2: Kinect face databases employed in our experiments.

Database	# Subjects	# Samples	Challenges
FaceWarehouse [23]	150	20	Pose and expression
IIIT-D [46, 47]	106	11-254	Expression and pose
CurtinFaces [65]	52	97	Pose, expression, lighting and disguise

Examples of the depth and RGB face images for a person from CurtinFaces database are illustrated in Fig. 4-4.

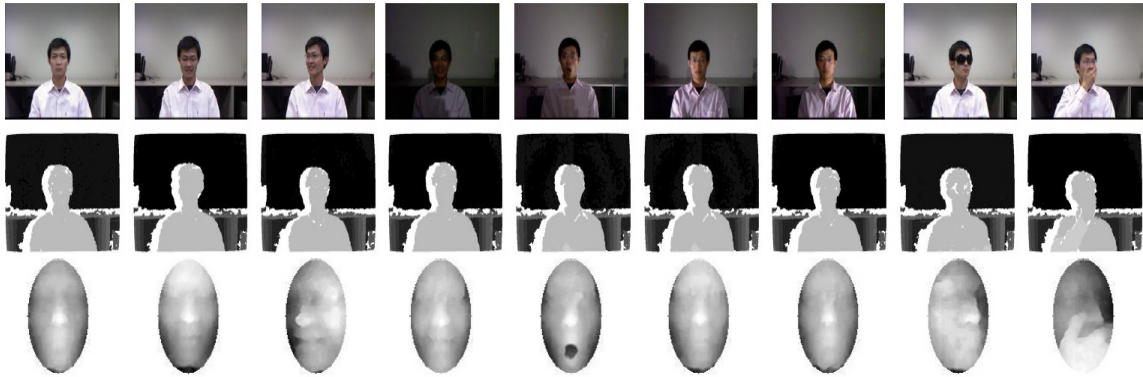


Figure 4-4: Face images samples from a subject of the CurtinFaces database. Top: RGB faces, middle: their corresponding raw depth maps and bottom: depth cropped face.

#### 4.4.2 Setup

In this section, we provide details about the parameters used in different experiments and evaluation protocols. First, for each of the four features, as the aim of our study is not to optimize the performances, we used default parameters with no adjustments. Uniform LBP patterns are extracted with a radius  $R = 2$  and neighborhood  $P = 8$ . The window size in LPQ is set to 5. HoG features are quantized with 9 bin histograms.

The filters used in BSIF are learned from patches of  $11 \times 11$  and coded with 8 bits. For each feature, histograms are computed from non-overlapped blocks of  $16 \times 16$  pixels, for both RGB and depth images, and concatenated to form the face feature vector.

For identity recognition, five images per subject are used for training and the rest for test. In gender and ethnicity classification, 10 subjects<sup>7</sup> per class are used to train the models and the other subjects are used for test. We note that for gender and ethnicity classification, subjects belonging to train and test subsets are mutually exclusive in order to avoid the identity bias in classification. Ethnicity evaluation is performed on FaceWarehouse (Chinese vs. White) and CurtinFaces (Caucasian, Chinese and Indian) databases only since IIIT-D database includes only one ethnicity.

Finally, the performances are assessed in terms of correct classification rates. For all the experiments, five-fold cross validation strategy is performed and the mean classification rate and standard deviation are reported.

### 4.4.3 Experimental results

Tables 4.3, 4.4 and 4.5 summarize the average accuracy and standard deviation for the three face analysis problems.

Table 4.3: Mean classification rates (%) and standard deviation using RGB and depth for face identity classification on FaceWarehouse, IIIT-D and CurtinFaces databases.

Method	Database					
	FaceWarehouse		IIIT-D		CurtinFaces	
	RGB	Depth	RGB	Depth	RGB	Depth
LBP	99.6 $\pm$ 0.1	85.3 $\pm$ 0.4	93.8 $\pm$ 1.6	84.4 $\pm$ 1.0	66.2 $\pm$ 0.6	84.0 $\pm$ 1.1
LPQ	99.7 $\pm$ 0.1	85.4 $\pm$ 0.4	93.4 $\pm$ 1.4	84.7 $\pm$ 1.8	57.6 $\pm$ 1.0	73.8 $\pm$ 1.1
HoG	98.4 $\pm$ 0.4	86.4 $\pm$ 0.6	92.5 $\pm$ 1.5	82.8 $\pm$ 1.3	68.2 $\pm$ 1.0	83.8 $\pm$ 1.0
BSIF	99.8 $\pm$ 0.1	88.5 $\pm$ 0.4	91.5 $\pm$ 1.7	77.8 $\pm$ 1.2	72.2 $\pm$ 1.0	77.8 $\pm$ 1.1

The analysis of the results points out that, generally, better performances on the FaceWarehouse database and IIIT-D database compared to the CurtinFaces database.

<sup>7</sup>In case the number of subjects for a given class is less than 20, half of the subjects are used for training and the other half for testing.

Table 4.4: Mean classification rates (%) and standard deviation using RGB and depth for face gender classification on FaceWarehouse, IIIT-D and CurtinFaces databases.

Method	Database					
	FaceWarehouse		IIIT-D		CurtinFaces	
	RGB	Depth	RGB	Depth	RGB	Depth
LBP	74.7 $\pm$ 1.7	77.6 $\pm$ 2.7	87.5 $\pm$ 1.6	76.4 $\pm$ 5.5	86.3 $\pm$ 3.2	84.3 $\pm$ 4.5
LPQ	78.4 $\pm$ 2.6	78.8 $\pm$ 1.7	88.0 $\pm$ 2.4	77.4 $\pm$ 4.5	85.3 $\pm$ 3.8	83.5 $\pm$ 3.9
HoG	78.6 $\pm$ 2.3	77.5 $\pm$ 1.5	86.1 $\pm$ 2.5	70.1 $\pm$ 3.3	86.8 $\pm$ 2.1	85.0 $\pm$ 4.1
BSIF	78.9 $\pm$ 3.0	78.2 $\pm$ 1.7	86.2 $\pm$ 3.2	70.3 $\pm$ 1.9	87.7 $\pm$ 2.6	85.2 $\pm$ 2.5

Table 4.5: Mean classification rates (%) and standard deviation using RGB and depth for facial ethnicity classification on FaceWarehouse and CurtinFaces database. Results are not provided for IIIT-D database as only one ethnicity is represented in this database.

Method	Database					
	FaceWarehouse		IIIT-D		CurtinFaces	
	RGB	Depth	RGB	Depth	RGB	Depth
LBP	90.6 $\pm$ 4.3	95.3 $\pm$ 1.1	-	-	70.5 $\pm$ 3.1	69.4 $\pm$ 3.2
LPQ	93.8 $\pm$ 3.9	96.5 $\pm$ 1.0	-	-	71.3 $\pm$ 3.0	68.6 $\pm$ 3.0
HoG	94.6 $\pm$ 4.0	96.8 $\pm$ 1.6	-	-	69.3 $\pm$ 3.3	67.8 $\pm$ 2.4
BSIF	96.0 $\pm$ 2.7	98.4 $\pm$ 0.6	-	-	74.9 $\pm$ 3.6	70.2 $\pm$ 2.7

CurtinFaces database is indeed more challenging in terms of variations of pose, expression and illumination.

In overall, the RGB images yield in better performances compared to the depth images. Nevertheless, the results of the depth images alone are still good and actually much better than our expectations based on the human perception. It is indeed quite hard to visually distinguish the subjects using only the depth images. One can also notice from the results on CurtinFaces database through the three tables that depth images may compete or even outperform RGB images under challenging illumination and pose variations. Another important remark is that the difference in classification accuracy between depth and RGB images is less significant in gender and ethnicity classification than it is in identity classification. In particular, depth outperforms RGB in ethnicity classification on FaceWarehouse database. These results point out the usefulness of Kinect depth images in some face classification problems.

Regarding the performance of different features, the four descriptors perform comparably across the three databases. However, in most of the cases, the new BSIF descriptor yields in the best classification rates. Our extensions to BSIF to describe depth images by learning dedicated depth filters demonstrated interesting results, making BSIF generally better than the three other descriptors.

Figure 4-5 visually illustrates the obtained results on FaceWarehouse database. From this figure, one can easily notice that RGB clearly outperforms depth in identity classification. The performance difference is becoming less significant in gender classification problem. In ethnicity classification, the depth surprisingly outperforms the RGB based methods.

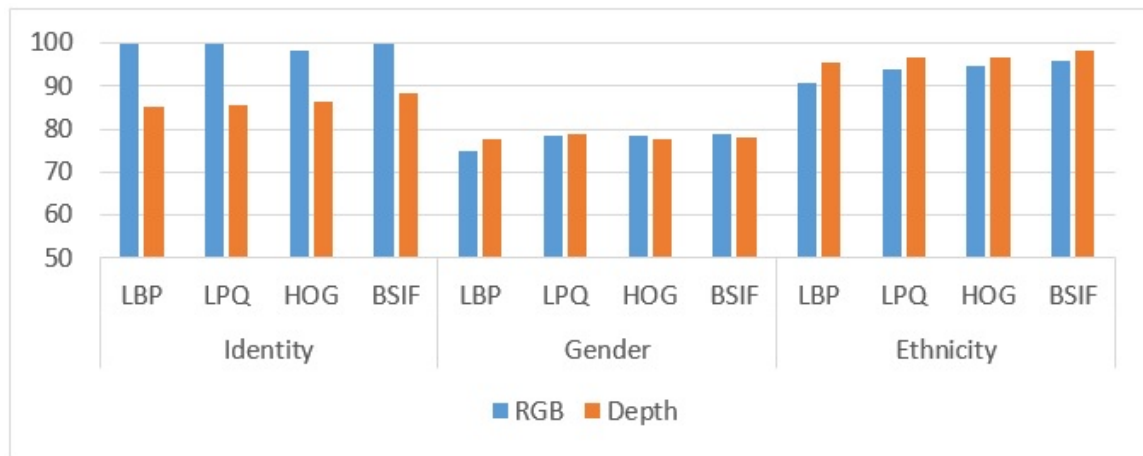


Figure 4-5: Classification accuracy for identity, gender and ethnicity using RGB and depth on FaceWarehouse database.

Our main goal through this work is to compare the performance of Kinect depth and RGB images in different face analysis tasks. Thus, we did not aim at optimizing the overall performance using complex methods.

The depth images provided by Kinect sensor are of low quality and noisy thus requiring a crucial preprocessing before analysis. The outcomes on such images are highly depending on the preprocessing step and hence cannot be easily generalized or compared to previously reported results if a different preprocessing is applied. Even though, for completeness, we summarize in Table 4.6 the performances reported by other authors in the literature dealing with face analysis tasks on publicly available



Kinect face datasets. Again, one cannot fairly compare the different methods since each method uses different data and/or different evaluation protocols. Furthermore, most of the reported works combine RGB and depth modalities but omit to report the performance of each modality separately.

Table 4.6: Summary of reported performance of literature work on face analysis using Kinect sensor.

Method	Application	Dataset	Accuracy
RISE[47]	Face recognition	III-D	81.0 % (RGB-D)
		Eurecom	89.0 % (RGB-D)
COV+LBP[29]	Face recognition	CurtinFaces	84.6% (RGB-D)
Depth+DCS[66]	Face recognition	CurtinFaces	88.7 % (D)
			91.1% (RGB)
			96.7% (RGB-D)
DLQP[80]	Face recognition	HRRFace	63.95% (D)
G-LBP[56]	Gender recognition	Eurecom	87.1% (D)
3DLBP[56]	Gender recognition	Eurecom	85.9% (D)
Curvature [103]	Expression recognition	SBIA	77.4% (D)
			84.9% (RGB)
			89.4% (RGB-D)

As an indication, Li et al. [66] reported a face recognition accuracy of 88.7% using complex depth preprocessing steps, including symmetric filling of face depth maps, on CurtinFaces dataset while we achieved 84.0% using simple LBP feature only. Our performance is comparable to the work of Ciaccio et al. [29] combining LBP and covariance features on the same dataset. Gender recognition was tackled by Huynh et. [56] achieving 87.1% accuracy using depth images on Eurecom dataset. Our experiments on larger and more challenging databases yield better results as can be noticed from tables. To the best of our knowledge, the ethnicity classification has not been previously addressed using Kinect data.

## 4.5 Conclusion

In this chapter, we presented a review on using Kinect depth data for different face analysis problems. The review of the literature revealed that the recently introduced consumer low-cost depth sensors have attracted a big interest from researchers work-

ing on face analysis tasks. The device was mainly used for face recognition and face detection, segmentation and tracking as well as head pose estimation and normalization. To this end, the depth maps are either considered alone or combined with RGB channels.

To gain more insight, we presented the first comprehensive study in the literature exploring the usefulness of the depth information acquired by the low-cost depth sensor in different face analysis tasks including face identification, gender recognition and ethnicity classification. We carried out intensive experimental evaluation with four state-of-the-art local face descriptors on three publicly available Kinect face databases. While it is difficult to visually distinguish the subjects using only the depth images, the obtained results confirmed that the depth facial information alone provides promising classification results beyond the expectations based on the human perception. Moreover, we found depth maps to perform better than RGB images under severe illumination, expression and viewpoint changes. Regarding the best performing methods, the introduced BSIF features derived from a new set of filters showed interesting results for both RGB and depth images.



# Chapter 5

## Kinship verification from videos

This chapter deals with automatic kinship verification from face videos. Kinship verification from faces is a challenging task. Indeed, it inherits the research problems of face verification from images captured in the wild under adverse pose, expression, illumination and occlusion conditions. In addition, kinship verification should deal with wider intra-class and inter-class variations, as persons from the same family may look very different while faces of persons with no kin relation may look similar. Moreover, automatic kinship verification can face new challenges since a pair of input images may be from persons of different sex (e.g. brother-sister kin) and/or with a large age difference (e.g. father-daughter kin).

The published papers and organized competitions (e.g. [76, 75]) dealing with automatic kinship verification over the past few years showed some promising results. Typical current best-performing methods combine several face descriptors, apply metric learning approaches and compute Euclidean distances between pairs of features for kinship verification. One can remark that these works are based on handcrafted features extracted from images while kinship verification is less investigated using deep learning and videos. In the present chapter, we aim to exploit the temporal information present in face videos, investigating the use of both spatio-temporal shallow features and deep features describing faces.

This chapter is organized as follows. Section 5.1 briefly overviews the related work and motivates our approach. The proposed approach for kinship verification

from videos is described in Section 5.2. Experiments and analysis are then given in Section 5.3. In Section 5.4, we give the conclusions.

## 5.1 Background and motivation

Kinship verification from face is receiving increasing interest by the research community. This is mainly motivated by its potential applications, especially in analyzing daily shared data in social web. The first approaches to tackle kinship verification were based on low level handcrafted feature extraction and SVM or  $k$ -NN classifiers. For instance, Zhou et al. [132] used a spatial pyramid learning descriptor; Gabor gradient orientation pyramid has been used by Zhou et al. [133]; and Self-similarity of Weber faces was utilized by Kohli et al. [64]. Several types of face features are then combined by many researchers and used for verifying the kin relation. For example, in the second kinship competition [75], all the proposed methods used three or more descriptors. The best performing method in this competition employed four different local features (LBP, HOG, over-complete LBP - OCLBP - and Fisher vectors).

On the other hand, different metric learning approaches have been investigated for tackling the kinship verification problem. Lu et al. [77] learned a distance metric where the face pairs with a kin relation are pulled close to each other and those without a kin relation are pushed away. Recently, Zhou et al. [134] applied ensemble similarity learning for solving the kinship verification problem. They learned an ensemble of sparse bi-linear similarity bases from kinship data by minimizing the violation of the kinship constraints between pairs of images and maximizing the diversity of the similarity bases. Yan et al. [121] and Hu et al. [54] learned multiple distance metrics based on various features, by simultaneously maximizing the kinship constraint (pairs with a kinship relation must have a smaller distance than pairs without a kinship relation) and the correlation of different features.

Motivated by the impressive success of deep learning approaches in various image representation and classification [105] in general and face recognition in particular [107], Zhang et al. [128] recently proposed a convolution neural network archi-

itecture for face-based kinship verification. The proposed architecture is composed by two convolution max pooling layers followed by a convolution layer then a fully connected layer. A two-way soft max classifier is used as the final layer to train the network. The network takes a pair of RGB face images of different persons as an input, checking the possible kin relations. However, their reported results do not outperform the shallow methods presented in the FG15 kinship competition on the same datasets [75]. The reason behind this may be the scarcity of training data, since deep learning approaches require the availability of enough training samples which is not the case for available face kinship databases.

While most of the published works cope with kinship problem from images, to our knowledge the only work that performed kinship from videos was conducted by Dibeklioglu et al. [34]. The authors combined facial expression dynamics with facial appearance as features and used SVM for classification.

It appears that most of literature works on kinship verification are mainly based on shallow handcrafted features and hence are not associated with the recent significant progress which has been made in machine learning suggesting the use of deep features. Moreover, the role of facial dynamics in kinship verification is mostly unexplored as most existing works focus on analyzing still facial images instead of video sequences. Based on these observations, we propose to approach the problem of kinship verification from spatio-temporal point of view and also exploit the recent progress in deep learning.

## 5.2 Video-based kinship verification

This section describes our approach for kinship verification from videos. In the following, we first present an overview of the proposed approach, then we provide the details of each step.

### 5.2.1 Approach overview

Fig. 5-1 depicts an overview of our approach for kinship verification from videos. Given two face video sequences, to verify their kin relationship, our proposed approach starts with detecting, cropping and aligning the face images based on facial landmarks. Then, two types of descriptors are extracted: shallow spatio-temporal texture features and deep features. As spatio-temporal features, we extract local binary patterns (LBP) [2], local phase quantization (LPQ) [4] and binarized statistical image features (BSIF) [60]. These features are all extracted from three orthogonal planes (TOP) of the videos. Deep features are extracted by convolutional neural networks (CNNs) [92]. The pairs of features are then combined to be used as inputs to support vector machines (SVM) for classification. A score level fusion is then performed, to combine all the features' results, and the issued score is used to decide whether the two persons in the input videos have a kin relation or not. The details of the proposed approach are presented in the following sections.

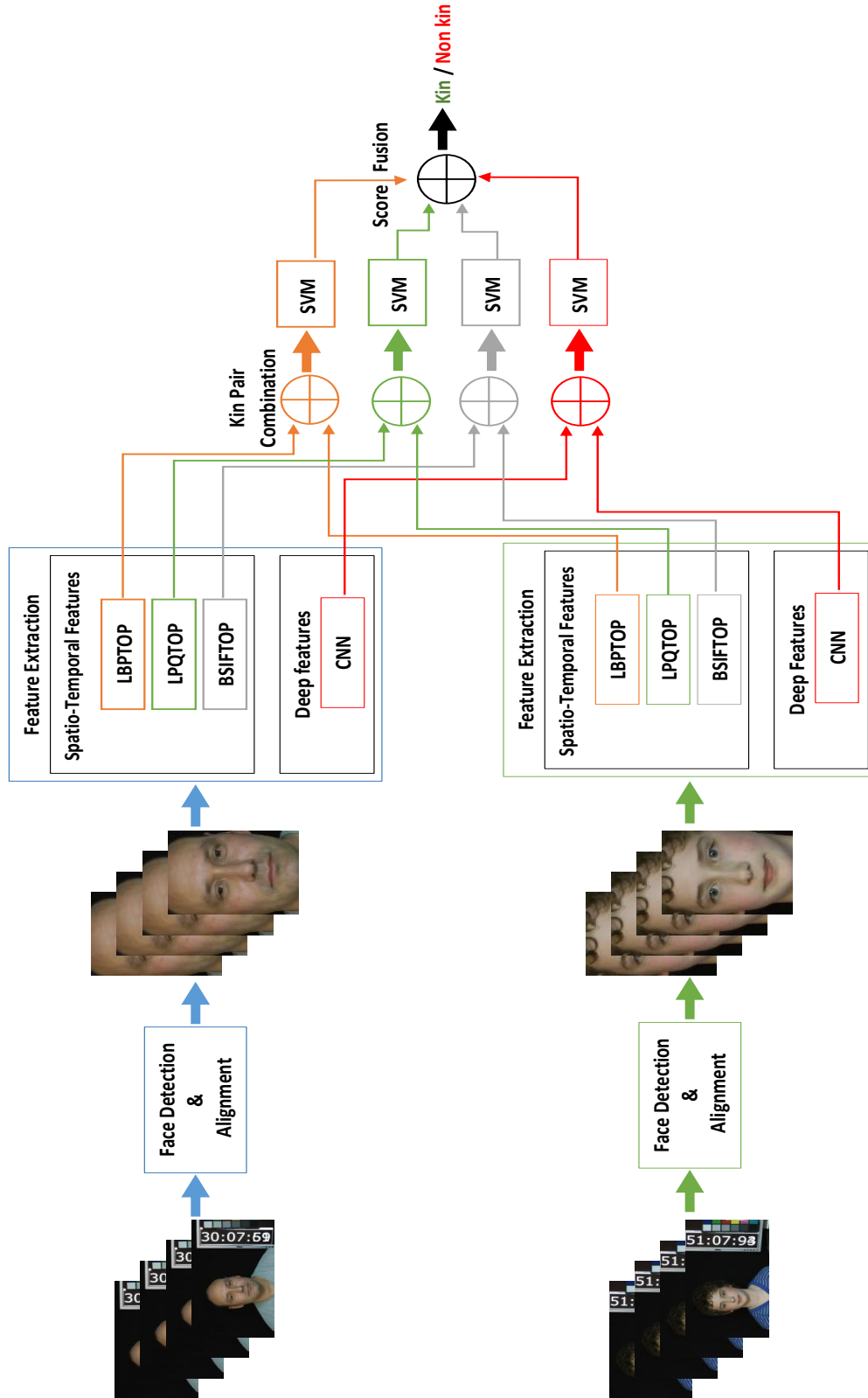


Figure 5-1: Overview of the proposed approach for kinship verification from videos.



### 5.2.2 Face detection and tracking

The first step in our proposed approach is to segment the face region from each video sequence. Therefore, we employed an active shape model (ASM) [30] based approach. ASM is a statistical model of the shape of an object. It represents an object by the distribution of a set of points. The model is built based on a set of training images annotated with landmark points. To detect a new instance of the object, the ASM iteratively deforms to fit the object in the new image. Therefore, two steps are alternatively performed to match the model to the new instance: generating a suggested shape by inspecting the neighborhood of each point and adapting the suggested shape to the model.

In our case, we detect 68 facial landmarks tracking them along the video. Faces are then cropped from all the frames of the video and aligned based on the detected landmarks. Fig. 5-2 illustrates an example of the detected face landmarks in one frame and the cropped face.



Figure 5-2: Example of face cropping: (left) a frame annotated with the detected landmarks, and (right) the cropped and aligned face region.

### 5.2.3 Face description

For describing faces from videos, we use two types of features: texture spatio-temporal features and deep learning features. These features are introduced hereafter.

#### Spatio-temporal features

Spatio-temporal texture features have been shown to be efficient for describing faces in various face analysis tasks, such as face recognition [63] and facial expression classification [131]. The spatio-temporal textural dynamics of the face in a video are extracted from three orthogonal planes XY, XT, and YT [96, 130, 7], separately. X and Y are the horizontal and vertical spatial axes of the video, and T refers to the time axis. An example of the orthogonal planes at a pixel of the video is given in Fig. 5-3. This approach characterizes the video sequence in three ways: a stack of XY planes in axis T, a stack of XT planes in axis Y and a stack of YT planes in axis X. The XT and YT planes provide information about the space-time transitions while XY plane represents the spatial information.

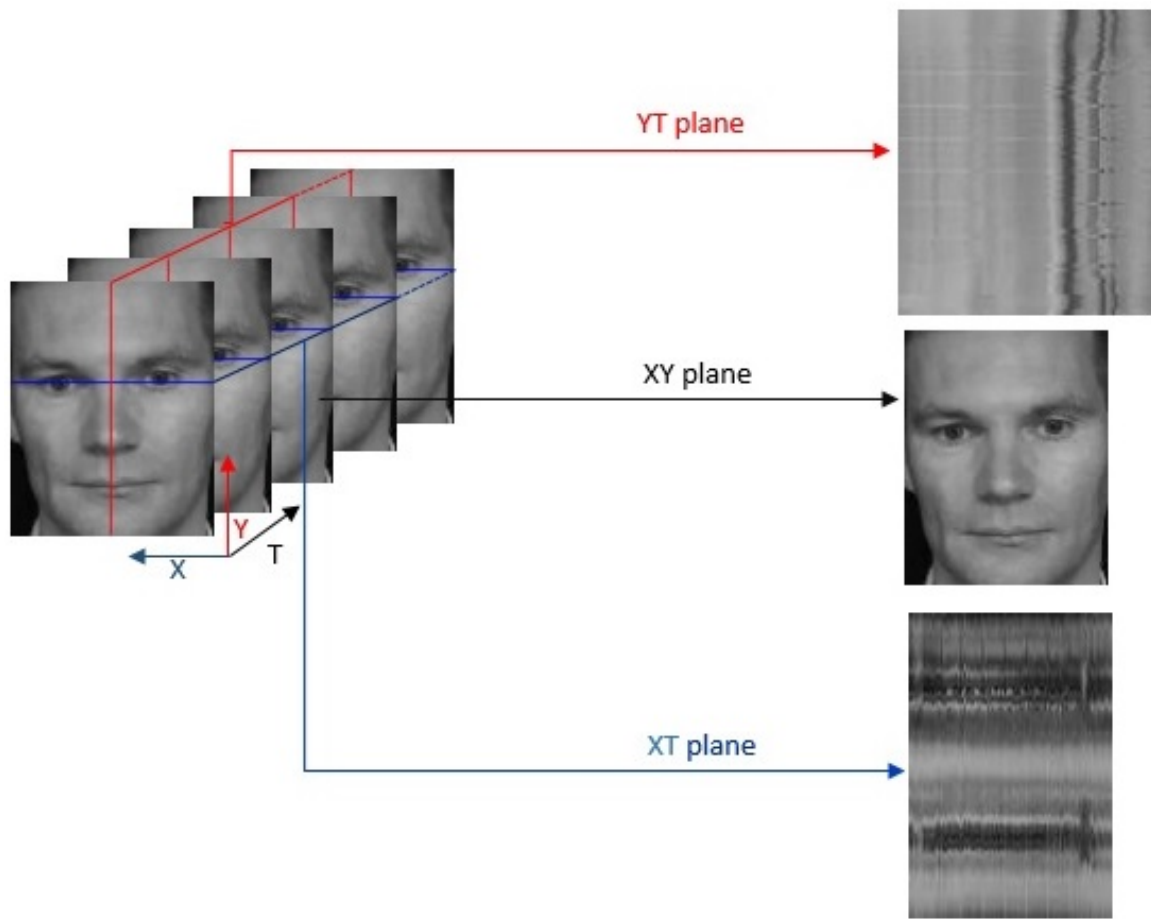


Figure 5-3: Illustration of three orthogonal planes used to extract dynamic textural face descriptors from a video.

The face video is subdivided into smaller volumes (see Fig. 5-4) in order to maintain the facial spatial structure. For each region, the texture features of each plane are summarized in a separate histogram and then the three histograms are concatenated into a single feature vector (Fig. 5-5). The final face descriptor is composed by the concatenation of all the regions' features.

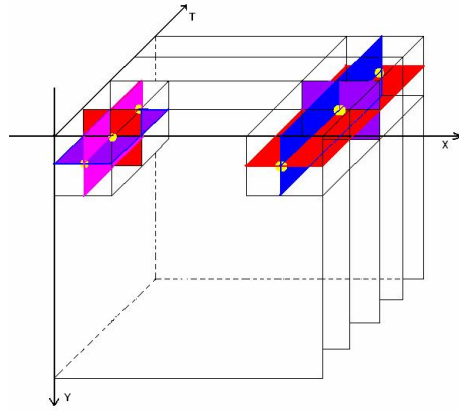


Figure 5-4: Division of video into region volumes.

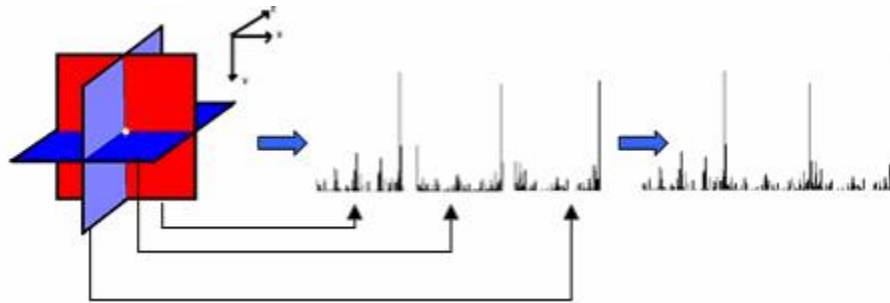


Figure 5-5: Three plan feature vector.

Three local texture descriptors ( LBP [2], LPQ [4] and BSIF [60]), used in the previous chapter for still images, are extended here to describe face appearance from videos. The features are extracted by applying the previous regions three planes strategy. Furthermore, the three features are extracted at multiple scales, to take benefit of the multi-resolution representation [25], by varying their parameters. Hence, the

utilized parameters of LBP are  $P = \{8, 16, 24\}$  and  $R = \{1, 2, 3\}$ ; and for LPQ and BSIF descriptors, the filter sizes were selected as  $W = \{3, 5, 7, 9, 11, 13, 15, 17\}$ . The feature dimension sizes for the three neighborhoods of LBP are 3540, 14580 and 33300, respectively. For both LPQ and BSIF the feature size is 15360 for each filter.

## Deep learning features

Deep neural networks have been recently outperforming the state of the art in various classification tasks [101]. Particularly, convolutional neural networks (CNNs) demonstrated impressive performance in object classification in general and face recognition in particular [110]. Two factors are mainly behind this success of deep learning approaches. The first one is the abundance of web scale training data. Indeed, the networks used to beat the state of the art in image detection and classification [101] are very deep architectures (e.g. Google network (GoogLeNet) has 22 layers [109] ) trained with millions of samples and thousands of classes. The second factor is the advance made by hardware computation speed, especially GPU, enabling the training of very deep architectures with billions of parameters. Even though, training of very deep architectures still require days or even months with the current available hardware.

The deep learning approaches have many advantages. First, deep neural networks are scalable models having the capacity to learn highly complex representations of thousands of categories. Once trained, a deep model stores its knowledge compactly in learned parameters, making it easy to deploy in any environment. It can then be easily used for fast prediction of new inputs with no need for storing additional data. Additionally, deep learning approaches learn to extract discriminative features in contrast to hand-engineered feature extractors, such as LBP and its variants. Moreover, in a deep learning model both feature extraction and classification steps are optimized at the same time, which is not the case of classical approaches.

In this work, we utilize a convolutional neural network (CNN) for extracting deep face features. CNNs are hierarchical machine learning models which are able to learn complex representations of images and signals using vast amounts of training

data. Inspired by the human visual system, CNNs progressively extract sophisticated representation of the input by learning transformations in multiple layers. Fig. 5-6 illustrates an example of a deep CNN. A deep CNN is formed by alternating many convolutional and subsampling layers. Usually, the top of the network is composed by one or more fully connected layers and a classification layer.

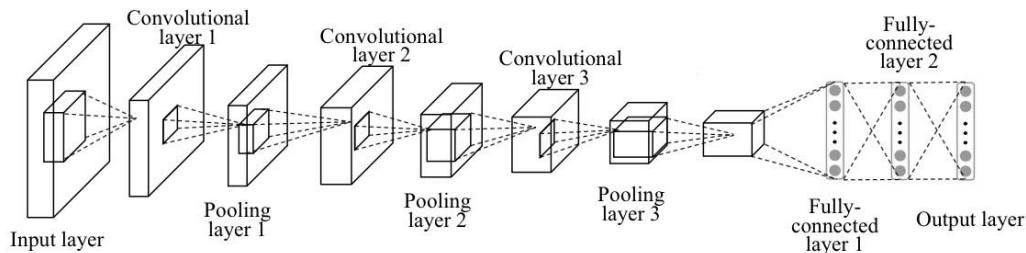


Figure 5-6: Example of a convolutional neural network.

As stated before, deep neural networks require a huge amount of training data to learn efficient features, which is not the case for the available kinship databases. Indeed, our preliminary experiments using a Siamese CNN architecture [28] as well as deep architecture proposed by a previous work [128] for kinship verification yielded lower performance than shallow features. An alternative for extracting deep face features is to use a pre-trained network. A number of very deep pre-trained architectures has already been made available by researchers. In our case, we use the VGG-face [92] network which has been initially trained for face recognition on a reasonably large dataset of 2.6 million images of 2622 people. This network has been evaluated for face verification from both pairs of images and videos showing interesting performance compared against state of the art. This motivated us to use VGG-face network for extracting deep face features for kinship verification.

The detailed parameters of the VGG-face CNN are provided by Table 5.1. The input of the network is an RGB face image of size  $224 \times 224$  pixels. The network is composed of 13 linear convolution layers (conv), each followed by a non-linear rectification layer (relu). Some of these rectification layers are followed by a non-linear max pooling layer (mpool). Following are two fully connected layers (fc) both

outputting a vector of size 4096. At the top of the initial network are a last fully connected layer with the size of classes to predict (2622) and a softmax layer for computing the class posterior probabilities.

To extract deep face features for kinship verification, we input the video frames one by one to the CNN and collect the feature vector issued by the fully connected layer fc7 (all the layers of the CNN except the class predictor fc8 layer and the softmax layer are used). All the frames' features of a given face video are finally averaged to obtain the video descriptor.

Table 5.1: VGG-face CNN architecture.

layer	0	1	2	3	4	5	6	7	8	9
type	input	conv	relu	conv	relu	mpool	conv	relu	conv	relu
name		conv1_1	relu1_1	conv1_2	relu1_2	pool1	conv2_1	relu2_1	conv2_2	relu2_2
support		3	1	3	1	2	3	1	3	1
filt dim		3		64			64		128	
num filts		64		64			128		128	
stride		1	1	1	1	2	1	1	1	1
pad		1	0	1	0	0	1	0	1	0
layer	10	11	12	13	14	15	16	17	18	
type	mpool	conv	relu	conv	relu	conv	relu	mpool	conv	
name	pool2	conv3_1	relu3_1	conv3_2	relu3_2	conv3_3	relu3_3	pool3	conv4_1	
support	2	3	1	3	1	3	1	2	3	
filt dim		128		256		256			256	
num filts		256		256		256			512	
stride	2	1	1	1	1	1	1	2	1	
pad	0	1	0	1	0	1	0	0	1	
layer	19	20	21	22	23	24	25	26	27	28
type	relu	conv	relu	conv	relu	mpool	conv	relu	conv	relu
name	relu4_1	conv4_2	relu4_2	conv4_3	relu4_3	pool4	conv5_1	relu5_1	conv5_2	relu5_2
support	1	3	1	3	1	2	3	1	3	1
filt dim		512		512			512		512	
num filts		512		512			512		512	
stride	1	1	1	1	1	2	1	1	1	1
pad	0	1	0	1	0	0	1	0	1	0
layer	29	30	31	32	33	34	35	36	37	
type	conv	relu	mpool	conv	relu	conv	relu	conv	softmax	
name	conv5_3	relu5_3	pool5	fc6	relu6	fc7	relu7	fc8	prob	
support	3	1	2	7	1	1	1	1	1	
filt dim	512			512		4096		4096		
num filts	512			4096		4096		2622		
stride	1	1	2	1	1	1	1	1	1	
pad	1	0	0	0	0	0	0	0	0	

### 5.2.4 Classification

To classify a pair of face features as positive (the two persons have a kinship relation) or negative (no kinship relation between the two persons), we use a bi-class linear support vector machine classifier. Before feeding the features and their labels to the SVM, each pair of features has to be transformed into a single feature vector as imposed by the classifier. We have examined various ways for combining a pair of features, such as concatenation and vector distances. We have empirically found that utilizing the normalized absolute difference shows the best performance. Therefore, in our work, a pair of feature vectors  $X = \{x_1, \dots, x_d\}$  and  $Y = \{y_1, \dots, y_d\}$  is represented by the vector  $F = \{f_1, \dots, f_d\}$  where :

$$f_i = \sum_i \frac{|x_i - y_i|}{\sum_i (x_i + y_i)} \quad (5.1)$$

## 5.3 Experiments

### 5.3.1 Database and test protocol

To evaluate the proposed approach, we use UvA-NEMO Smile database [33], which is , to the best of our knowledge, the only available video kinship database. The database was initially collected for analyzing posed versus spontaneous smiles of subjects. Videos are recorded with a resolution of  $1920 \times 1080$  pixels at a rate of 50 frames per second under controlled illumination conditions. A color chart is placed on the background of the videos to allow further illumination and color normalization. The ages of the subjects in the database vary from 8 to 76 years. Many families participated in the database collection, allowing its use for evaluation of automatic kinship from videos. A total of 95 kin relations were identified between 152 subjects in the database. There are seven different kin relations between pairs of videos: Sister-Sister (S-S), Brother-Brother (B-B), Sister-Brother (S-B), Mother-Daughter (M-D), Mother-Son (M-S), Father-Daughter (FD), and Father-Son (F-S). The association of the videos of persons having kinship relations gives 228 pairs of spontaneous and



287 pairs of posed smile videos. The statistics of the database are summarized in Table 5.2.

Table 5.2: Kinship statistics of UvA-NEMO Smile database.

Relation	Spontaneous		Posed	
	Subj. #	Vid. #	Subj. #	Vid. #
S-S	7	22	9	32
B-B	7	15	6	13
S-B	12	32	10	34
M-D	16	57	20	76
M-S	12	36	14	46
F-D	9	28	9	30
F-S	12	38	19	56
All	75	228	87	287

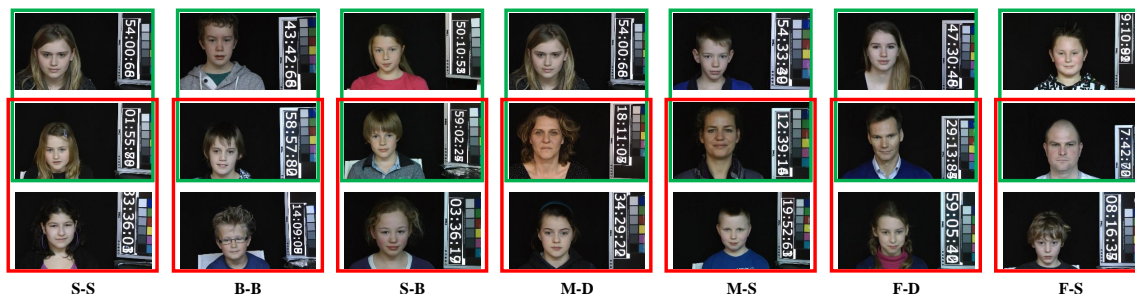


Figure 5-7: Samples of pair images from UvA-NEMO Smile database for different kin relations. Positive pairs are combinations of first row with second row (green rectangles) and negative pairs are combinations of second row with third row (red rectangles).

Following [34], we randomly generate negative kinship pairs corresponding to each positive pair. Therefore, for each positive pair we associate the first video with another video of a person within the same kin subset while ensuring there is no relation between the two subjects. Examples of the positive pairs and the generated negative pairs are illustrated by Fig. 5-7. For all the experiments, we perform a per-relationship evaluation and report the average accuracy (rate of correctly classified pairs) of spontaneous and posed videos. The accuracy for the whole database, obtained by pooling all the relations, is also provided. Since the number of pairs of each relation is small,

we apply the leave-one-out evaluation scheme.

The performances in different experiments are assessed in terms of ROC curves and accuracy (correct classification rates):

$$accuracy = \frac{TP + TN}{P + N}, \quad (5.2)$$

where  $TP$  is the number of correctly classified positive pairs,  $TN$  is the number of correctly classified negative pairs,  $P$  is the number of all positive pairs, and  $N$  is the number of all negative pairs.

### 5.3.2 Results and analysis

We have performed various experiments to assess the performance of the proposed approach. In the following, we present the obtained results for each experiment and discuss them.

#### Comparing deep features against shallow features

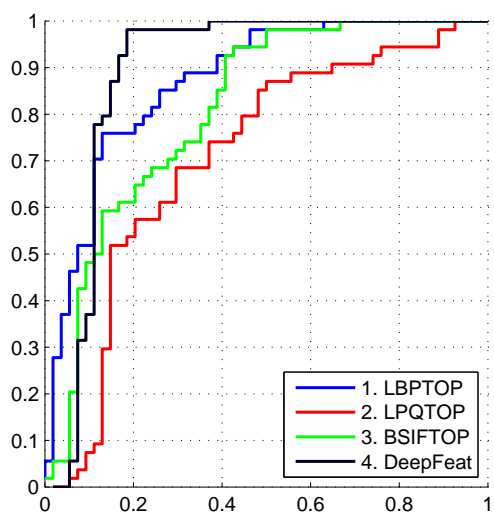
First we compare the performance of the deep features against the spatio-temporal features. The results for different features are reported in Table 5.3. The ROC curves for separate relations as well as for the whole database are depicted in Fig. 5-8. The performances of the three spatio-temporal features (LBPTOP, LPQTOP and BSIFTOP) show competitive results on different kinship relations. Considering the average accuracy and the accuracy of all the kinship relations, LPQTOP is the best performing method, closely followed by the BSIFTOP, while LBPTOP shows the worst performance.

On the other hand, deep features report the best performance on all kinship relations significantly improving the verification accuracy. The gain in verification performance of the deep features varies between 2% and 9%, for different relations, compared with the best spatio-temporal accuracy. These results highlight the ability of CNNs in learning face descriptors. Even though the network has been trained for face recognition, it generates highly discriminative face features for the task of kinship

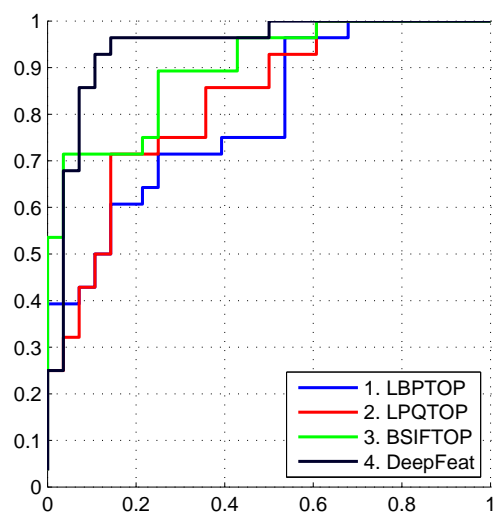
Table 5.3: Accuracy (in %) of kinship verification using spatio-temporal and deep features on UvA-NEMO Smile database.

Method	S-S	B-B	S-B	M-D	M-S	F-D	F-S	Mean	All
BSIFTOP	75.07	83.46	71.23	82.46	72.37	81.67	79.84	78.01	75.83
LPQTOP	69.67	78.21	82.54	71.71	83.30	78.57	83.91	78.27	76.02
LBPTOP	80.47	77.31	70.50	78.29	72.37	84.40	71.50	76.41	72.82
DeepFeat	<b>88.92</b>	<b>92.82</b>	<b>88.47</b>	<b>90.24</b>	<b>85.69</b>	<b>89.70</b>	<b>92.69</b>	<b>89.79</b>	<b>88.16</b>

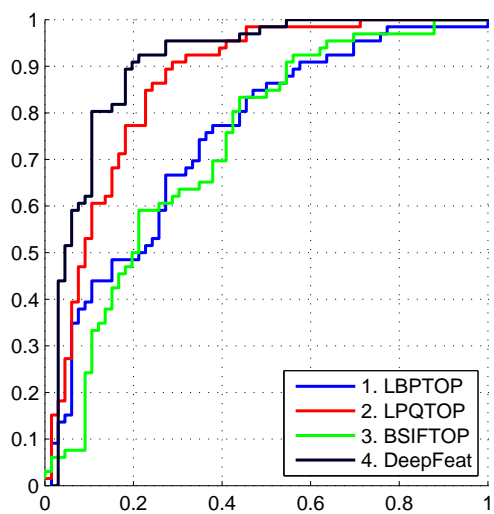
verification.



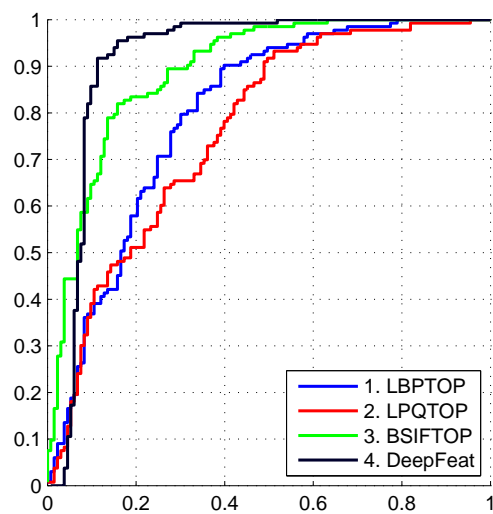
(a) Sister-Sister



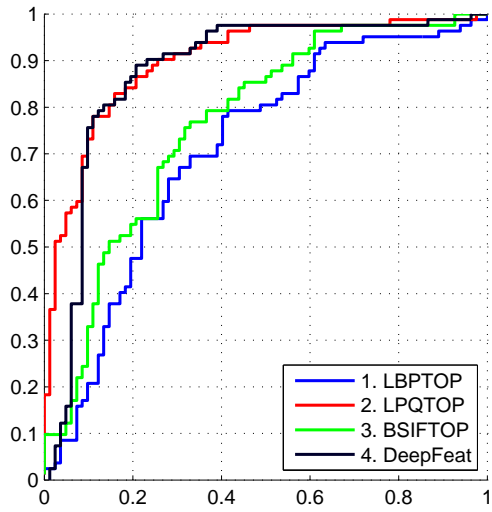
(b) Brother-Brother



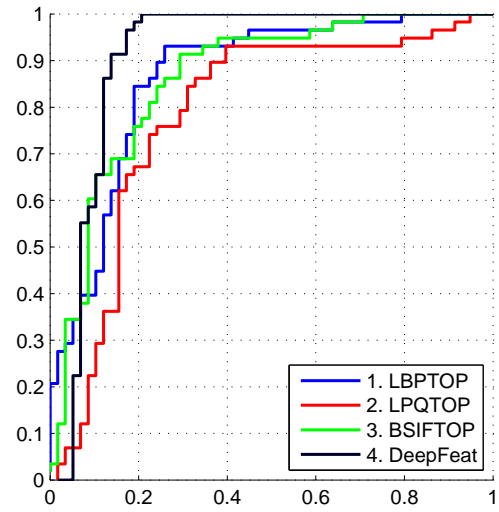
(c) Sister-Brother



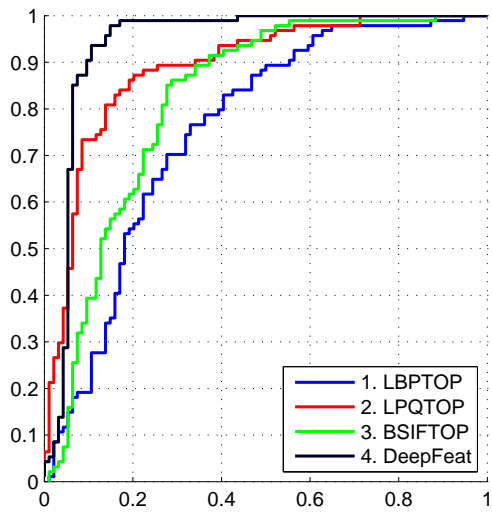
(d) Mother-Daughter



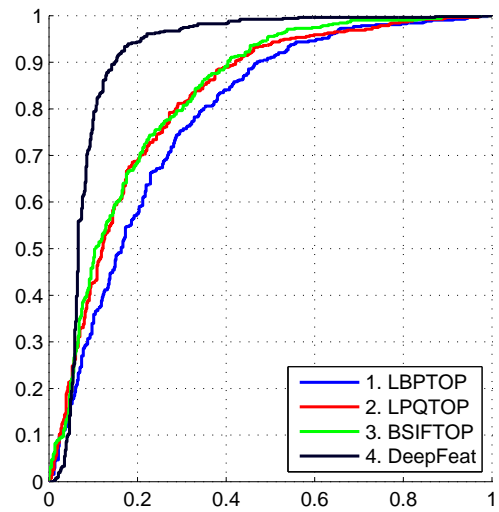
(e) Mother-Son



(f) Father-Daughter



(g) Father-Son



(h) All

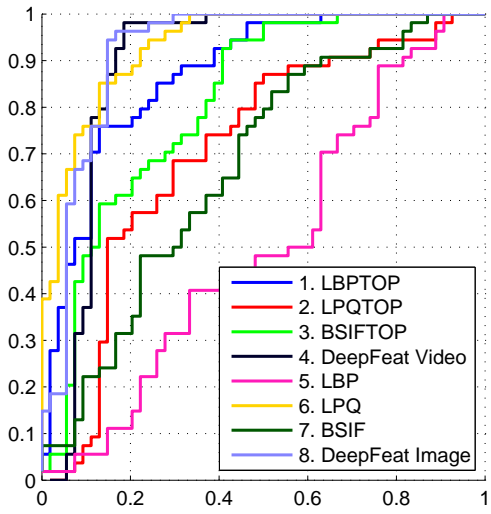
Figure 5-8: Comparing deep vs. shallow features on UvA-NEMO Smile database.

### **Comparing different relations**

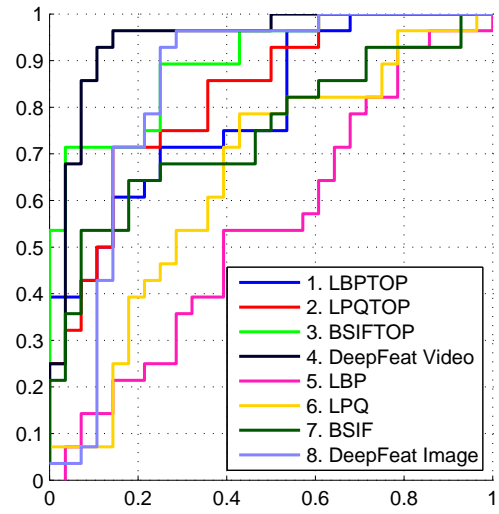
Regarding different types of kin relations, the best verification accuracy is obtained for B-B and F-S while the lowest are S-B and M-S. These results are maybe due to the different sex of the pairs. One can conclude that checking the kinship relation is easier between persons of the same gender. However, a further analysis of this point is needed as the accuracy of S-S is average in our case. Unfortunately, this analysis is not easy with the currently available data. It is also noticed that the performance of kinship between males (B-B and F-S) is better than between females (M-D and S-S). Moreover, the difference in age of the persons has an effect on the kinship verification accuracy. For instance, the difference in age of brothers (best performance) is lower than it is for M-S (lowest performance).

### **Comparing videos against images**

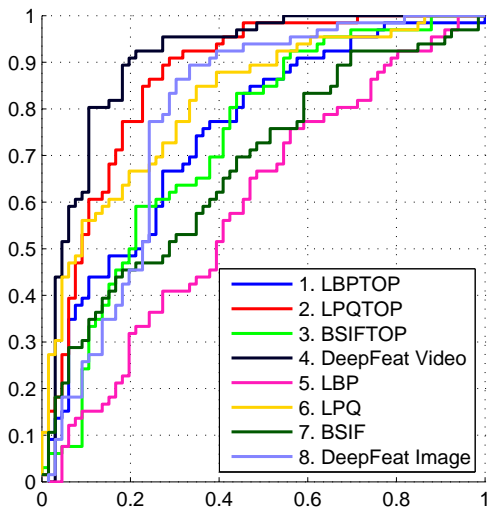
We have carried out an experiment to check if verifying kinship relations from videos instead of images is worthy. Therefore, in this experiment, we employ the first frame from each video of the database. For this experiment, spatial variants of texture features (LBP, LPQ and BSIF) and deep features are extracted from the face images. Fig. 5-9 shows the ROC curve comparing the performance of videos against still images for each relation as well as for the pool of all relationships. The superiority of the performance of videos compared with still images is obvious for each feature, demonstrating the importance of face dynamics in verifying kinship between persons. Again, deep features extracted from still face images demonstrate high discriminative ability, outperforming both the spatial texture features extracted from images and the spatio-temporal features extracted from videos. We note that, in still images (see Fig. 5-9), LPQ feature outperforms both LBP and BSIF.



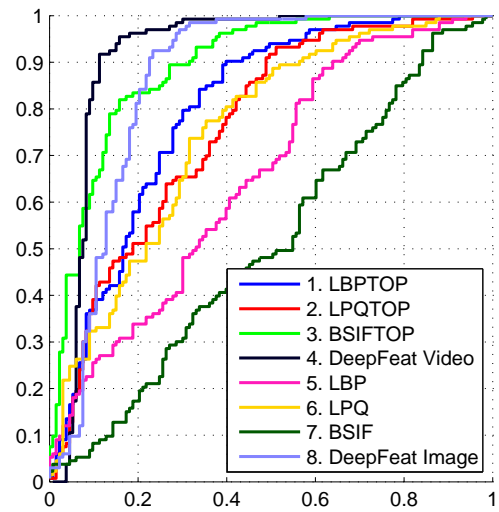
(a) Sister-Sister



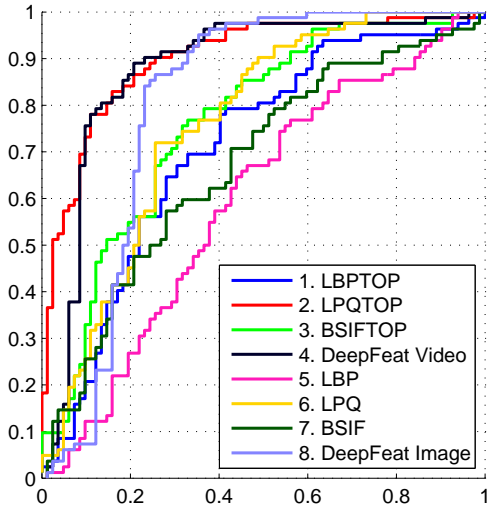
(b) Brother-Brother



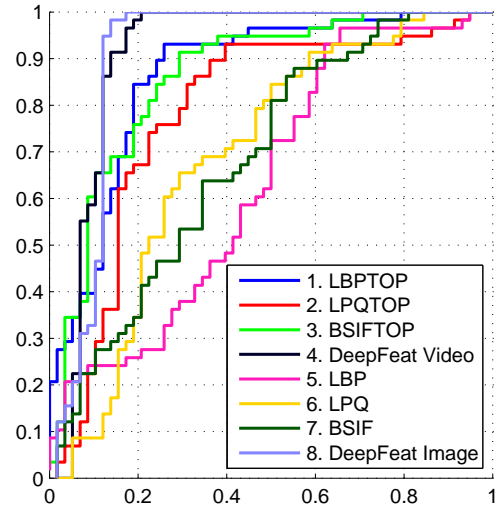
(c) Sister-Brother



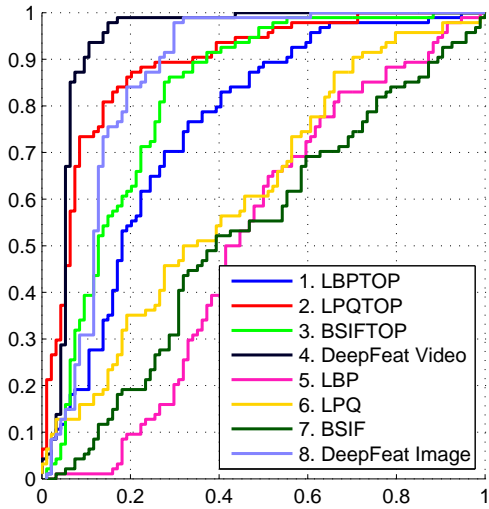
(d) Mother-Daughter



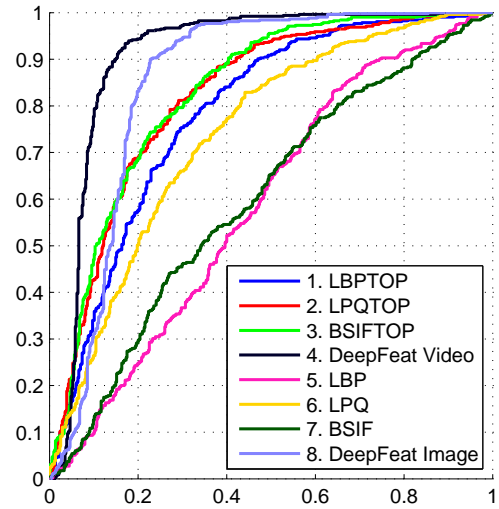
(e) Mother-Son



(f) Father-Daughter



(g) Father-Son



(h) All

Figure 5-9: Comparing videos vs. still images for kinship verification on UvA-NEMO Smile database.



Table 5.4: Comparison of our approach for kinship verification against state of the art on UvA-NEMO Smile database.

Method	S-S	B-B	S-B	M-D	M-S	F-D	F-S	Mean	All
Fang <i>et al.</i> [41]	61.36	56.67	56.25	56.14	55.56	57.14	55.26	56.91	53.51
Guo & Wang [49]	65.91	56.67	60.94	58.77	62.50	67.86	55.26	61.13	56.14
Zhou <i>et al.</i> [133]	63.64	70.00	60.94	57.02	56.94	66.07	60.53	62.16	58.55
Dibeklioglu <i>et al.</i> [34]	75.00	70.00	68.75	67.54	75.00	75.00	78.95	72.89	67.11
Our DeepFeat	88.92	92.82	88.47	90.24	85.69	89.70	<b>92.69</b>	89.79	88.16
Our Deep+Shallow	<b>88.93</b>	<b>94.74</b>	<b>90.07</b>	<b>91.23</b>	<b>90.49</b>	<b>93.10</b>	88.30	<b>90.98</b>	<b>88.93</b>

### Feature fusion

We have fused spatio-temporal features and deep features to check their complementarity. For simplicity, we have opted for a simple sum at the score-level to perform the fusion. Table 5.4 shows a comparison of the fusion results with the previous works. Overall, the fusion enhanced the verification accuracy by a significant margin. The effect is more evident in the relationships depicted by different sex and higher age variation, such as M-S (improved by 4.8%) and F-D (improved by 3.4%).

### Comparison against state of the art

Comparing our results against the state-of-the-art ones demonstrates considerable improvements in all the kinship subsets as shown in Table 5.4. For better illustration we depict in Fig. 5-10 the performance of our approach the best one from the state of the art [34]. Depending on the relation type, the improvement in verification accuracy of our approach compared with the best performing method by Dibeklioglu *et al.* [34] ranges from 9% to 23%. The average accuracy of all the kin relations has been improved by over 18%.

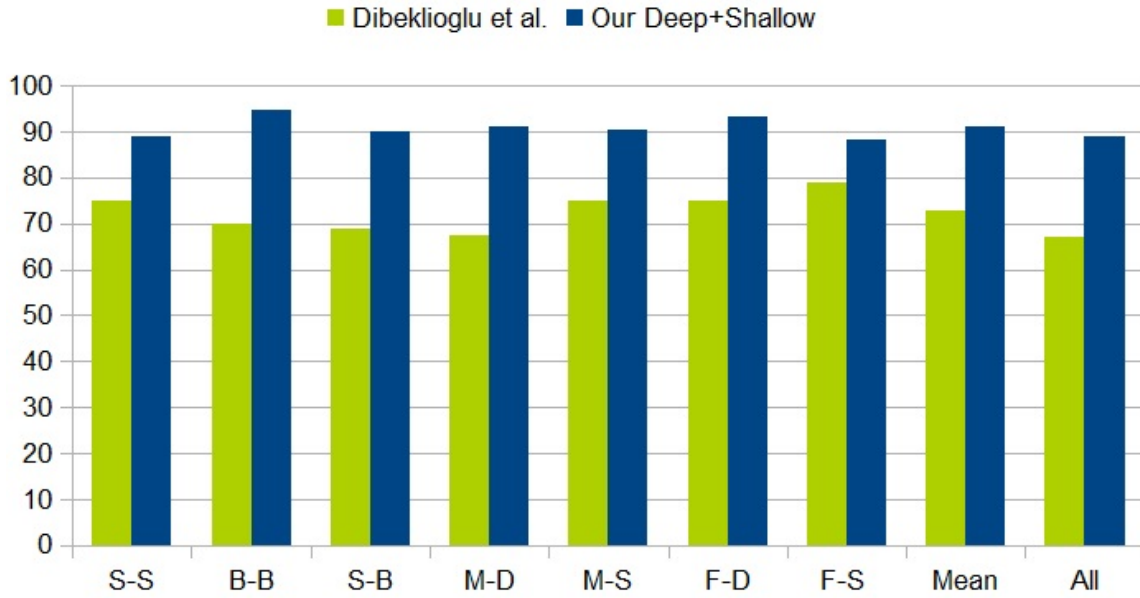


Figure 5-10: Performance of our approach against the best state-of-the-art one.

### Classification examples

Finally, in Fig.5-11 and Fig.5-12 we provide some examples of positive pairs correctly classified and positive pairs wrongly classified by our fusion approach, respectively.



Figure 5-11: Examples of correctly classified positive kin pairs by our approach using both spatio-temporal features and deep features.



Figure 5-12: Examples of wrongly classified positive kin pairs by our approach using both spatio-temporal features and deep features.

## 5.4 Conclusion

In this chapter, we have investigated the kinship verification problem from face video sequences. Faces are described using both spatio-temporal features and deep learned features. Experimental evaluation has been performed on the kinship part of UvA-NEMO Smile video database. Our study demonstrates the high efficiency of deep features in describing faces for inferring kinship relations. Further fusion of spatio-temporal features and deep features exhibited interesting improvements in verification accuracy. We have also shown the out-performance of videos against still images in kinship verification. Furthermore, comparison of our approach against the previous similar work indicates significant improvements in verification accuracy.

Using a CNN pre-trained for face recognition, we obtained improved results for kinship verification demonstrating the generalization ability of deep features to similar tasks. Even though the deep features results in our work are very promising, these features are extracted in a frame basis way. Employing a video deep architecture would lead into better results. However, the scarcity of kinship videos prevented us from opting to a such solution.



# Chapter 6

## Summary and future work

This thesis investigated several face analysis tasks, namely face verification and identification, gender recognition, ethnicity classification and kinship verification, from RGB images depth maps and videos. In this chapter, the thesis contributions are summarized and perspectives are elaborated.

### 6.1 Summary

In the first part of the thesis, we have proposed two novel approaches for improving face description and modeling based on local binary patterns. Both approaches are evaluated on face authentication problem showing interesting enhancements in terms of verification performance. The two proposed approaches share the same intuition of reinforcing a user-specific model by making use of generic face model, exploiting the shared similarities of human faces, which is adapted to each person specificity. The first method is theoretically well established. A compact feature vector is automatically selected from face region's LBP codes by clustering each region codes of a pool of background faces. The maximum *a posteriori* paradigm is employed to infer a specific model for a given person. The second approach keeps the simplicity of histogram representation, which is strengthened via a new improved estimation. A face model is estimated as weighted sum of a generic model and the person specific model. We have fused both approaches yielding in further improvements compared

to the LBP-baseline as well as similar previous works.

The 3D facial scans have been shown to outperform RGB images in face analysis under adversarial illumination, head pose and expression conditions. However, high resolution 3D scanners, given their cost, size and scan speed, are impractical for deployment of face analysis applications. The recent advance in 3D sensing technology provides very promising alternatives to old scanners. The thesis contributes in this scope by the use of facial depth maps, captured with Microsoft Kinect, which are of low resolution but of low cost and rendered at video rates. Moreover, Kinect like sensors are today being miniaturized and integrated in portable devices, opening new perspectives for using such depth images in many exiting applications. Motivated by these benefits, we conducted an in-depth study on three databases involving four different descriptors to compare depth maps against RGB images for three face analysis tasks. While humans are unable to infer any useful information from the kinect noisy depth images, we showed that machines are successful in predicting identity, gender and ethnicity from such images. Moreover, we demonstrated that Kinect depth images outperform their RGB counterparts under sever illumination, expression and head pose challenges.

The thesis contributed to automatic face-based kinship verification, which is a relatively new and challenging research problem in computer vision. While most of the existing works extract shallow handcrafted features from still face images, we approached this problem from spatio-temporal point of view and explored the use of both shallow texture features and deep features for characterizing faces. Promising results, especially those of deep features, are obtained. Our experiments also showed the superiority of using videos over still images, hence pointing out the important role of facial dynamics for kinship verification. Furthermore, the fusion of the two types of features (i.e. shallow spatio-temporal texture features and deep features) yielded significant performance improvements compared to state-of-the-art methods. Our experiments also pointed out the impact of gender and wide age differences on the problem of kinship verification.

To sum up, since efficient face description is a key step in the face analysis system,

in this thesis, we mainly focused on employing efficient local texture features for describing faces. We first extracted these features from still images, which we have later extended to depth maps and videos. In the last part of the thesis, we have considered the promising deep features, which exhibited remarkable performance improvements. Moreover, efficient face modeling approaches have also been developed by the first part of the thesis. All our contributions have been validated through extensive evaluation on publicly available face databases and fairly compared against state of the art.

## 6.2 Future directions

The work presented in this thesis opens up some perspectives and suggests some future research directions which are elaborated hereafter:

Firstly, though limited to some specific face analysis problems, the work of the present thesis can easily be extended to handle other similar face analysis tasks, such as age estimation, expression recognition, pain detection, etc.

Our proposed VQMAP face model generates a compact and efficient representation instead of a high dimensional LBP feature vector. It is worth to apply the proposed model to other LBP variants and LBP-like features which generate higher size features, especially those involving multi-resolution and over complete representations. Furthermore, it is of interest to investigate other metrics in both clustering and matching steps in the VQMAP model. For instance, as Hamming distance is more appropriate for binary series matching, it would yield further performance improvements, given the binary nature of LBP codes. We note also that our histogram adaptation approach is directly applicable to all other histogram-based image descriptors.

Regarding face analysis from 3D scans, even though a number of face databases acquired with Kinect has already been made available for research purposes (see our paper [18] for a detailed description of the available Kinect face databases), most of these databases are small-sized and collected in controlled environments. Be-



sides, there is no standard evaluation protocol associated with the publicly available datasets. Thus, each published paper designs its own evaluation methodology making it difficult to fairly compare various research results. Therefore, it is crucial to define standard evaluation protocols for each database.

Besides, the depth sensing is being developed and improved rapidly. Actually, a new version of Kinect (named Kinect 2), with enhanced depth sensing providing better quality depth maps, has been recently released by Microsoft. Google has also recently integrated a depth sensor in its Tango mobile devices. To the best of our knowledge, there is only one small publicly available Kinect 2 depth face database (HRRFaceD [80]) while no depth face database acquired with mobile devices exists. Thus, collecting new datasets with the latest versions of RGB-D sensors considering real world challenges and defining standard evaluation protocols is a key issue to be considered by the research community. Another promising research path is exploring 3D videos (i.e. 4D data) by analyzing faces from spatio-temporal depth data.

The lack of databases is also noticed for kinship problem. In this thesis, because of training data scarcity, we have been constrained to use a CNN pre-trained (for face recognition), in our experiments. Even though the deep features we extracted gave are very promising results, these features are extracted in a frame basis way. Employing a video deep architecture would lead into better results. However, deep learning approaches require the availability of huge training data, which is not the current case for Kinship. Therefore, further work includes the collection of a large kinship video database encompassing real world challenges to enable learning deep video features.



# Appendix A

## Vector quantization maximum *a posteriori*

This appendix presents the vector quantization maximum *a posteriori* (VQ-MAP) [51] model. We provide the formulation and detail mathematical development of the model.

The goal of vector quantization is to estimate the parameter vector, denoted as  $\Theta = (c_1^t, \dots, c_K^t)^t$ , which models the data. Here,  $c_i$  are the centroids and  $K$  is the model size, which is a trade-off between the representation accuracy and the data model size.

The maximum *a posteriori* modeling paradigm, irrespective of the actual model in question, is formulated as a way to seek  $\Theta$  that maximizes the posterior probability density function (pdf). Formally:

$$\begin{aligned}\Theta_{MAP} &= \arg \max_{\Theta} P(\Theta/X) \\ &= \arg \max_{\Theta} P(X/\Theta)g(\Theta),\end{aligned}\tag{A.1}$$

where  $P(X/\Theta)$  is the likelihood of the training set  $X = \{x_1, \dots, x_N\}$  given the parameters  $\Theta$ , and  $g(\Theta)$  is the prior pdf of the parameters. Three subproblems need to be solved so that a maximization algorithm can be derived:

- The likelihood function  $P(X/\Theta)$  needs to be defined in terms of vector quanti-

zation;

- An appropriate prior distribution  $g(\Theta)$  needs to be defined;
- The prior distribution contains its own set of parameters, which also needs to be estimated.

In the following, these points are addressed and the maximization algorithm is derived.

## A.1 Modeling VQ as a Gaussian mixture

For the VQ-MAP algorithm, one must formulate Equation (A.1) in the vector quantization framework. Since VQ is not a parametric probabilistic model, one needs to specify a likelihood pdf that corresponds to the mean squared error (MSE), which defines the VQ model. The likelihood  $P(X/\Theta)$  can be modeled as a Gaussian mixture as in [13]. The density of the  $k$ th component is defined as:

$$p(x/c_k, \Sigma_k) = \frac{1}{2\pi\epsilon} \exp \left\{ -\frac{1}{2\epsilon} \|x - c_k\|^2 \right\}, \quad (\text{A.2})$$

where  $\Sigma_k = I\epsilon$ , and  $\epsilon$  is constant. It is shown in [13] that with this model, the EM algorithm reduces to k-means algorithm and that component prior weights  $\pi_k$  do not play any role in the algorithm. The weights just reflect the proportion of the data vectors in a given cluster.

## A.2 Defining the prior density

When selecting the appropriate prior density  $g(\Theta)$ , a good choice would be the conjugate prior of the  $p(x/c_k, \Sigma_k)$  as in [13]. Prior distribution is called a conjugate prior if its algebraic form is the same as the resulting posterior distribution. The conjugate prior of a multivariate Gaussian with a known covariance matrix is a multivariate

Gaussian. Therefore the prior of the component  $k$  is modeled as:

$$p(c_k/\mu_k, \hat{\Sigma}_k) = B_k \exp \left\{ -\frac{1}{2}(c_k - \mu_k)^t \hat{\Sigma}_k^{-1} (c_k - \mu_k) \right\}, \quad (\text{A.3})$$

where  $\hat{\Sigma}_k$  is the covariance matrix of the prior distribution, and

$$B_k = \frac{1}{(2\pi)^{D/2} \left| \hat{\Sigma}_k \right|^{1/2}}. \quad (\text{A.4})$$

Assuming independence between the parameters of the individual mixture components, as was done in [45], the prior model can be written as:

$$g(\Theta) \propto \prod_{k=1}^K g(c_k/\mu_k, \hat{\Sigma}_k). \quad (\text{A.5})$$

### A.3 MAP estimates for vector quantization

In order to maximize the posterior pdf in Equation (A.1), one needs to jointly determine the observation posteriors and the model parameters of each component. Unfortunately, the maximization cannot be performed directly [45]. Instead, locally optimal solution can be obtained by EM algorithm [13] for the Gaussian mixture models and by k-means algorithm for the vector quantization models. Both algorithms work essentially in a similar manner:

1. find observation posteriors (E-step);
2. given the posteriors, re-estimate the parameters (M-step).

In k-means, the observation posteriors correspond to hard partitioning of the dataset. In the M-step, the parameters are maximized by calculating new centroid estimates. Now the corresponding steps need to be defined in the new framework so that MAP parameters can be optimized.

Interestingly, the term  $g(\Theta)$  affects the maximization of the posterior distribution only in the M-step [13]. Optimal  $\Theta$  with respect to observation posteriors can then

be calculated by maximizing the following auxiliary function [45]:

$$R(\Theta, \hat{\Theta}) = Q(\Theta, \hat{\Theta}) + \log(\Theta), \quad (\text{A.6})$$

where  $\hat{\Theta}$  are the parameters estimated in the previous iteration, and  $\Theta$  are the parameters to be estimated. The function  $Q$  is the expectation of the complete-data log likelihood [13] and can be expressed as:

$$Q(\Theta, \hat{\Theta}) = \sum_{i=1}^N \sum_{j=1}^K \gamma_{ik} \{ \ln \pi_k + \ln p(x/c_k, \Sigma_k) \}, \quad (\text{A.7})$$

where  $\pi_k$  is the prior weight of the component  $k$ , and  $\gamma_{ik}$  is the posterior probability of the observation  $i$  for the component  $k$ . By letting  $\epsilon \rightarrow 0$  in Equation (A.2), the complete-data log likelihood function becomes the MSE [13]:

$$Q(\Theta, \hat{\Theta}) = -\frac{1}{2} \sum_{i=1}^N \sum_{j=1}^K r_{ik} \|x_i - c_k\|^2. \quad (\text{A.8})$$

The values of  $r_{ik}$  form a binary matrix, where

$$r_{ik} = \begin{cases} 1, & \text{if } k = \arg \min_j \|x_i - c_j\|; \\ 0, & \text{otherwise.} \end{cases} \quad (\text{A.9})$$

In vector quantization literature, MSE describes the distortion when observations  $x_i$  are encoded as their nearest centroids  $c_j$ .

By substituting (A.5) and (A.8) into (A.6), one arrives at a new auxiliary function form:

$$R(\Theta, \hat{\Theta}) = -\sum_{i=1}^N \sum_{j=1}^K r_{ik} \|x_i - c_k\|^2 - \sum_{k=1}^K (c_k - \mu_k^t) \hat{\Sigma}_k^{-1} (c_k - \mu_k). \quad (\text{A.10})$$

$c_k$  needs to be found such for each component that minimizes the above equation. The  $\mu_k$  and  $\hat{\Sigma}_k$  are the prior parameters for the component  $k$ , and they are selected from a previously trained universal background model as in [99]. However, in the

VQ model, covariance matrices (variance parameters) are not recorded as a part of the UBM. Therefore, for all components the covariances are set to  $\hat{\Sigma}_k = I$ . This is motivated by the model assumptions in Equation (A.2). Now,  $R(\Theta, \hat{\Theta})$  can be written as:

$$R(\Theta, \hat{\Theta}) = r_{11} \|x_1 - c_1\|^2 + \dots + r_{NK} \|x_N - c_K\|^2 + \|c_1 - \mu_1\|^2 + \dots + \|c_K - \mu_K\|^2. \quad (\text{A.11})$$

Now, let  $S_k = \{x_1, \dots, x_{|S_k|}\}$  denotes the set of training vectors that are mapped to  $c_k$ .  $R_k$  denotes the terms of  $R(\Theta, \hat{\Theta})$  that contain centroid  $c_k$ :

$$\begin{aligned} R_k &= \|x_1 - c_k\|^2 + \dots + \|x_{|S_k|} - c_k\|^2 + \|c_k - \mu_k\|^2 \\ &= 2|S_k| \langle \bar{x}_k, c_k \rangle + |S_k| \|c_k\|^2 \|c_k - \mu_k\|^2 \\ &= 2|S_k| \langle \bar{x}_k, c_k \rangle + (|S_k| + 1) \|c_k\|^2 + 2 \langle c_k, \mu_k \rangle, \end{aligned} \quad (\text{A.12})$$

where  $|S_k|$  is the number of vectors mapped to centroid  $c_k$ , and  $\bar{x}_k$  is the average of all vectors in the same cluster. Taking the gradient with respect to  $c_k$  from Equation (A.12), the centroid re-estimation formula for the M-step as is obtained:

$$c_k = \frac{|S_k|}{|S_k| + 1} \bar{x}_k + \frac{1}{|S_k| + 1} \mu_k. \quad (\text{A.13})$$





# Bibliography

- [1] Y. Adini, Y. Moses, and S. Ullman. Face recognition: the problem of compensating for changes in illumination direction. *IEEE Transactions on Pattern Analysis and Machine Intelligence*, 19(7):721–732, Jul 1997.
- [2] T. Ahonen, A. Hadid, and M. Pietikäinen. Face description with local binary patterns: Application to face recognition. *IEEE Transactions on Pattern Analysis and Machine Intelligence*, 28(12):2037–2041, 2006.
- [3] T. Ahonen and M. Pietikäinen. Pixelwise local binary pattern models of faces using kernel density estimation. In M. Tistarelli and M. Nixon, editors, *Advances in Biometrics*, volume 5558 of *Lecture Notes in Computer Science*, pages 52–61. Springer Berlin Heidelberg, 2009.
- [4] T. Ahonen, E. Rahtu, V. Ojansivu, and J. Heikkilä. Recognition of blurred faces using local phase quantization. In *International Conference on Pattern Recognition (ICPR)*, pages 1–4, Dec 2008.
- [5] P. Anasosalu, D. Thomas, and A. Sugimoto. Compact and accurate 3D face modeling using an RGB-D camera: Let’s open the door to 3D video conference. In *International Conference on Computer Vision Workshops (ICCVW)*, pages 67–74, Dec 2013.
- [6] M. Andersen, T. Jensen, P. Lisouski, A. Hansen, T. Gregersen, and P. Ahrendt. Kinect depth sensor evaluation for computer vision applications. Technical report, Department of Engineering, Aarhus University, Denmark, 2012.
- [7] S. Arashloo and J. Kittler. Dynamic texture recognition using multiscale binarized statistical image features. *IEEE Transactions on Multimedia*, 16(8):2099–2109, Dec 2014.
- [8] A. B. Ashraf, S. Lucey, J. F. Cohn, T. Chen, Z. Ambadar, K. M. Prkachin, and P. E. Solomon. The painful face – pain expression recognition using active appearance models. *Image and Vision Computing*, 27(12):1788 – 1796, 2009. Visual and multimodal analysis of human spontaneous behaviour:.
- [9] E. Bailly-Baillié, S. Bengio, F. Bimbot, M. Hamouz, J. Kittler, J. Mariéthoz, J. Matas, K. Messer, V. Popovici, F. Porée, B. Ruiz, and J.-P. Thiran. The banca database and evaluation protocol. In J. Kittler and M. Nixon, editors, *Audio- and Video-Based Biometric Person Authentication*, volume 2688 of *Lecture Notes in Computer Science*, pages 625–638. Springer Berlin Heidelberg, 2003.

- [10] O. Barkan, J. Weill, L. Wolf, and H. Aronowitz. Fast high dimensional vector multiplication face recognition. In *IEEE International Conference on Computer Vision (ICCV)*, pages 1960–1967, Dec 2013.
- [11] M. S. Bartlett, G. Littlewort, I. Fasel, and J. R. Movellan. Real time face detection and facial expression recognition: Development and applications to human computer interaction. In *Computer Vision and Pattern Recognition Workshop, 2003. CVPRW'03. Conference on*, volume 5, pages 53–53. IEEE, 2003.
- [12] P. N. Belhumeur, J. P. Hespanha, and D. J. Kriegman. Eigenfaces vs. fisherfaces: recognition using class specific linear projection. *IEEE Transactions on Pattern Analysis and Machine Intelligence*, 19(7):711–720, Jul 1997.
- [13] C. M. Bishop. *Pattern Recognition and Machine Learning (Information Science and Statistics)*. Springer-Verlag New York, Inc., Secaucus, NJ, USA, 2006.
- [14] V. Blanz and T. Vetter. Face recognition based on fitting a 3D morphable model. *IEEE Transactions on Pattern Analysis and Machine Intelligence*, 25(9):1063–1074, Sept 2003.
- [15] W. W. Bledsoe. The model method in facial recognition. Technical report, Panoramic Research, Inc., Palo Alto, California, 1964.
- [16] E. Boutellaa, M. Bengherabi, S. Ait-Aoudia, and A. Hadid. How much information kinect facial depth data can reveal about identity, gender and ethnicity? In L. Agapito, M. M. Bronstein, and C. Rother, editors, *Computer Vision - ECCV 2014 Workshops*, volume 8926 of *Lecture Notes in Computer Science*, pages 725–736. Springer International Publishing, 2015.
- [17] E. Boutellaa, M. Bordallo, S. Ait-Aoudia, X. Feng, and A. Hadid. Kinship verification from videos using spatio-temporal texture features and deep learning. In *international conference on biometrics (ICB)*. IEEE, 2016. Accepted.
- [18] E. Boutellaa, A. Hadid, M. Bengherabi, and S. Ait-Aoudia. On the use of kinect depth data for identity, gender and ethnicity classification from facial images. *Pattern Recognition Letters*, 68, Part 2:270 – 277, 2015. Special Issue on Soft Biometrics.
- [19] E. Boutellaa, F. Harizi, M. Bengherabi, S. Ait-Aoudia, and A. Hadid. Face verification using local binary patterns and maximum a posteriori vector quantization model. In *Advances in Visual Computing*, pages 539–549. Springer, 2013.
- [20] E. Boutellaa, F. Harizi, M. Bengherabi, S. Ait-Aoudia, and A. Hadid. Face verification using local binary patterns and generic model adaptation. *International Journal of Biometrics*, 7(1):31–44, 2015.
- [21] S. Brahmam, L. Jain, L. Nanni, and A. Lumini, editors. *Local Binary Patterns: New Variants and Applications*. Spinger, 2014.
- [22] C. Cao, Y. Weng, S. Lin, and K. Zhou. 3D shape regression for real-time facial animation. *ACM Transactions on Graphics*, 32(4):41:1–41:10, July 2013.

- [23] C. Cao, Y. Weng, S. Zhou, Y. Tong, and K. Zhou. Facewarehouse: A 3D facial expression database for visual computing. *IEEE Transactions on Visualization and Computer Graphics*, 20(3):413–425, March 2014.
- [24] Y. Cao and B.-L. Lu. Real-time head detection with kinect for driving fatigue detection. In M. Lee, A. Hirose, Z.-G. Hou, and R. Kil, editors, *Neural Information Processing*, volume 8228 of *Lecture Notes in Computer Science*, pages 600–607. Springer Berlin Heidelberg, 2013.
- [25] C. H. Chan, M. Tahir, J. Kittler, and M. Pietikäinen. Multiscale local phase quantization for robust component-based face recognition using kernel fusion of multiple descriptors. *IEEE Transactions on Pattern Analysis and Machine Intelligence*, 35(5):1164–1177, May 2013.
- [26] Y.-L. Chen, H.-T. Wu, F. Shi, X. Tong, and J. Chai. Accurate and robust 3D facial capture using a single RGB-D camera. In *International Conference on Computer Vision (ICCV)*, pages 3615–3622, Dec 2013.
- [27] Y.-Y. Chen, W. H. Hsu, and H.-Y. M. Liao. Discovering informative social subgraphs and predicting pairwise relationships from group photos. In *Proceedings of the 20th ACM International Conference on Multimedia*, MM '12, pages 669–678, New York, NY, USA, 2012. ACM.
- [28] S. Chopra, R. Hadsell, and Y. LeCun. Learning a similarity metric discriminatively, with application to face verification. In *IEEE Computer Society Conference on Computer Vision and Pattern Recognition*, volume 1, pages 539–546 vol. 1, June 2005.
- [29] C. Ciaccio, L. Wen, and G. Guo. Face recognition robust to head pose changes based on the RGB-D sensor. In *International Conference on Biometrics: Theory, Applications and Systems (BTAS)*, pages 1–6, Sept 2013.
- [30] T. Cootes, C. Taylor, D. Cooper, and J. Graham. Active shape models—their training and application. *Computer Vision and Image Understanding*, 61(1):38 – 59, 1995.
- [31] T. F. Cootes, G. J. Edwards, and C. J. Taylor. Active appearance models. In H. Burkhardt and B. Neumann, editors, *European Conference on Computer Vision*, pages 484–498, Berlin, Heidelberg, 1998. Springer Berlin Heidelberg.
- [32] N. Dalal and B. Triggs. Histograms of oriented gradients for human detection. In *Conference on Computer Vision and Pattern Recognition*, volume 1, pages 886–893 vol. 1, June 2005.
- [33] H. Dibeklioglu, A. Salah, and T. Gevers. Are you really smiling at me? spontaneous versus posed enjoyment smiles. In A. Fitzgibbon, S. Lazebnik, P. Perona, Y. Sato, and C. Schmid, editors, *Computer Vision ECCV 2012*, volume 7574 of *Lecture Notes in Computer Science*, pages 525–538. Springer Berlin Heidelberg, 2012.
- [34] H. Dibeklioglu, A. Salah, and T. Gevers. Like father, like son: Facial expression dynamics for kinship verification. In *IEEE International Conference on Computer Vision (ICCV)*, pages 1497–1504, Dec 2013.

- [35] H. Drira, B. Ben Amor, A. Srivastava, M. Daoudi, and R. Slama. 3D face recognition under expressions, occlusions, and pose variations. *IEEE Transactions on Pattern Analysis and Machine Intelligence*, 35(9):2270–2283, Sept 2013.
- [36] M. V. Duc, A. Masselli, and A. Zell. Real time face detection using geometric constraints, navigation and depth-based skin segmentation on mobile robots. In *International Symposium on Robotic and Sensors Environments (ROSE)*, pages 180–185, Nov 2012.
- [37] G. Edwards, C. Taylor, and T. Cootes. Interpreting face images using active appearance models. In *International Conference on Automatic Face and Gesture Recognition*, pages 300–305, Apr 1998.
- [38] G. Fanelli, M. Dantone, J. Gall, A. Fossati, and L. Van Gool. Random forests for real time 3D face analysis. *International Journal of Computer Vision*, 101(3):437–458, February 2013.
- [39] G. Fanelli, J. Gall, and L. Van Gool. Real time 3D head pose estimation: Recent achievements and future challenges. In *International Symposium on Communications Control and Signal Processing (ISCCSP)*, pages 1–4, May 2012.
- [40] G. Fanelli, T. Weise, J. Gall, and L. Gool. Real time head pose estimation from consumer depth cameras. In *Pattern Recognition*, volume 6835, pages 101–110. Springer Berlin Heidelberg, 2011.
- [41] R. Fang, K. Tang, N. Snavely, and T. Chen. Towards computational models of kinship verification. In *IEEE International Conference on Image Processing (ICIP)*, pages 1577–1580, Sept 2010.
- [42] B. Fasel and J. Luetttin. Automatic facial expression analysis: a survey. *Pattern Recognition*, 36(1):259 – 275, 2003.
- [43] P. F. Felzenszwalb and D. P. Huttenlocher. Pictorial structures for object recognition. *International Journal of Computer Vision*, 61(1):55–79, 2005.
- [44] A. Gallagher and T. Chen. Understanding images of groups of people. In *IEEE Conference on Computer Vision and Pattern Recognition*, pages 256–263. IEEE, 2009.
- [45] J. Gauvain and C.-H. Lee. Maximum a posteriori estimation for multivariate gaussian mixture observations of markov chains. *IEEE Transactions on Speech and Audio Processing*, 2(2):291–298, Apr 1994.
- [46] G. Goswami, S. Bharadwaj, M. Vatsa, and R. Singh. On RGB-D face recognition using kinect. In *International Conference on Biometrics: Theory, Applications and Systems (BTAS)*, pages 1–6, Sept 2013.
- [47] G. Goswami, M. Vatsa, and R. Singh. RGB-D face recognition with texture and attribute features. *IEEE Transactions on Information Forensics and Security*, 9(10):1629–1640, Oct 2014.

- [48] D. B. Graham and N. M. Allinson. Face recognition from unfamiliar views: subspace methods and pose dependency. In *Proceedings. Third IEEE International Conference on Automatic Face and Gesture Recognition*, pages 348–353, Apr 1998.
- [49] G. Guo and X. Wang. Kinship measurement on salient facial features. *IEEE Transactions on Instrumentation and Measurement*, 61(8):2322–2325, Aug 2012.
- [50] J. Han, L. Shao, D. Xu, and J. Shotton. Enhanced computer vision with microsoft kinect sensor: A review. *IEEE Transactions on Cybernetics*, 43(5):1318–1334, Oct 2013.
- [51] V. Hautamaki, T. Kinnunen, I. Karkkainen, J. Saastamoinen, M. Tuononen, and P. Franti. Maximum a posteriori adaptation of the centroid model for speaker verification. *IEEE Signal Processing Letters*, 15:162–165, 2008.
- [52] B. Heisele, P. Ho, J. Wu, and T. Poggio. Face recognition: component-based versus global approaches. *Computer Vision and Image Understanding*, 91(12):6 – 21, 2003. Special Issue on Face Recognition.
- [53] M. Hernandez, J. Choi, and G. Medioni. Laser scan quality 3D face modeling using a low-cost depth camera. In *Proceedings of the 20th European Signal Processing Conference (EUSIPCO)*, pages 1995–1999, Aug 2012.
- [54] J. Hu, J. Lu, J. Yuan, and Y.-P. Tan. Large margin multi-metric learning for face and kinship verification in the wild. In *Computer Vision–ACCV 2014*, pages 252–267. Springer, 2015.
- [55] D. Huang, C. Shan, M. Ardabilian, Y. Wang, and L. Chen. Local binary patterns and its application to facial image analysis: a survey. *IEEE Transactions on Systems, Man, and Cybernetics, Part C: Applications and Reviews*, 41(6):765–781, 2011.
- [56] T. Huynh, R. Min, and J.-L. Dugelay. An efficient LBP-based descriptor for facial depth images applied to gender recognition using RGB-D face data. In J.-I. Park and J. Kim, editors, *Computer Vision Workshops (ACCVW)*, volume 7728 of *Lecture Notes in Computer Science*, pages 133–145. Springer Berlin Heidelberg, 2013.
- [57] A. K. Jain, S. C. Dass, K. Nandakumar, and K. N. Soft biometric traits for personal recognition systems. In *Proceedings of International Conference on Biometric Authentication*, pages 731–738, 2004.
- [58] A. K. Jain and A. Ross. Bridging the gap: from biometrics to forensics. *Philosophical Transactions of the Royal Society of London B: Biological Sciences*, 370(1674), 2015.
- [59] Q. Jin, J. Zhao, and Y. Zhang. Facial feature extraction with a depth AAM algorithm. In *International Conference on Fuzzy Systems and Knowledge Discovery (FSKD)*, pages 1792–1796, May 2012.
- [60] J. Kannala and E. Rahtu. BSIF: Binarized statistical image features. In *International Conference on Pattern Recognition (ICPR)*, pages 1363–1366, 2012.

- [61] T. Kinnunen, J. Saastamoinen, V. Hautamaki, M. Vinni, and P. Franti. Comparing maximum a posteriori vector quantization and gaussian mixture models in speaker verification. In *IEEE International Conference on Acoustics, Speech and Signal*, pages 4229–4232, 2009.
- [62] J. C. Klontz and A. K. Jain. A case study on unconstrained facial recognition using the boston marathon bombings suspects. Technical Report MSU-CSE-13-4, Department of Computer Science, Michigan State University, East Lansing, Michigan, May 2013.
- [63] S. Koelstra, M. Pantic, and I. Y. Patras. A dynamic texture-based approach to recognition of facial actions and their temporal models. *IEEE Transactions on Pattern Analysis and Machine Intelligence*, 32(11):1940–1954, 2010.
- [64] N. Kohli, R. Singh, and M. Vatsa. Self-similarity representation of weber faces for kinship classification. In *IEEE Fifth International Conference on Biometrics: Theory, Applications and Systems (BTAS)*, pages 245–250, Sept 2012.
- [65] B. Li, W. Liu, S. An, and A. Krishna. Tensor based robust color face recognition. In *International Conference on Pattern Recognition (ICPR)*, pages 1719–1722, Nov 2012.
- [66] B. Li, A. Mian, W. Liu, and A. Krishna. Using kinect for face recognition under varying poses, expressions, illumination and disguise. In *Workshop on Applications of Computer Vision (WACV)*, pages 186–192, Jan 2013.
- [67] S. Li, K. Ngan, and L. Sheng. A head pose tracking system using RGB-D camera. In M. Chen, B. Leibe, and B. Neumann, editors, *Computer Vision Systems*, volume 7963 of *Lecture Notes in Computer Science*, pages 153–162. Springer Berlin Heidelberg, 2013.
- [68] S. Z. Li and A. K. Jain, editors. *Encyclopedia of Biometrics*. Springer, USA, 2009.
- [69] S. Z. Li and A. K. Jain, editors. *Handbook of Face Recognition, 2nd Edition*. Springer-Verlag London, 2011.
- [70] X. Li, J. Chen, G. Zhao, and M. Pietikinen. Remote heart rate measurement from face videos under realistic situations. In *2014 IEEE Conference on Computer Vision and Pattern Recognition*, pages 4264–4271, June 2014.
- [71] S. Liao, X. Zhu, Z. Lei, L. Zhang, and S. Li. Learning multi-scale block local binary patterns for face recognition. In S.-W. Lee and S. Li, editors, *Advances in Biometrics*, volume 4642 of *Lecture Notes in Computer Science*, pages 828–837. Springer Berlin Heidelberg, 2007.
- [72] Y. Linde, A. Buzo, and R. Gray. An algorithm for vector quantizer design. *IEEE Transactions on Communications*, 28(1):84–95, 1980.
- [73] C. Liu and H. Wechsler. Gabor feature based classification using the enhanced fisher linear discriminant model for face recognition. *IEEE Transactions on Image processing*, 11(4):467–476, 2002.

- [74] D. G. Lowe. Distinctive image features from scale-invariant keypoints. *International Journal of Computer Vision*, 60(2):91–110, 2004.
- [75] J. Lu, J. Hu, V. Liong, X. Zhou, A. Bottino, I. Ul Islam, T. Figueiredo Vieira, X. Qin, X. Tan, S. Chen, S. Mahpod, Y. Keller, L. Zheng, K. Idrissi, C. Garcia, S. Duffner, A. Baskurt, M. Castrillon-Santana, and J. Lorenzo-Navarro. The FG 2015 kinship verification in the wild evaluation. In *IEEE International Conference and Workshops on Automatic Face and Gesture Recognition*, volume 1, pages 1–7, May 2015.
- [76] J. Lu, J. Hu, X. Zhou, J. Zhou, M. Castrillón-Santana, J. Lorenzo-Navarro, L. Kou, Y. Shang, A. Bottino, and T. Figueiredo Vieira. Kinship verification in the wild: The first kinship verification competition. In *IEEE International Joint Conference on Biometrics (IJCB)*, pages 1–6. IEEE, 2014.
- [77] J. Lu, X. Zhou, Y.-P. Tan, Y. Shang, and J. Zhou. Neighborhood repulsed metric learning for kinship verification. *IEEE Transactions on Pattern Analysis and Machine Intelligence*, 36(2):331–345, 2014.
- [78] J. MacQueen. Some methods for classification and analysis of multivariate observations. In *Fifth Berkeley Symp. on Math. Statist. and Prob.*, volume 1, pages 1281–297. Univ. of Calif. Press, 1967.
- [79] F. Malawski, B. Kwolek, and S. Sako. Using kinect for facial expression recognition under varying poses and illumination. In D. Slezak, G. Schaefer, S. Vuong, and Y.-S. Kim, editors, *Active Media Technology*, volume 8610 of *Lecture Notes in Computer Science*, pages 395–406. Springer International Publishing, 2014.
- [80] T. Mantecon, C. Del-Bianco, F. Jaureguizar, and N. Garcia. Depth-based face recognition using local quantized patterns adapted for range data. In *IEEE International Conference on Image Processing (ICIP)*, pages 293–297, Oct 2014.
- [81] K. Messer, J. Matas, J. Kittler, and K. Jonsson. XM2VTSDB: The extended M2VTS database. In *In Second International Conference on Audio and Video-based Biometric Person Authentication*, pages 72–77, 1999.
- [82] G. Meyer and M. Do. Real-time 3D face modeling with a commodity depth camera. In *International Conference on Multimedia and Expo Workshops (ICMEW)*, pages 1–4, July 2013.
- [83] R. Min, J. Choi, G. Medioni, and J. Dugelay. Real-time 3D face identification from a depth camera. In *International Conference on Pattern Recognition (ICPR)*, pages 1739–1742, Nov 2012.
- [84] R. Min, A. Hadid, and J. L. Dugelay. Improving the recognition of faces occluded by facial accessories. In *IEEE International Conference on Automatic Face Gesture Recognition and Workshops (FG 2011)*, pages 442–447, March 2011.
- [85] E. Murphy-Chutorian and M. M. Trivedi. Head pose estimation in computer vision: A survey. *IEEE Transactions on Pattern Analysis and Machine Intelligence*, 31(4):607–626, April 2009.

- [86] R. Niese, P. Werner, and A. Al-Hamadi. Accurate, fast and robust realtime face pose estimation using kinect camera. In *International Conference on Systems, Man, and Cybernetics (SMC)*, pages 487–490, Oct 2013.
- [87] E. Nowak, F. Jurie, and B. Triggs. Sampling strategies for bag-of-features image classification. In *Computer Vision–ECCV 2006*, pages 490–503. Springer, 2006.
- [88] T. Ojala, M. Pietikäinen, and T. Mäenpää. Multiresolution gray-scale and rotation invariant texture classification with local binary patterns. *IEEE Transactions on Pattern Analysis and Machine Intelligence*, 24(7):971–987, 2002.
- [89] V. Ojansivu and J. Heikkil. Blur insensitive texture classification using local phase quantization. In A. Elmoataz, O. Lezoray, F. Nouboud, and D. Mammass, editors, *Image and Signal Processing*, volume 5099 of *Lecture Notes in Computer Science*, pages 236–243. Springer Berlin Heidelberg, 2008.
- [90] P. Paderleris, X. Zabulis, and A. Argyros. Head pose estimation on depth data based on particle swarm optimization. In *Conference on Computer Vision and Pattern Recognition Workshops (CVPRW)*, pages 42–49, June 2012.
- [91] M. Pamplona Segundo, S. Sarkar, D. Goldgof, L. Silva, and O. Bellon. Continuous 3D face authentication using RGB-D cameras. In *Conference on Computer Vision and Pattern Recognition Workshops (CVPRW)*, pages 64–69, June 2013.
- [92] O. M. Parkhi, A. Vedaldi, and A. Zisserman. Deep face recognition. In *British Machine Vision Conference*, 2015. 1(3), p.6.
- [93] A. Pentland, B. Moghaddam, and T. Starner. View-based and modular eigenspaces for face recognition. In *IEEE Computer Society Conference on Computer Vision and Pattern Recognition*, pages 84–91, Jun 1994.
- [94] P. Phillips, P. Flynn, T. Scruggs, K. Bowyer, J. Chang, K. Hoffman, J. Marques, J. Min, and W. Worek. Overview of the face recognition grand challenge. In *Conference on Computer Vision and Pattern Recognition (CVPR)*, volume 1, pages 947–954 vol. 1, 2005.
- [95] M. Pietikäinen, A. Hadid, G. Zhao, and T. Ahonen. *Computer Vision Using Local Binary Patterns*. Springer-Verlag London, 2011.
- [96] J. Pivrinta, E. Rahtu, and J. Heikkil. Volume local phase quantization for blur-insensitive dynamic texture classification. In A. Heyden and F. Kahl, editors, *Image Analysis*, volume 6688 of *Lecture Notes in Computer Science*, pages 360–369. Springer Berlin Heidelberg, 2011.
- [97] A. Rattani, C. Chen, and A. Ross. Evaluation of texture descriptors for automated gender estimation from fingerprints. In L. Agapito, M. M. Bronstein, and C. Rother, editors, *Computer Vision - ECCV 2014 Workshops*, volume 8926 of *Lecture Notes in Computer Science*, pages 764–777. Springer International Publishing, 2015.



- [98] X.-M. Ren, X.-F. Wang, and Y. Zhao. An efficient multi-scale overlapped block LBP approach for leaf image recognition. In D.-S. Huang, J. Ma, K.-H. Jo, and M. Gromiha, editors, *Intelligent Computing Theories and Applications*, volume 7390 of *Lecture Notes in Computer Science*, pages 237–243. Springer Berlin Heidelberg, 2012.
- [99] D. A. Reynolds, T. F. Quatieri, and R. B. Dunn. Speaker verification using adapted gaussian mixture models. *Digital Signal Processing*, 10(1-3):19–41, 2000.
- [100] Y. Rodriguez and S. Marcel. Face authentication using adapted local binary pattern histograms. In A. Leonardis, H. Bischof, and A. Pinz, editors, *Computer Vision ECCV 2006*, volume 3954 of *Lecture Notes in Computer Science*, pages 321–332. Springer Berlin Heidelberg, 2006.
- [101] O. Russakovsky, J. Deng, H. Su, J. Krause, S. Satheesh, S. Ma, Z. Huang, A. Karpathy, A. Khosla, M. Bernstein, A. C. Berg, and L. Fei-Fei. ImageNet Large Scale Visual Recognition Challenge. *International Journal of Computer Vision (IJCV)*, 115(3):211–252, 2015.
- [102] F. S. Samaria and A. C. Harter. Parameterisation of a stochastic model for human face identification. In *Applications of Computer Vision, 1994., Proceedings of the Second IEEE Workshop on*, pages 138–142, Dec 1994.
- [103] A. Savran, R. Gur, and R. Verma. Automatic detection of emotion valence on faces using consumer depth cameras. In *International Conference on Computer Vision Workshops (ICCVW)*, pages 75–82, Dec 2013.
- [104] B. Schlkopf, A. Smola, E. Smola, and K.-R. Müller. Nonlinear component analysis as a kernel eigenvalue problem. *Neural Computation*, 10:1299–1319, 1998.
- [105] K. Simonyan and A. Zisserman. Very deep convolutional networks for large-scale image recognition. *CoRR*, abs/1409.1556, 2014.
- [106] Q. Sun, Y. Tang, P. Hu, and J. Peng. Kinect-based automatic 3D high-resolution face modeling. In *International Conference on Image Analysis and Signal Processing (IASP)*, pages 1–4, Nov 2012.
- [107] Y. Sun, X. Wang, and X. Tang. Deep learning face representation from predicting 10,000 classes. In *Proceedings of the 2014 IEEE Conference on Computer Vision and Pattern Recognition, CVPR '14*, pages 1891–1898, Washington, DC, USA, 2014. IEEE Computer Society.
- [108] M. Suwa, N. Sugie, and K. Fujimora. preliminary note on pattern recognition of human emotional expression. In *Proceedings of the Fourth International Joint Conference on Pattern Recognition*, pages 408–410, 1978.
- [109] C. Szegedy, W. Liu, Y. Jia, P. Sermanet, S. Reed, D. Anguelov, D. Erhan, V. Vanhoucke, and A. Rabinovich. Going deeper with convolutions. *CoRR*, abs/1409.4842, 2014.

- [110] Y. Taigman, M. Yang, M. Ranzato, and L. Wolf. Deepface: Closing the gap to human-level performance in face verification. In *IEEE Conference on Computer Vision and Pattern Recognition (CVPR)*, pages 1701–1708, June 2014.
- [111] X. Tan, S. Chen, Z. H. Zhou, and J. Liu. Face recognition under occlusions and variant expressions with partial similarity. *IEEE Transactions on Information Forensics and Security*, 4(2):217–230, June 2009.
- [112] R. Tomari, Y. Kobayashi, and Y. Kuno. Multi-view head detection and tracking with long range capability for social navigation planning. In *International Conference on Advances in Visual Computing - Volume Part II*, ISVC, pages 418–427, Berlin, Heidelberg, 2011. Springer-Verlag.
- [113] M. Turk and A. Pentland. Eigenfaces for recognition. *J. Cognitive Neuroscience*, 3(1):71–86, Jan. 1991.
- [114] P. Viola and M. Jones. Rapid object detection using a boosted cascade of simple features. In *Computer Vision and Pattern Recognition, 2001. CVPR 2001. Proceedings of the 2001 IEEE Computer Society Conference on*, volume 1, pages I–511–I–518 vol.1, 2001.
- [115] G. Wang, A. Gallagher, J. Luo, and D. Forsyth. Seeing people in social context: Recognizing people and social relationships. In K. Daniilidis, P. Maragos, and N. Paragios, editors, *European Conference on Computer Vision*, pages 169–182. Springer Berlin Heidelberg, Berlin, Heidelberg, 2010.
- [116] K. Wang, X. Wang, Z. Pan, and K. Liu. A two-stage framework for 3D face reconstruction from RGB-D images. *IEEE Transactions on Pattern Analysis and Machine Intelligence*, 36(8):1493–1504, Aug 2014.
- [117] Z. M. Wang and J. H. Tao. Reconstruction of partially occluded face by fast recursive pca. In *International Conference on Computational Intelligence and Security Workshops*, pages 304–307, Dec 2007.
- [118] T. Weise, S. Bouaziz, H. Li, and M. Pauly. Realtime performance-based facial animation. *ACM Transactions on Graphics*, 30(4):77:1–77:10, July 2011.
- [119] L. Wiskott, J. M. Fellous, N. Kuiger, and C. von der Malsburg. Face recognition by elastic bunch graph matching. *IEEE Transactions on Pattern Analysis and Machine Intelligence*, 19(7):775–779, Jul 1997.
- [120] J. Wright, A. Y. Yang, A. Ganesh, S. S. Sastry, and Y. Ma. Robust face recognition via sparse representation. *IEEE Transactions on Pattern Analysis and Machine Intelligence*, 31(2):210–227, Feb 2009.
- [121] H. Yan, J. Lu, W. Deng, and X. Zhou. Discriminative multimetric learning for kinship verification. *IEEE Transactions on Information Forensics and Security*, 9(7):1169–1178, July 2014.
- [122] J. Yang, W. Liang, and Y. Jia. Face pose estimation with combined 2D and 3D hog features. In *International Conference on Pattern Recognition (ICPR)*, pages 2492–2495, Nov 2012.

- [123] M. H. Yang. Kernel eigenfaces vs. kernel fisherfaces: Face recognition using kernel methods. In *Fifth IEEE International Conference on Automatic Face and Gesture Recognition*, pages 215–220, May 2002.
- [124] M.-H. Yang, D. J. Kriegman, and N. Ahuja. Detecting faces in images: a survey. *IEEE Transactions on Pattern Analysis and Machine Intelligence*, 24(1):34–58, Jan 2002.
- [125] Z. Yang and H. Ai. Demographic classification with local binary patterns. In S.-W. Lee and S. Z. Li, editors, *Advances in Biometrics: International Conference, ICB 2007, Seoul, Korea, August 27-29, 2007. Proceedings*, pages 464–473, Berlin, Heidelberg, 2007. Springer Berlin Heidelberg.
- [126] S. Zafeiriou, C. Zhang, and Z. Zhang. A survey on face detection in the wild: Past, present and future. *Computer Vision and Image Understanding*, 138:1 – 24, 2015.
- [127] J. Zhang, H. Wang, S. Liu, F. Davoine, C. Pan, and S. Xiang. Active learning based automatic face segmentation for kinect video. In *International Conference on Acoustics, Speech and Signal Processing (ICASSP)*, pages 1816–1820, May 2013.
- [128] K. Zhang, Y. Huang, C. Song, H. Wu, and L. Wang. Kinship verification with deep convolutional neural networks. In *Proceedings of the British Machine Vision Conference (BMVC)*, pages 148.1–148.12. BMVA Press, September 2015.
- [129] W. Zhang, Q. Wang, and X. Tang. Real time feature based 3-D deformable face tracking. In *European Conference on Computer Computer Vision - ECCV*, pages 720–732, 2008.
- [130] G. Zhao and M. Pietikainen. Dynamic texture recognition using local binary patterns with an application to facial expressions. *IEEE Transactions on Pattern Analysis and Machine Intelligence*, 29(6):915–928, June 2007.
- [131] G. Zhao and M. Pietikäinen. Boosted multi-resolution spatiotemporal descriptors for facial expression recognition. *Pattern recognition letters*, 30(12):1117–1127, 2009.
- [132] X. Zhou, J. Hu, J. Lu, Y. Shang, and Y. Guan. Kinship verification from facial images under uncontrolled conditions. In *Proceedings of the 19th ACM International Conference on Multimedia*, MM ’11, pages 953–956, New York, NY, USA, 2011. ACM.
- [133] X. Zhou, J. Lu, J. Hu, and Y. Shang. Gabor-based gradient orientation pyramid for kinship verification under uncontrolled environments. In *Proceedings of the 20th ACM International Conference on Multimedia*, MM ’12, pages 725–728, New York, NY, USA, 2012. ACM.
- [134] X. Zhou, Y. Shang, H. Yan, and G. Guo. Ensemble similarity learning for kinship verification from facial images in the wild. *Information Fusion*, pages –, 2015.
- [135] M. Zollhöfer, M. Martinek, G. Greiner, M. Stamminger, and J. Süßmuth. Automatic reconstruction of personalized avatars from 3D face scans. *Journal of Visualization and Computer Animation*, 22(2-3):195–202, 2011.